CONTRIBUTIONS TO LTE IMPLEMENTATION

Teză destinată obţinerii
titlului ştiinţific de doctor inginer
la
Universitatea "Politehnica" din Timişoara
în domeniul INGINERIE ELECTRONICA
ŞI TELECOMUNICAŢII
de către

Ing. Jamal Mountassir

Conducător ştiinţific:	prof.univ.dr.ing. Alexandru Isar
Referenţi ştiinţifici:	prof.univ.dr.ing. Miranda Nafornita
	conf.univ.dr.ing. Constantin Paleologu
	conf.univ.dr.ing. Romulus Terebes

Ziua susţinerii tezei: 28.06.2013

Seriile Teze de doctorat ale UPT sunt:

1. Automatică
2. Chimie
3. Energetică
4. Ingineria Chimică
5. Inginerie Civilă
6. Inginerie Electrică
7. Inginerie Electronică şi Telecomunicaţii
8. Inginerie Industrială
9. Inginerie Mecanică
10. Ştiinţa Calculatoarelor
11. Ştiinţa şi Ingineria Materialelor

Universitatea „Politehnica” din Timişoara a iniţiat seriile de mai sus în scopul diseminării expertizei, cunoştinţelor şi rezultatelor cercetărilor întreprinse în cadrul şcolii doctorale a universităţii. Seriile conţin, potrivit H.B.Ex.S Nr. 14 / 14.07.2006, tezele de doctorat susţinute în universitate începând cu 1 octombrie 2006.

România, 300159 Timişoara, Bd. Republicii 9,
tel. 0256 403823, fax. 0256 403221
e-mail: editura@edipol.upt.ro

Acknowledgement

This thesis has been elaborated while working as a researcher in the Communication Department of the Electronics and Telecommunications Faculty, "Politehnica" University of Timisoara, Romania. During the past three years working towards my PhD degree, I was very fortunate enough to come across many great individuals and I am very grateful for it.

First, I would like to give the utmost gratitude to my thesis advisor Alexandru ISAR from "Politehnica" University of Timisoara. Not only was he generous enough to guide my thesis research during his busy schedules, but he was also my role model as a great teacher. Through numerous discussions and one-on-one meetings, I learned so much from him and I greatly appreciate all the advice and wisdom, big and small.

I would like to thank the members of the thesis committee, for their time and valuable feedback on my research. I am honored to have them on the committee.

I would like to thank my colleagues and friends for the fruitful talks and friendly environment they have provided me.

Last but not least, I would like to thank my family for all the love, support and interest in my career.

Timişoara, June 2013 Jamal MOUNTASSIR

To my Family.

MOUNTASSIR, Jamal

Contributions to LTE Impelentation

Teze de doctorat ale UPT, Seria 7, Nr. 63, Editura Politehnica, 2013, 112 pagini, 74 figuri, 5 tabele.

ISSN: 1842-7014

ISBN: 978-606-554-680-6

Keywords: 3GPP LTE, OFDMA, SC-FDMA, PAPR, Blind Estimation

Abstract,

The third Generation Partnership Project Long Term Evolution (3GPP LTE) is one of the choices for next generation wireless networks. LTE is designed to provide a peak data rate of about 100 Mbps in Downlink and 50 Mbps in Uplink, and to ensure high mobility at speed up to 350 km/h. LTE's objectives include a radio interface physical layer to support transmission bandwidth up to 20 MHz together with new transmission schemes and advanced multi-antenna technologies.

In order to achieve its target, LTE specified a new radio interface based on Orthogonal Frequency Division Multiple Access (OFDMA) in Downlink and Single Carrier Frequency Division Multiple Access (SC-FDMA) in Uplink, which is based on OFDMA implemented by Discrete Fourier Transform (DFT) precoding, along with Multiple Input Multiple Output (MIMO) antenna processing and all services are supported on IP based architectures. This new OFDMA based air interface is utilized under Evolved UMTS terrestrial Radio Access Network (E-UTRAN) and supported with a new flatter- IP core termed as Evolved Packet Core (EPC).

The principal advantage of SC-FDMA is its low Peak-to-Average Power Ratio (PAPR) of the transmitted signal. This parameter is one of the drawbacks of OFDMA. The transmitter in most radio systems uses High power Amplifier (HPA), the HPA introduce inter-modulation between subcarriers and additional interferences into the system due to its saturation, as a consequence high PAPR of OFDM systems and leads to an increased Bit Error Rate (BER)

In this thesis, we analyze the PAPR characteristics for both OFDMA and SCFDMA, we investigate the most used PAPR reduction techniques and we propose new techniques in order to further reduce the PAPR by taking in consideration the signal degradation that appears usually after applying a PAPR reduction technique.

A new blind estimation technique using a denoising method, based on wavelets, is also proposed in this Thesis. This technique is simpler than the non blind estimation methods, because it does not require the channel estimation and it provides a solution for estimation problem in LTE DL and UL, improving substantially the performance of both types of communication systems.

CONTENTS

List of Figures

List of Tables

Abbreviations

1xEVO-DO	Evolution Data Only
3GPP LTE	The Third Generation Partnership Project Long Term Evolution
ACE	Active Constellation Extension
ACK	ACKnowledgement
AMBR	Aggregate Maximum Bit Rate
AP	Application Protocol
ARP	Allocation and Retention Priority
ARQ	Automatic Repeat Request
AWGN	Additive White Gaussian Noise
BCH	Broadcast Channel
BER	Bit Error Rate
BRICC	Bearer Independent Call Control
BSR	Buffer Status Report
BS	Base Station
CAZAC	Constant Amplitude Zero Auto-Correlation
CCDF	Complementary Cumulative Distribution Function
CDMA	Code Division Multiple Access
CM	Constant Modulus
CMA	Constant Modulus Algorithm
CP	Cyclic Prefix
CQI	Channel Quality Indicator
CS	Circuit Switched
D/A	Digital to Analog
DAC	Digital to Analog Converter
DCT	Discrete Cosine Transform
DFDMA	Distributed FDMA
DFT	Discrete Fourier Transform
DL	Downlink
DL-SCH	Downlink Shared Channel
DST	Discrete Sine Transform

DwPTS	Downlink Pilot Time Slot
DWT	Discrete Wavelet Transform
EDGE	Enhanced Data GSM Environment
eNodeB	evolved NodeBs
EPC	Evolved Packet Core
E-UTRAN	Evolved UMTS terrestrial Radio Access Network
FDD	Frequency Division Duplex
FDM	Frequency Division Multiplexing
FEC	Forward Error Correcting
FTT	Fast Fourier Transform
FWHT	Fast Walsh–Hadamard Transform
GBR	Guaranteed Bit Rate
GMSK	Gaussian Minimum Shift Keying
GP	Guard Period
GPRS	General Packet Radio Services
GSM	Global System for Mobile Communications
HARQ	Hybrid Automatic repeat ReQuest
HLR	Home Location Register
HPA	High Power Amplifier
HSDPA	High Speed Downlink Packet Access
HSS	Home Subscriber Server
HSUPA	High Speed Uplink Packet Access
ICI	Inter Carrier Interference
IDFT	Inverse Discrete Fourier Transform
IDWT	Inverse DWT
IFDMA	Interleaved FDMA
IFFT	Inverse Fast Fourier Transform
IMS	IP Multimedia System
IP	Evolved Packet Core
ISI	Inter-Symbol Interference
LFDMA	Localized FDMA
LMMSE	Linear Minimum Mean Square Error
LOS	Line of Sight

LS	Least Square
MAC	Media Access Control
MBR	Maximum Bit Rate
MBS	Multimedia Broadcast Services
MBSMS	Multimedia Broadcast and Multicast Services
MIMO	Multiple Input Multiple Output
MME	Mobile Management Entity
MMSE	Minimum Mean Square Error
MSE	Mean Square Error
NACK	Negative ACKnowledgement
NAS	Non Access Stratum
OFDM	Orthogonal Frequency Division Multiplexing
OFDMA	Orthogonal Frequency Division Multiple Access
PAPR	Peak-to-Average-Power Ratio
PBCH	Physical Broadcast Channel
PCH	Paging Channel
PCRF	Policy and Charging Rules Function
PDCCH	Physical Downlink Control Channel
PDCP	Packet Data Convergence Protocol
PDN	Packet Data Network
PDSCH	Physical Downlink Shared Channel
PDU	Protocol Data Units
P-GW	PDN Gateway
PHY	Physical
PLMN	Public Land Mobile Networks
PRACH	Physical Access Channel
PS	Packet Switched
PTS	Partial Transmit Sequence
PUSCH	Physical Uplink Shared Channel
QAM	Quadrature Amplitude Modulation
QoS	Quality of Service
QPSK	Quadrature Phase Shift Keying
RACH	Random Access Channel

RC	Raised-Cosine
RLC	Radio Link Control
RRC	Radio Resource Control
RTP	Real-time Transport Protocol
SC-FDMA	Single Carrier Frequency Division Multiple Access
SER	Symbol Error Rate
SGSN	Serving GPRS Support Node
S-GW	Serving Gateway
SIB	System Information Blocks
SLM	Selected Mapping
SNR	Signal to Noise ratio
SOS	Second Order Statistics
SVD	Singular Value Decomposition
TA	Tracking Areas
TCP	Transmission Control Protocol
TDD	Time Division Duplex
TDMA	Time Division Multiple Access
TR	Tone Reservation
UDP	User Datagram Protocol
UE	User Equipment
UL	Uplink
UL-CH	Uplink Shared Channel
UMTS	Universal Mobile Telecommunications System
UpPTS	Uplink Pilot Time Slot
VoIP	Voice over Internet Protocol
WHT	Walsh-Hadamard Transform
WiMAX	Worldwide Interoperability for Microwave Access

CHAPTER 1

INTRODCUTION

In this chapter, we present the motivation of the work and a short outline of the thesis.

1.1. Motivation

The evolution of wireless networks process is an ongoing phenomenon. There is always a need for high data rates, reduced packet latency or delay, high spectral efficiency and lower cost. The third Generation Partnership Project Long Term Evolution (3GPP LTE) is one of the choices for next generation wireless networks. LTE can be described as an evolution for both Universal Mobile Telecommunications System (UMTS) and Code Division Multiple Access (CDMA) (as for example CDMA Evolution Data Only, 1xEVO-DO) networks [1]. LTE's objectives include a radio interface physical layer to support transmission bandwidth up to 20 MHz together with new transmission schemes and advanced multi-antenna technologies. LTE is designed to provide a peak data rate of about 100 Mbps in Downlink and 50 Mbps in Uplink, and to ensure high mobility at speed up to 350 km/h; LTE is also expected to support voice and real time service quality without interruption [2].

In order to achieve its target, LTE specified a new radio interface based on Orthogonal Frequency Division Multiple Access (OFDMA) in Downlink and Single Carrier Frequency Division Multiple Access (SC-FDMA) in Uplink, which is based on OFDMA implemented by Discrete Fourier Transform (DFT) precoding, along with Multiple Input Multiple Output (MIMO) antenna processing and all services are supported on IP based architectures. This new OFDMA based air interface is utilized under Evolved UMTS terrestrial Radio Access Network (E-UTRAN) and supported with a new flatter- IP core termed as Evolved Packet Core (EPC) [2].

The principal advantage of SC-FDMA is its low Peak-to-Average Power Ratio (PAPR) of the transmitted signal. The PAPR value should be low because any power amplifier of a transmitter is nonlinear and saturates if the entry signal exceeds a certain threshold (corresponding to the big peak power value). After saturation of the power amplifier, the signal waveform is distorted resulting an Inter-symbol Interference (ISI) and the subcarriers separation becomes very difficult at the receiver.

The subject of wireless networks is multi-disciplinary. One of the research fields that profited most from the development of wireless networks is signal processing theory. Due to the evolution of wireless networks, new branches of signal processing were developed, such as space-time processing, time-frequency processing, detection and estimation theory. Among the most important problems revealed by wireless communication networks should be mentioned: communication channel estimation: estimation of channel's parameters (rank of channel's matrix, coherence time of the channel, coherence bandwidth of the channel, Doppler frequency maximum deviation, angle of arrival of each multiple path composing the channel); physical layer programming (the choice of digital modulation used, the choice of subcarriers used … etc) depending on the identified channel parameters (this is for the Media Access Control –MAC layer protocol stack) and sharing access

to multiple users. Given the complexity of these problems, it is often preferable to replace theoretical analysis of communications network with performance analysis based on simulations. Therefore, in recent years, many network simulators are designed. Among the most important network simulators, there are those that simulate the physical layer [3]. Using such a simulator, different MAC level decisions and scenarios can be created for the corresponding physical layer. Based on the analysis of wireless network performance made by simulations, the opportunity of some decisions, which must be made in the MAC layer, can be evaluated and rules to optimize these decisions can be established.

Also, one can imagine scenarios for the identification of physical layer parameters, such as for example the cell topography or location of users, taking into consideration the roads belonging to a cell specified or the laws of motion of mobile users.

In this thesis, a new blind estimation technique using a denoising method, based on wavelets, is proposed. This technique is simpler than the non blind estimation methods, because it does not require the channel estimation and it provides a solution for estimation problem in LTE DL and UL, improving substantially the performance of both types of communication systems. So, the contribution of this technique is very important.

As PAPR is very important in OFDMA, another objective of this thesis is PAPR reduction. It is accomplished by analyzing and simulating different precoding techniques in OFDMA and by combining different PAPR reduction techniques in order to build new techniques with new properties. The present thesis provide a solution to the PAPR reduction problem by taking in consideration the signal degradation that usually appears after applying a PAPR reduction technique.

1.2. Thesis Outline

The outline of the thesis is as follow:

- Chapter 1, introduction, presents a short presentation of the context, the present work relies in and an overview of the structure of the thesis.

- Chapter 2, Overview of Third Generation Partnership Project Long Term Evolution, presents the evolution to LTE, E-UTRAN and the EPC. LTE protocol layers and channel are also described and then life of LTE User Equipment (UE), traffic handling and the mobility of users are discussed.

- Chapter 3, Multiple Access schemes in LTE, includes a presentation of LTE UL and DL (OFDMA and SC-FDMA) architectures and different subcarrier mapping schemes are compared.

- Chapter 4, Peak-to-Average Power Ratio, gives an overview of PAPR parameters in OFDMA and SC-FDMA. Different PAPR reduction techniques in OFDM are presented; we analyze pre-coding techniques in OFDM system for PAPR reduction and then we introduce a new PAPR reduction technique for OFDM, obtained by combining Partial Transmit Sequence (PTS) and Companding techniques. We use soft reduction companding for PAPR reduction in SC-FDMA as well, which gives good PAPR reduction results without deteriorating the Bit Error Rate curves.

- Chapter 5, Channel Estimation, investigates the wireless channels. We introduce some estimation techniques; we first present the non blind estimation techniques based on Pilot Arrangement which is generally divided in three categories: Block Type, Comb-type, and Lattice Type. Next, the channel estimation techniques based on training symbols are presented. Next, we illustrate the most used blind channel estimation techniques, which are based on subspace methods and Constant Modulus Algorithm (CMA). Finally, we develop and introduce a new blind estimation technique based on denoising, and then we implement this new technique in OFDMA and SC-FDMA for one user case.

- Chapter 6, Conclusions, presents the summary of the work, the conclusions drawn and future perspectives.

The thesis ends with a list of references, containing a number of 87 references.

CHAPTER 2

OVERVIEW OF 3GPP LONG TERM EVOLUTION

2.1. Introduction

LTE introduces important changes in comparison with its precursor communication technologies, in three major areas: Air interface, Radio network Architecture, and Core Network [4]. The Air interface changes produced in comparison with Worldwide Interoperability for Microwave Access (WiMAX) technology consist of the implementation of Single Carrier Frequency Division Multiple Access (SC-FDMA) in Uplink (UL), along with the fully-integrated use of Multiple Antenna Techniques. As a result of these changes, the Air interface supports high data rates. LTE changes the hierarchical architecture of UMTS or 1xEV-DO network and converts the radio network into IP-based distributed network. IP-based backhaul networks will reduce the backhaul cost. In the Core network, a fully packetized IP-based Core Network will replace the separate Circuit Switched (CS) and the Packet Switched (PS) Core Networks which provide scalability and reduced cost. The new service can be introduced via IP Multimedia System (IMS). The LTE architecture is presented in Figure 2.1.

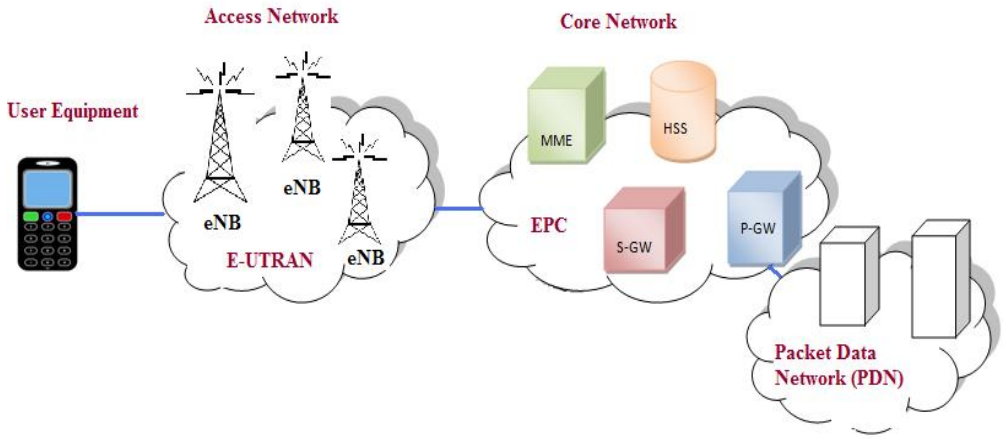

Figure 2.1: LTE architecture

The sub-systems in Figure 2.1 will be described in following sections.

2.2. Evolution to LTE

LTE supports data rates of over 300 Mbps in DL and more than 80 Mbps in UL. It reduces latency by reducing the number of nodes in the network and supports both Time Division Duplex (TDD) and Frequency Division Duplex (FDD) modes of

operation. As it was already said, LTE represents an evolution of technologies previously used as UMTS or CDMA. This evolution can be observed on the following figure.

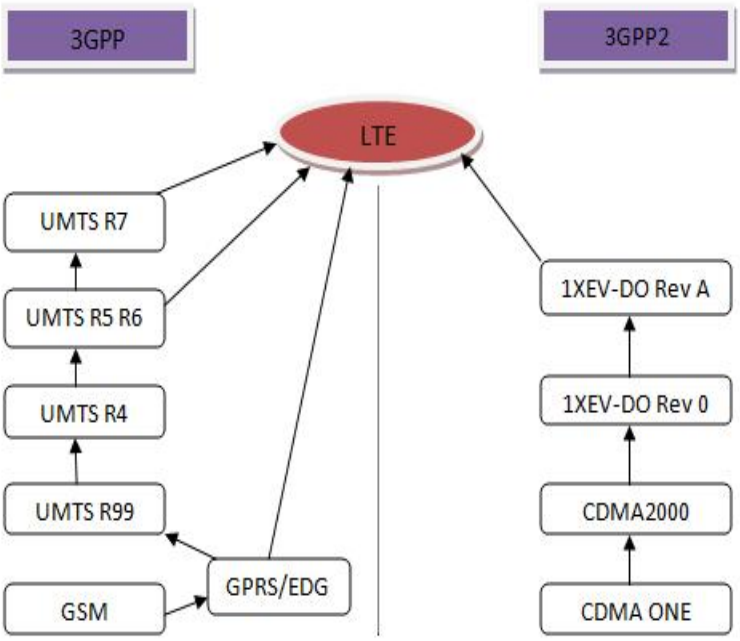

Figure 2.2: The evolution to LTE options from both UMTS and 1xEV-DO networks.

The path to UMTS begins with the Global System for Mobile Communications (GSM) voice network [5]. General Packet Radio Services (GPRS) is the packet data network with the theoretical data rate of 171 kbps. GPRS shares access network with GSM, but has separate core network [6]. With some coding and modulation enhancement, GPRS becomes Enhanced Data GSM Environment (EDGE) and offers approximately 3 times the data rate of GPRS [7]. LTE can evolve directly from a GPRS/EDGE network without the need to evolve through UMTS Release 99 [8], the first Release of UMTS. UMTS is characterized by change in access technology from Time Division Multiple Access (TDMA) to CDMA [9]. The theoretical data rate for UMTS R99 is 2 Mbps. UMTS R4 [10] does not impact the data rate, but through the introduction of Bearer Independent Call Control (BICC), UMTS R4 provides a more efficient core network. UMTS R5 [11] and R6 [12] introduce significant improvements in data rates, by introducing IMS supporting all IP networking and the High Speed Downlink Packet Access (HSDPA) which increases the peak DL data rate to about 14 Mbps. UMTS R6 introduces both multimedia Broadcast Services (MBS) capable of supporting services such as mobile TV, and the High Speed Uplink Packet Access (HSUPA) which increases the peak UL data rate to about 5.76 Mbps.

UMTS R7 is also referred to as HSPA+ [13], [14]. This release introduces Multi Input Multi Output (MIMO) systems, which uses multiple antennas concurrently sending and receiving parallel data streams, to further improve the efficiency of the network. UMTS R7 offers peak data of 42 Mbps DL and 22 Mbps UL.

LTE can evolve directly from either UMTS R5, R6 without upgrading to UMTS R7, or it can evolve from a UMTS R7 network.

The path to LTE through EV-Do begins with CDMA ONE based on old IS 95 standard [15]. As with GSM, CDMA ONE [16] is basically a voice and low speed circuit switched data network. Packed switching was added with the evolution to CDMA 2000 [17]. CDMA 2000 has a maximum data rate of about 614 kbps, but more practically it supports about 150 kbps. 1xEV-DO Rev 0 is a packet data network that offers peak data rate of about 2.45 Mbps DL and 153 kbps UL. Rev 0 provides bandwidth on demand and gives the users the feel that they are always connected. A short coming of Rev 0 is that it does not support the real time services [18].

1xEV-DO Rev A extends the downlink data rate only a small amount from 2.45 Mbps to 3.07 Mbps. Moreover the peak uplink data rate increases from about 153 kbps to 1.8 Mbps [18].

An important feature introduced with Rev A is the ability to support real time services. This enables the deployment of Voice over Internet Protocol (VoIP) services. VoIP is a real time application rapidly growing in popularity.

The targets for downlink and uplink peak data rate requirements were set to 100 Mbps for the downlink and 50 Mbps for the Uplink with a spectrum allocation of 20 MHz [19].

2.3. Evolved UTRAN Architecture

The Evolved UMTS Terrestrial Radio Access Network (E-UTRAN) is the radio access network of LTE. It consists only of cell sites, or evolved NodeBs (eNBs), which are the base stations of LTE and responsible to provide the E-UTRAN user plane and control plane protocol terminations towards the User Equipment (UE). The inter-eNB communication is referenced in standards as X2. Inter-cell communications using the X2 interface between the eNBs is new and unique to LTE. Similarly, the reference for UE-to-eNB communications known as the LTE-Uu, and E-UTRAN-to-Evolved Packet Core (EPC) communications is designated as S1. The S1 interface is separated by control plane signaling and user plane traffic. The variant of S1 used for control plane signaling is referred to as S1-Mobile Management Entity (MME), and for the user plane as S1-U [20]. The architecture of E-UTRAN is presented in Figure 2.3.

According to [2], the eNB performs the following functions:

1. Transfer of user data across the E-UTRAN between the S1 and LTE-Uu (air) interfaces.
2. Radio channel ciphering and deciphering in order to protect transmitted data over the air against unauthorized third party. The key for ciphering and deciphering is derived through signaling or session dependent information.
3. Integrity protection in order to avoid alteration of the transmitted data by an unauthorized third party.
4. Header compression for a particular network layer or protocol combination such as TCP/IP and RTP/UDP/IP.
5. Mobility Control functions:
   - Handover manages the radio interface by radio measurements, and it is used to maintain the Quality of Service (QoS) requested by EPC at the transition from a cell into a neighborhood one. The context is transferred during handover to target eNB;

- Paging provides a mechanism to a UE to contact the E-UTRAN when it is in LTE idle state;
- Positioning in order to provide physical location information for UE;

6. Connection setup and release in order to participate in processing of the end-to-end connection setup and release; maintains and manages the end-to-end connection;
7. Load balancing in order to distribute to uneven load distribution to keep the call dropping probabilities minimum. Load balancing may result in handover or cell reselection;
8. Distribution function for Non Access Stratum (NAS) messages in order to transfer the messages transparently for Radio Resource Control (RRC) and S1 –Application Protocol (AP);
9. NAS node selection function in order to select the MME/Serving Gateway (S-GW) for UE;
10. Synchronization in order to maintain the timing between different nodes within the network;
11. Radio access network sharing for multiple Public Land Mobile Networks (PLMNs). This mechanism directs the UE to appropriate PLMN. E-TRAN broadcasts the PLMN-ids in the air line (up to 6). The UE selects one of the PLMN-id and notifies E-UTRAN in random access procedure;
12. Multimedia Broadcast and Multicast Services (MBMS) function in order to ensure the transmission of the same data to a multiple recipients;

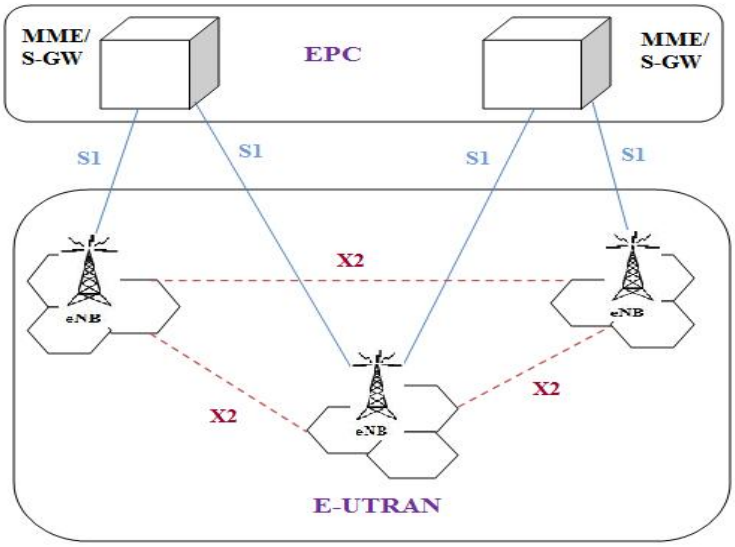

Figure 2.3: E-UTRAN architecture [20].

Subscriber and equipment trace. Traces are initiated by core network and a trace setup is transferred on X2 or S1 interface during handover.

As mentioned earlier, eNBs collaborate with each other over the X2 interface for functions like handover and interference management. The eNBs communicate with the EPC network's MME via the S1-MME interface and to the S-GW with the S1-U interface (see Figure 2.3). It exchanges user data with the S-GW over the S1-U

interface. The eNBs and the EPC have a many-to-many relationship to support load sharing and redundancy among MMEs and S-GWs. The eNB selects an MME from a group of MMEs so the load can be shared by multiple MMEs to avoid congestion.

2.4. Core Network

The LTE architecture has only one core network defined as EPC, which is dedicated to packet data. Voice services are established like other IP packet data services as voice over IP (VoIP), typically using IMS services environment beyond the EPC. This greatly simplifies the architecture since voice is no longer handled as an exception case. The migration also enables improved internetworking with other fixed and wireless communication networks as we can see in the following figure.

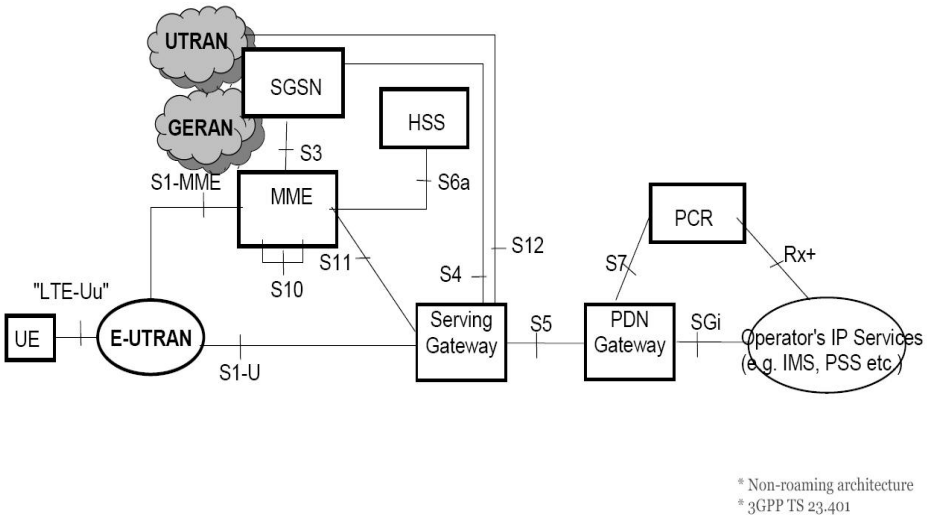

Figure 2.4: LTE network Architecture [2].

The EPC consists of several network elements that provide functions like the management of mobiles within its domain, authentication of subscribers and establishment of the bearer path to transport traffic between the UE and the Packet Data Network (PDN). The functions are supported in the EPC by entities like the MME, the S-GW, the PDN Gateway (P-GW), the Home subscriber Server (HSS) and the PCR (Policy and Charging Rules) function.

2.4.1. Mobility Management Entity

The MME performs the role of the Serving GPRS Support Node (SGSN) in GPRS networks. It manages UEs within the LTE EPC. As such, the MME manages subscriber authentication, maintains a context for authenticated UEs, establishes data bearer paths in the network for user traffic and keeps track of the location of idle mobiles which have not detached from the network. For idle UEs that need to be reconnected to the access network to receive downstream data, the MME will initiate

paging to locate the UE and re-establish the bearer paths to and through the E-UTRAN [2].

A mobile's MME is selected by the eNB from which the mobile initiates system access. The MME could be a part of the pool of MMEs in the EPC for load sharing and redundancy. In the establishment of the user's data bearer paths, the MME is responsible for selecting the P-GW and the S-GW which will make up the ends of the data path through the EPC.

2.4.2. Serving Gateway

The S-GW works primarily as an IP packet data router. From a network architecture perspective, the S-GW is the UE's bearer path anchor in the EPC; as the UE moves from one eNB to another during mobility operations, the S-GW remains the same and the bearer path towards the E-UTRAN is switched to talk to the new eNB serving the UE. If the UE moves to the domain of another S-GW, the MME is responsible for transferring all of the UE's bearer paths to the new S-GW [20].

Within the EPC, the S-GW, acting upon direction from the MME, establishes bearer paths for the UE to one or more P-GWs. If the downstream data should be received for an idle UE, the S-GW will buffer the downstream packets and request the MME to locate and re-establish the bearer paths to and through the E-UTRAN.

2.4.3. PDN Gatway

The P-GW is the gateway between the LTE network and a PDN. While the P-GW works primarily as a router for user traffic, there are some significant functions the P-GW performs on behalf of the UE. These functions include IP address allocation for the UE, packet filtering of downstream user traffic to ensure it is placed on the appropriate bearer path, enforcement of downstream Quality of Services (QoS), including the data rate. Depending upon the services a subscriber is using, there may be multiple user data bearer paths between the UE and a P-GW.

It is also possible that the subscriber is using services on PDNs served by different P-GWs. In this case, the UE will have at least one bearer path established to each P-GW. During handover of the UE from one eNB to another, if the S-GW is also changing, the bearer path from the P-GW is switched to the new S-GW.

2.4.4. Home Subscriber System

The Home Subscriber System (HSS) is responsible for both updating and storing the database containing all the user subscription information. The HSS can be thought of as the master database for the PLMN, as it incorporates both the functions of the Home Location Register (HLR) and the Authentication Center (AuC).

2.4.5. Policy and Charging Rules Function

The Policy and Charging Rules Function (PCRF) is responsible for flow based charging control functionalities and policy control decisions, it provides the network control with regard to gating, QoS and flow based charging and service data flow detection. In addition, the PCRF also authorizes the QoS resources and provides the charging filter rules [2].

2.5. LTE Protocol Layers

Some of the protocol layers used in LTE networks are presented in following figure.

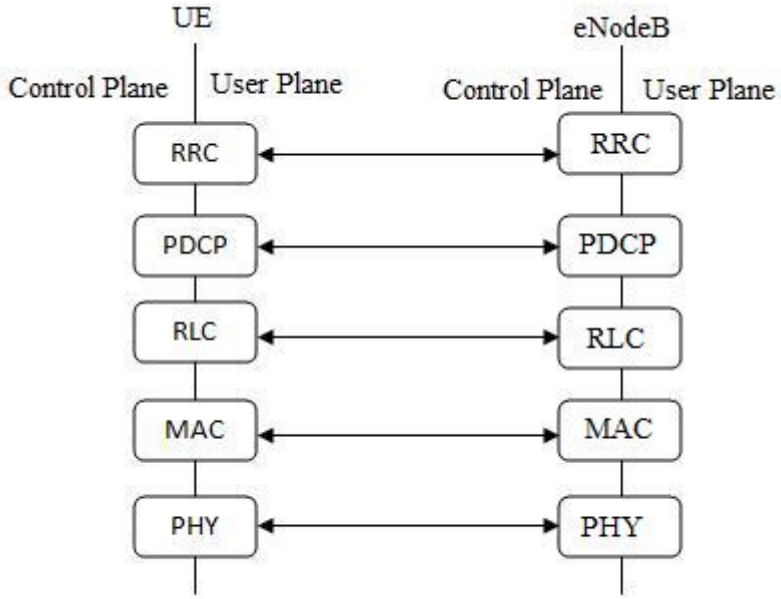

Figure 2.5: Protocol layers in LTE-Uu (between UE and e-NB).

Let us examine the LTE-Uu control plane protocol.
The Physical (PHY) layer in LTE supports the following functions [2]:

- Hybrid Automatic repeat ReQuest (HARQ) with soft combining,
- OFDMA-based physical layer,
- Uplink power control,
- Multi-stream transmission and reception (MIMO).

The Medium Access Control (MAC) sub-layer performs the following functions [21]:

- Scheduling,
- Error handling across UEs as well as across different logical channels of a UE,
- In-sequence delivery of Radio Link Control (RLC) Protocol data Units (PDUs),
- Multiplexing/de-multiplexing of different RLC bearers into/from the physical layer on transport channel.

The RLC sub-layer supports functions such as [22]:

- Transfer of super layer PDUs,
- Error correction through Automatic Repeat Request (ARQ),
- Flow control and concatenation or re-assembly of packets.

The Packet Data Convergence Protocol (PDCP) sub-layer performs:

- IP header compression,
- Ciphering,
- Supporting lossless mobility in case of inter-eNB handovers.

- Providing integrity protection to higher layer-control protocols [23].

The RRC sub-layer is between the UE and the eNB. It performs function such as [2]:

- Broadcasting system information,
- Paging,
- Connection management with UEs to allocate temporary identifiers,
- Radio bearer control,
- Mobility functions,
- UE measurement reporting and control.

2.5.1. Frame structures

Duplex schemes and frame structures are used in LTE. The LTE physical layer supports two types of duplexing: Frequency Division Duplex (FDD) and Time Division Duplex (TDD). In order to communicate with an eNB, a UE operates in FDD mode on two separate frequencies, one for uplink traffic and one for downlink traffic. With TDD, a UE needs only one frequency channel to communicate with an eNB. The uplink traffic and downlink traffic are allocated in different time slots on that channel.

LTE supports two types of frame structures. The frame structure type one can be used for both FDD and TDD duplex schemes and the frame structure type 2 can be used for TDD only.

Frame structure type 1

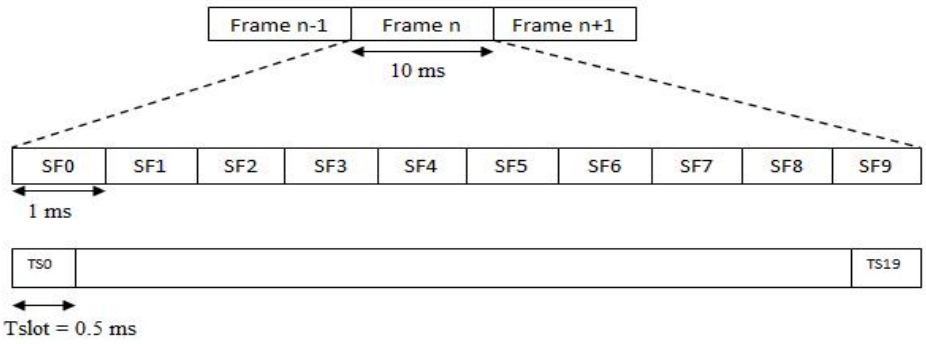

Figure 2.6: Frame structure type 1 applicable for TDD and FDD.

The frame structure type 1 is applicable for both FDD and TDD based transmissions. The LTE radio frame duration is of 10 ms. Each frame is divided into 10 sub-frames of 1ms duration each. Each sub-frame is further subdivided into two time slots of 0.5 ms each. To summarize, each frame has 20 time slots as it can be seen in Figure 2.6.

In LTE, each time slot is divided into many OFDM symbols. Each OFDM symbol consists of two parts: Cyclic Prefix (CP) followed by Useful Symbol. A CP is created by copying the tail end of the symbol to the beginning of the symbol period,

thus creating a guard time. CP helps combat Inter-symbol Interference (ISI) and Inter Carrier Interference (ICI). The duration of CP depends on the multipath delay spread characteristic of the radio environment, as can be seen in the following figure. LTE specifies two possible values for CP duration. The first one, called normal CP is defined for radio environments with low multipath delay spread. Typically urban environment LTE deployment use normal CP value which is about 5 microseconds. The second one, Extended CP, is used in Radio environments with high delay spread value. LTE defines Extended CP value to be approximately 15 microseconds.

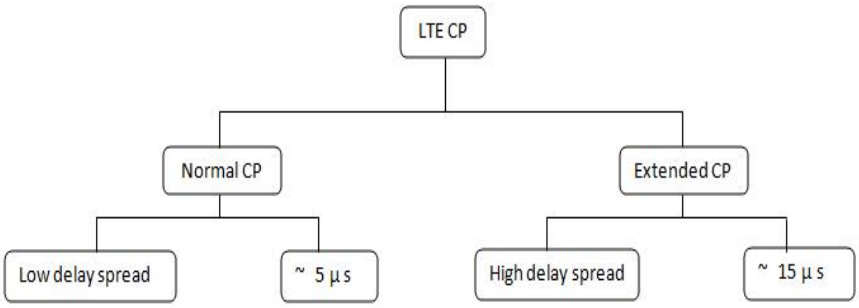

Figure 2.7: CP in LTE.

Each 10 ms frame in LTE is made up of twenty 0.5 ms duration slots. The numbers of OFDM symbols per slot will vary based on useful symbol time and length of CP. For non-multicast applications, LTE defines useful symbol time as 66.67 microseconds. When normal CP is used, each slot can transmit 7 OFDMA symbols. When extended CP is used, each slot can carries 6 OFDM symbols.

A UE requires radio resources to allow receiving information from the eNB in the DL direction and transmitting information to the eNB in the UL direction. The scheduler at eNB allocates the radio resources in terms of blocks to a UE. LTE defines a resource block as a group of 12 subcarriers assigned for one time slot. A base station may assign one or more resource blocks to a UE.

Frame structure type 2

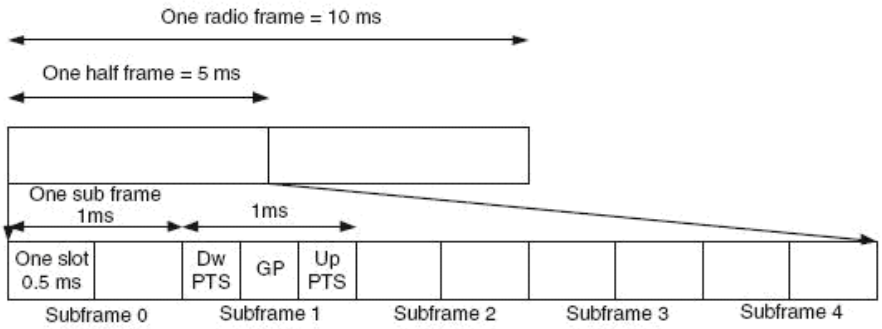

Figure 2.8: Frame structure type-2 [2]

It is applicable for TDD mode only. As is can be observed in Figure 2.8, each 10 ms radio frame consists of two half frames. Each half-frame is 5 ms long and contains 8 slots of length 0.5 ms each and 3 special fields: Downlink Pilot Time Slot (DwPTS), Guard Period (GP), and Uplink Pilot Time Slot (UpPTS) that have a total length of 1 ms. In a 10 ms radio frame, there is a total of 10 sub-frames (2 slots each) numbered from 0 to 9. Sub-frame 0 and 5 include DL synchronization reference signals. Sub-frame 1 is allocated for DwPTS for transmitting pilots in the DL. A guard period is kept between the special DwPTS and the special UpPTS. When there is a switch between UL and DL then the duration of one OFDM symbol is used as a switching interval. UpPTS is always used for UL transmission. There are multiple frame configurations that define which sub-frames are used in DL and UL. Sub-frame 6 is sometimes used for the 3 special fields. The remaining sub-frames can either be used for UL or DL depending on the specific configuration [2].

2.6. LTE Channels

There are many types of channels used in LTE. Some of them are presented in the following.

2.6.1. DL Physical channels

The classification of the physical DL channels is presented in Figure 2.9.

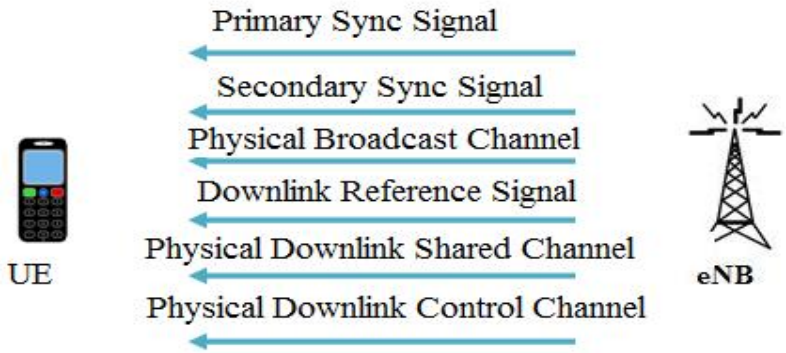

Figure 2.9: DL Physical Channel.

LTE defines two reference signals to help the UE to acquire the system and to achieve synchronization with the system. These reference signals are called Primary and Secondary synchronization signals. When a UE successfully acquires and locks on to these two signals, the UE has slot and frame level sync with the system. In addition to synchronization, the UE is able to uniquely identify this cell in that area [24].

LTE is defined for wide range of channel bandwidths starting from low values as 1.25 MHz to high values as 20 MHz. The network transmits a small amount of critical system information such as channel bandwidth used by the LTE on the physical broadcast channel.

LTE systems transmit a downlink reference signal. The UE uses the reference signal for coherent demodulation, channel estimation and handover functions. The Physical Downlink Shared Channel (PDSCH) is the main channel that carries user traffic, signaling messages, paging and system configuration messages.

The Physical Downlink Control Channel (PDCCH) is used to convey uplink and downlink allocation information. The PDCCH is also used to convey physical layer related acknowledgement information.

2.6.2. UL Physical Channels

The classification of UL physical channels is presented in Figure 2.10.

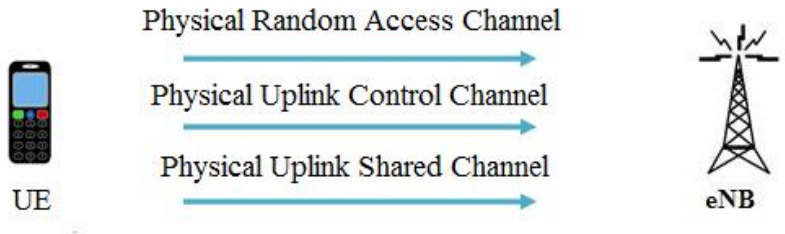

Figure 2.10: UL Physical Channels.

In the uplink, the Physical Random Access Channel (PRACH) is a collision-based access channel that enables multiple UEs to make initial requests. The Physical Uplink Control Channel (PUCCH) is used to carry ACKnowledgement/Negative ACKnowledgement (ACK/NACK) and Channel Quality Indicator (CQI) for downlink transmission. Also, this channel carries a scheduling request for uplink transmission. The Physical Uplink Shared Channel (PUSCH) carries uplink data transmission and signaling messages [30].

2.6.3. Transport Channels

The classification of transport channels is presented in Figure 2.11.

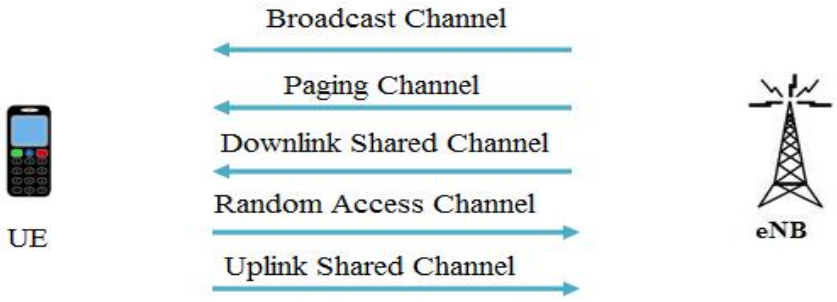

Figure 2.11: Transport Channels.

The following transport channels carry information in the downlink.

- The Broadcast Channel (BCH) transmits system configuration related broadcast messages.
- The Downlink Shared Channel (DL-SCH) carries user traffic and system messages. Its performance is enhanced by use of link adaptation and HARQ.
- The Paging Channel (PCH) is used to handle paging functions to trigger a transition from idle state.

The following transport channels carry MAC layer information in the uplink:

- The Random Access Channel (RACH) carries requests for initial access to the network and supports open loop power control.
- The Uplink Shared Channel (UL-SCH) carries user traffic and messages on the uplink. It also supports HARQ, link adaptation and request for resource allocation [24-25].

2.6.4. Mapping of transport Channel to Physical Channel

The mapping of transport channel to physical channel is represented in Figure 2.12.

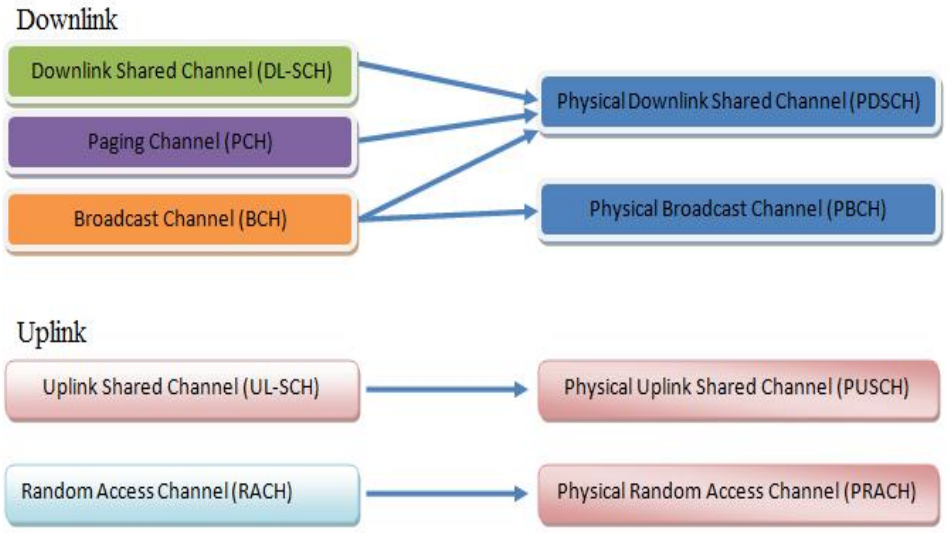

Figure 2.12: Mapping of Transport Channel to Physical Channel.

In downlink, the Downlink Shared Channel (DL-SCH) and the Paging Channel (PCH) are mapped to the Physical Downlink Shared Channel (PDSCH). The Broadcast Channel (BCH) maps to both the PDSCH and the Physical Broadcast Channel (PBCH).

In uplink, the Uplink Shared Channel (UL-SCH) is mapped to PUSCH and the Random Access Channel (RACH) is mapped to the Physical Access Channel (PRACH) [24].

2.7. Life of LTE UE

Figure 2.13: LIFE of a UE.

Let us review the life of an UE as it powers on, looks for the LTE network, registers with the selected network, and exchange data with the network. This cycle is represented in Figure 2.13. Each of these phases is detailed in the following:

1. When the UE is powered up, it uses programmed information or the most recently used network information to decide which frequency to use to start looking for an LTE network. After tuning its receiver to that frequency, the UE searches for LTE cell transmission on that frequency.
2. Once the UE finds LTE cell transmission, it starts listening to the system information that is broadcast in that cell. During this time, the UE is in "Idle" mode where it just listens to the system.
3. After the UE learns the LTE system information including system access parameters, the UE tries to access the network using random access channel procedures. Since multiple UEs may try to access the network at the same time using the same resources, collisions may occur. So random access procedures are defined to minimize and resolve collisions.
4. Typically, the UE now registers its presence with the network. The network authenticates the UE and allocates an IP address. Finally the network may allocate radio resources to the UE to enable efficient user traffic exchange.

Let us walk through each step in detail according to [1].

2.7.1. Step 1: System acquisition

We will examine the system acquisition procedure in detail. The UE will first retrieve configured information about the frequency band (for example 2.1 GHz) and channel frequency to start searching for an LTE system.

The UE now needs to figure out how wide is the bandwidth of LTE system it has found. LTE is defined to be scalable. It supports various channel bandwidths ranging from 1.25 MHz to 20 MHz. At this stage, in the system acquisition process, the UE may not know the channel bandwidth used by the system. To facilitate faster acquisition, LTE defines the initial acquisition procedure based on the smallest channel bandwidth supported, which is 1.25 MHz.

After frequency-based acquisition, the UE needs to synchronize with the system. Once timing synchronization is achieved; the UE can obtain critical system information including the channel bandwidth used by the LTE system.

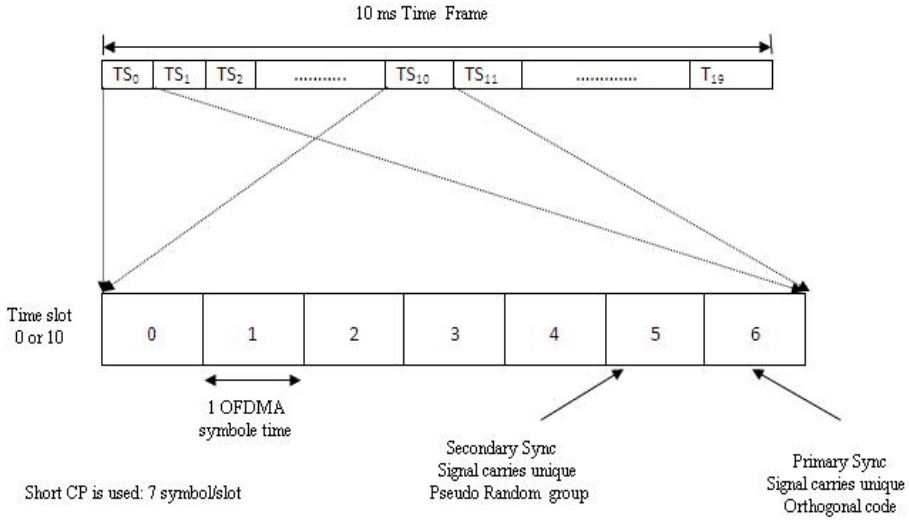

Figure 2.14: Timing Acquisition.

LTE defines a frame size of 10 ms. Each frame is subdivided into ten sub-frames of 1 ms duration. Each sub-frame is further subdivided into two half slots. In other words, each sub-frame consists of 20 slots. Each time slot contains 6 or 7 OFDMA symbols depending on the CP used. In Figure 2.14, the use of short CP is considered. When short CP is used, a slot carries 7 OFDMA symbols. LTE defines two physical layer reference signals to help UEs achieve time synchronization with the network. Both primary and secondary synchronization signals are transmitted on time slots 0 and 10 of every frame. Synchronization signals are transmitted only on the center (1.25 MHz) of the radio channel independent bandwidth.

The primary synchronization signal is always transmitted on the last OFDMA symbol duration of the time slot. The primary synchronization signal in each cell transmits one of three possible orthogonal sequences. The entire sequence is repeated in each time slot helping the UE to achieve slot level synchronization with the network.

The secondary synchronization signal is always transmitted on the second to last OFDMA symbol of time slots 0 and 10 of each frame. The secondary synchronization signal is made up of two binary sequences. When the UE acquires these sequences, it can reliably derive the start and the end of 10 ms frames, i.e. the UE achieves frames synchronization with the help of the secondary

synchronization signals. LTE systems use one of 170 possible sequences on the secondary synchronization signal. There are 510 possible combinations using three different sequences in primary sync signal and 170 possible sequences in secondary sync signal. This allows the UE to uniquely identify a cell in a given area.

2.7.2. Step 2. Idle mode

LTE systems broadcast critical system information such as LTE channel bandwidth using the Physical Broadcast Channel. This helps UEs during the acquisition stage. After acquiring critical system information, the UE moves on to listen to the PDSCH. The idle mode is represented in the following figure.

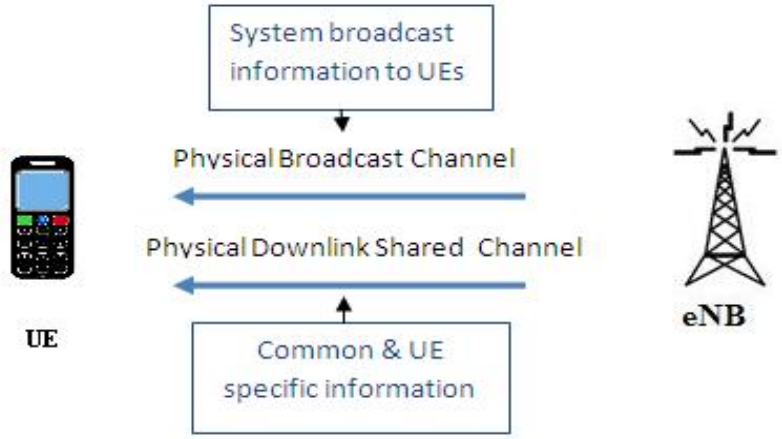

Figure 2.15: Idle Mode.

2.7.3. Step 3. Access procedure

The UE is now ready to register its presence with the network. Since the UE has just now required the LTE cell, the system has no idea of the UE's existence. So, the UE has to access the network through common resources for the purpose of initial access. Since multiple UE may be trying to access the network at the same time, collisions may occur over the air. Another key factor is the transmit power used by the UE for initial access. Since the UE could be anywhere in a cell, its uplink access transmission is going to increase the interference levels on the uplink. To minimize the impact of high power level during access, the network configures UEs to start at lower power level.

The LTE approach to access channel transmission is similar to other wireless technologies such as UMTS. In the following figure, we put together the higher level view of the access procedure.

a. First, the UE sends a preamble. When the first preamble does not get a response, the UE increases the transmit power by the configured power step value and sends the preamble again. We note that each successive preamble transmission has a random back off component in addition to a fixed timeout value. This approach minimizes the chance of the same

two UEs colliding again and again. Uplink preambles are sent to the PRACH.

b. When the eNB receives the last preamble transmission properly, it will compare the symbol arrival time from each preamble with that of other UEs already receiving traffic on the Shared Channel. The eNB determines the timing adjustment this UE should make to avoid collisions on uplink transmission and sends that value as a timing adjustment value. The eNB also sends an uplink transmission allocation to the UE along with the timing adjustment. The eNB sends the timing adjustment and allocation information on the PDCCH.

c. The UE uses the uplink allocation received to send its first message to the eNB. This message is sent on the PUSCH.

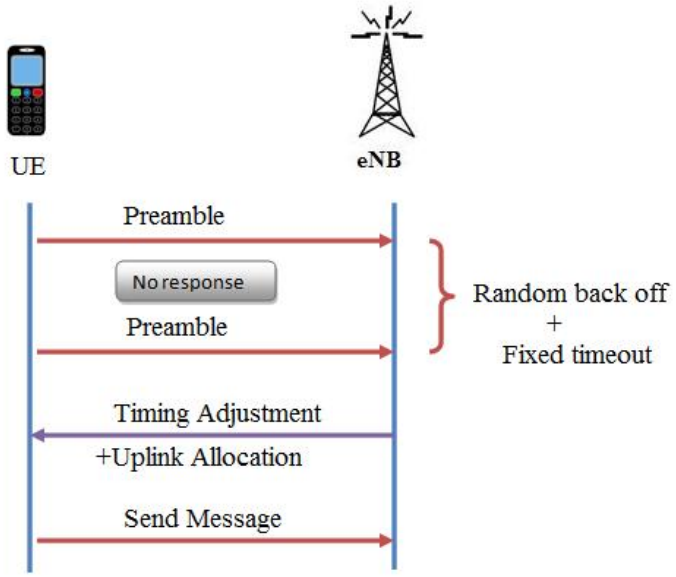

Figure 2.16: Access procedure message flow.

2.7.4. Step 4. Registration and traffic

The registration procedure starts with the UE sending an Attach message to the MME, where the UE requests to register with LTE network. The MME initiates the authentication procedure with the UE. When the authentication is successfully completed, the security mode is enabled to protect the information sent over the air. The MME selects the PDN-G to setup a default bearer between the S-GW and the P-GW. The P-GW eventually allocates an IP address for the UE. The UE can initiate packet data services using this default IP address (e.g., email). A default radio bearer and default S1 and S5 bearers are then set up. Now, the UE may trigger a request for other specific bearers or use the default bearer for IP services.

This completes the description of the high level service setup sequence. These steps are repeated for every new service instance.

2.7.5. Quality of Service: QoS

LTE is designed to support various applications with a wide range of data rate, error rate and latency requirements. A user may run applications such as VoIP, web browsing and streaming on his UE. The applications require QoS support from the network. For example, VoIP is a constant data rate, low latency application; on the other hand ,web browsing is bursty in nature but can tolerate delays better than VoIP applications. Streaming is somewhere in between; it needs higher data rates and low latency but can tolerate errors to a certain extent.

- **End-to-end bearer**

Let's look at how QoS of different services may be delivered in LTE network. From an application perspective, QoS can be supported by allocating resources to transport packets from a UE to application server and back. In LTE system, an end-to-end bearer is defined using two components. First is the EPS bearer which is defined between the UE and PDN-G. Second is the external bearer which is defined between the PDN-G and the external application server. For example, a VoIP application is setup between the UE and a VoIP server. For a streaming video application, when it is setup, QoS needs are understood and an LTE bearer is configured to meet the data rate, latency and error rate requirements. However, LTE does not control the external bearer setup. IP based QoS mechanisms including Service Level Agreements (SLA) will be used to setup QoS on the external. Similarly for each application, an EPS bearer and an external one will be constructed.

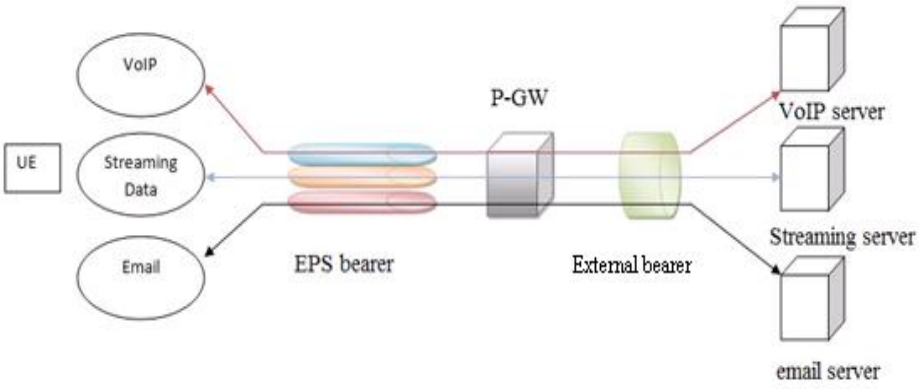

Figure 2.17: Bearers.

- **QoS functional elements**

There are two aspects of enforcing QoS in LTE. The first occurs during the service setup, LTE defines Allocation and Retention Priority (ARP) which is used to

enforce relative priorities between users and preemption decisions. The second aspect is to enforce QoS on individual traffic packets after service setup is completed. When the UE requests a service with certain QoS requirements, these requirements are eventually handed down to the PDN-G by the PCRF. The PDN-G then communicates with admission control at the MME/S-GW. Admission control at MME then verifies the subscriber profile and may change targeted QoS for the service. This updated QoS requirement is then forwarded to the admission control function at eNodeB. Now the eNodeB verifies its resources availability and load levels to see if the new requirements will be supporting by setting a new radio bearer. If yes, then the eNodeB will configure the new radio bearer to inform the UE. It will also trigger the schedulers to include the new radio bearer in scheduling computations. Finally the supported QoS information makes its way back to the PDN-G so that all the nodes are in sync with the QoS to be supported for this service (Figure 2.18).

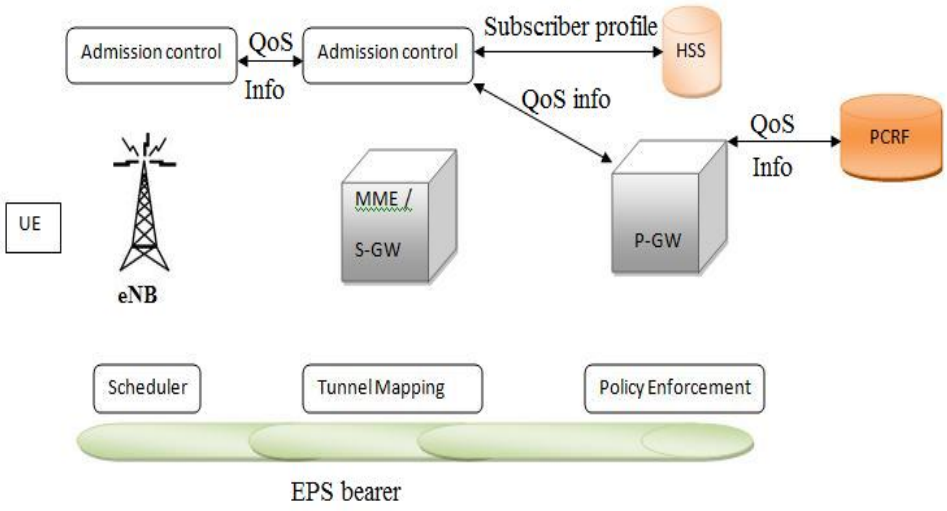

Figure 2.18: Admission control.

- **QoS enforcement**

Once the service is setup, traffic packets are processed at each node based on the allocated QoS. Traffic Characteristics are defined using error rate, latency and data rate requirements, as can be seen in Figure 2.19. From data rate perspective, LTE supports two types of bearers, Guaranteed Bit Rate (GBR) and non Guaranteed Bit Rate (non GBR); GBR is typically used for services with a known data rate requirements and more stringent latency requirements. The eNodeB scheduler logically reserves the resources for GBR bearer services. GBR is defined by two attributes, a Guaranteed Bit Rate and Maximum Bit Rate (MBR), traffic shaping will drop packets for data rates above the MBR values.

For non-GBR bearers, the network defines a single attribute called the Aggregate Maximum Bit Rate (AMBR). AMBR is the maximum bit rate for all non-GBR services within a single UE. The network may allocate traffic resources up to

the AMBR at any time. However, traffic mix within the AMBR limit is defined by relative priority between services and other factors.

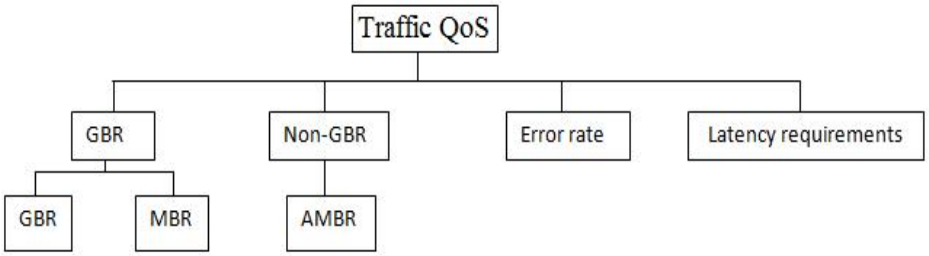

Figure 2.19: Traffic QoS.

- **SAE bearer**

An UE requests a service within certain QoS requirements; this may be trigged by the Policy Charging Rule Function (PCRF) indicating QoS needs to the PDN-G. The PDN gateway sets up a GTP tunnel between the PDN-G and the S-GW. This is called the S5 access bearer. Now, the admission control entity at the Gateway decides on the resources to be allocated for the services and sets up a GTP tunnel between the S-GW and the eNodeB. This is called the S1 access bearer. The admission control at eNodeB decides on the processing techniques and allocates the radio resource blocks to the UE for a particular service (Figure 2.20).

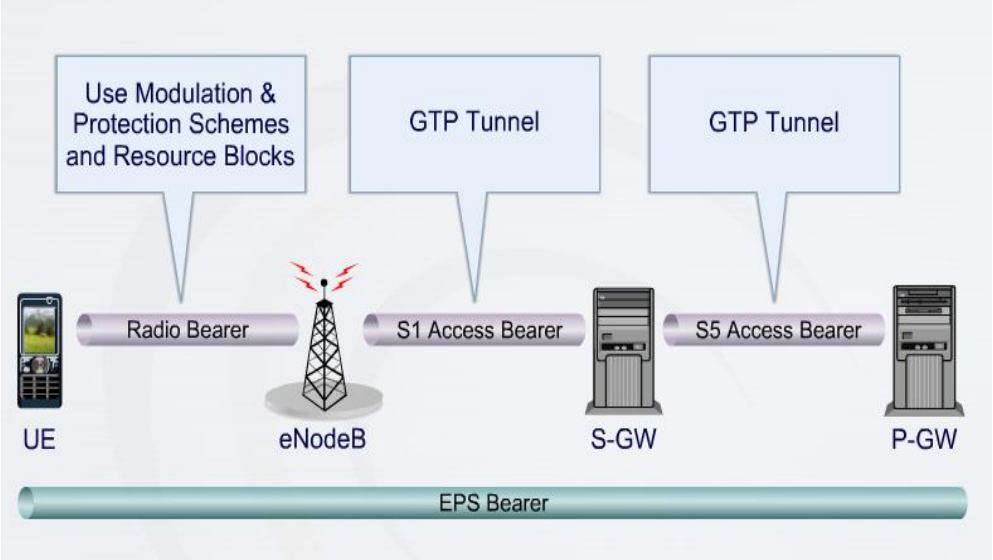

Figure 2.20: SAE bearer.

2.8. LTE Traffic handling

There are different handling procedures for DL and UL traffic.

2.8.1. DL traffic handling

When receiving packets from the video streaming server, the user's data arrives at eNodeB after traversing through the LTE Core network then it needs to be transmitted over the air. In this paragraph we describe the traffic handling process in LTE systems. In DL, traffic handling may be viewed as a four step process. The steps are presented in the following.

1. When a UE is assigned to LTE shared channels for exchanging data traffic, it is required to send a Channel Quality Indicator (CQI) report on a periodic basis. The UE measures the channel quality and reports the CQI using PUCCH.
2. The eNodeB has a scheduler responsible for allocating downlink radio resources to the UE. The Downlink Scheduler uses CQI reports as input along with other information such as the current buffer status for each UE and recent allocation history. It makes a decision as to which set of UE gets downlink resources at this time. The Scheduler also decides how much of the radio resources are allocated to each UE.
3. a. Allocation Information. When the downlink Scheduler makes resource allocation decisions, the eNodeB will use these resources to transmit traffic to those UEs. But all the UEs reported CQI values and so all of them are expecting traffic from the network! The eNodeB needs to ensure that the selected UEs understand their allocation of resources and receiving data. The eNodeB does this by sending the allocation information during the initial symbols of the allocation period followed by user traffic. Allocation information is sent to Physical Downlink Control CHannel (PDCCH).
   b. High Speed data Transmission. The eNodeB transmits traffic to the selected UEs on the PDSCH. Each user may receive different amounts of traffic based on their individual allocation.
4. ACK/NACK. When a UE receives its transmission, it will verify the checksum of the packet. If verification is successful, the UE sends a positive ACKnowledgement (ACK) for the packet. If not, the UE sends a Negative ACKnowledgment (NACK). The ACK/NACK is transmitted on PUCCH.

2.8.2. Uplink Traffic Handling

There are five basic steps involved in the process for the LTE user to transmit uplink data. These steps are presented in the following.

1. Uplink (UL) resources are also managed by the eNodeB. Each UE sends a scheduling request and Buffer Status Report (BSR) to inform the eNodeB of its current bandwidth needs.
2. The eNodeB gathers UL scheduling requests and BSRs from all of the UEs. The UL Scheduler then looks at all the requests, recent allocation history;

3. current UL load conditions and decides on the set of the UEs that would receive allocation at this time.
4. The UE performs data selection for UL transmission using current allocation from the eNodeB data in the buffer and UE capabilities.
5. Next, the UE forms the data packet for transmission. The UE transmits the data packet over the air based on identified transmission characteristics on the PUSCH. The UE also transmits associated control information as needed on the PUCCH.
6. The eNodeB send either an ACK or a NACK for the data it receives from the UE.

2.9. LTE Mobility

In LTE, an UE could be in one of two mobility states, idle and active. A UE is said to be in the idle mode when the UE is not actively exchanging traffic. A UE is said to be in active mode when it is actively exchanging traffic.

When a UE is in idle mode, it executes one of three mobility related procedures: cell selection, cell reselection, and Tracking Area (TA) update. In the active mode, LTE needs to support two possibilities. One is the case where a UE moves from one cell to another cell with no change in MME (i.e, intra-MME mobility). The second case is when a UE move to a cell that requires a change in MEE (i.e, inter-MME mobility). We explain the scenarios for both idle and active modes in this paragraph.

2.9.1. Idle Mode Mobility

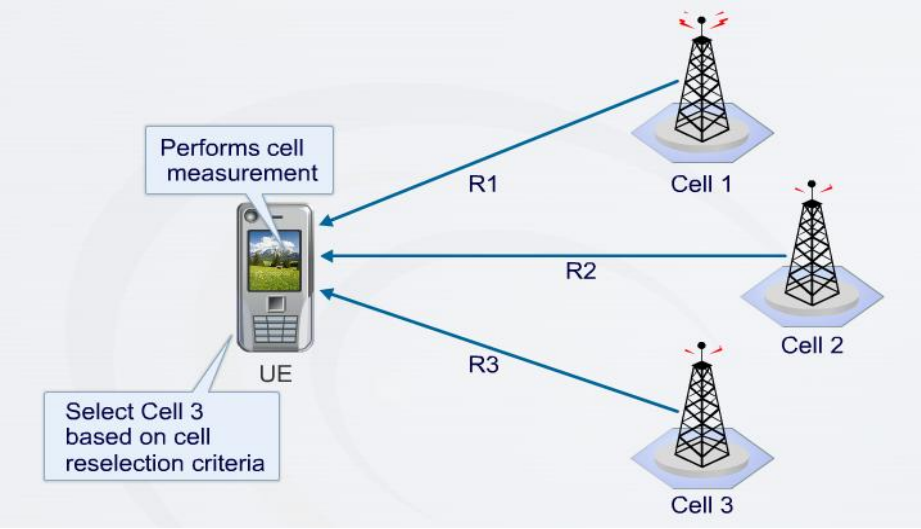

Figure 2.21: Cell reselection.

When the UE is first powered up, the UE decides, based on stored information, with which technology band and frequency it should start. If the UE is configured to look for an LTE network, it tries to acquire an LTE cell. The UE acquires an LTE cell by scanning for LTE reference signals. The UE then verifies that the network it has acquired is one of the valid networks per its configuration. The UE then receives system broadcast information which includes cell selection/reselection criteria and neighbor cell information. Cell reselection is the procedure to address UE mobility across cells when no active traffic exchange is taking place between the UE and the network. An example of cell reselection is given in Figure 2.21.

Cell reselection is controlled by the network through configuration data sent on System Information Blocks (SIBs). In idle state, the UE measures the signal quality of the neighbor cells. The type of measurement and the criteria to decide when to move to another cell is sent by the network as part of system information blocks. In Figure 2.21, Cell 1 has sent information about neighboring cells (e.g. cell 2 and cell 3) and cell reselection criteria. The UE measures the reference signals from cells 1, 2 and 3 on a periodic basis as configured. Let us assume that cell 3 meets the reselection criteria. Now the UE will start camping on cell 3.

The network needs to know the location of the UE to page it. LTE tracks the UE by requiring it to register its location with the network. If the UE is asked to update its location whenever it changes its cell, it may result in a lot of UL signaling just for the location updates. To minimize the location update and keep paging effective, we can track a UE at a higher granularity. For example, instead of tracking a UE at the cell level, we could track at larger area covered by group of cells.

LTE defines Tracking Areas (TAs) for location tracking. A tracking area is a group of cells. Each cell will broadcast the Tracking Area that it supports. If a UE moves from a cell in one TA to a cell in a different TA, then the UE will execute the tracking area update procedure. When data arrives for a UE at the S-GW, the UE will be paged on the last TA per its last TA update procedure.

2.9.2. Active Mode Mobility

In LTE Active Mode Mobility, when a UE moves between two LTE cells, "backward" handover or predictive handover is carried out.

2.9.3. Intra-MME/S-GW mobility

Let us suppose that the UE is currently located in cell C1 and has established the radio S1 and S5 bearers as shown in Figure 2.22.

As the UE moves from Cell C1 in direction of cell C2, the UE measures the neighboring cell C2's reference signal. When cell C2's reference signal quality meets the trigger criteria for a handover from cell C1, the handover procedure is initiated. In this scenario, we are assuming that cells C1 and C2 are both connected to the same S-GW.

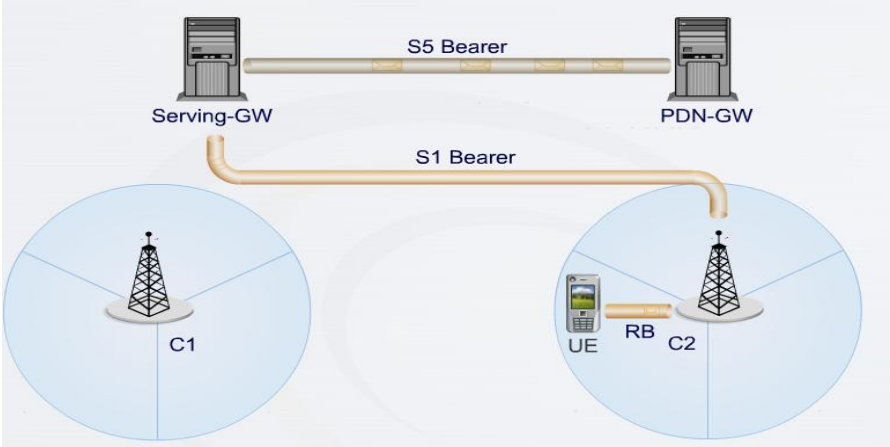

Figure 2.22: Intra-MME/S-GW mobility.

2.9.4. Handover overview

In LTE, the handover procedure goes through three distinct steps:

1. Handover preparation: the UE does handover measurements, detects a handover trigger condition and reports to the network. One the decision to proceed with the handover is made by the current serving cell and target cell will exchange information and set up necessary resources. Finally the serving cell will inform the UE of the decision to proceed with handover and convey the radio resource information.
2. Handover execution: the current cell starts forwarding data from its buffers to the target cell. At this time data is still forwarded to the original serving cell by the serving gateway. The UE acquires the new cell and conveys its presence. The radio bearer is established at the target cell.
3. Handover completion: the target cell sends a handover indication to the MME and the S-GW path switching is executed. Now the S-GW starts forwarding traffic to the new serving cell. A handover success notification is sent to the old serving cell to complete a successful handover.

2.10. Summary

As a conclusion, LTE introduces important changes in comparison with previous network technologies in three major areas:

1. Air interface: LTE uses OFDMA in the DL and SCFDMA in the UL along with MIMO techniques, allowing LTE air interface to support high data rates.

2. Radio network: LTE converts the radio network into an IP based distributed network; as a result, IP-based backhaul networks will reduce the backhaul cost.

3. Core network: LTE is based on full IP packet instead of separate Circuit Switched (CS) and Packet Switched (PS) core networks, which provide stability and reduce cost.

CHAPTER 3

Multiple Access Schemes in LTE

3.1. Introduction

Wireless digital communication is rapidly expanding, resulting in a growing demand for systems that are reliable and have a high spectral efficiency. The demand for higher data rate is leading to utilization of wider bandwidth, resulting severe frequency selectivity of the channel and thus the problem of Inter Symbol Interference (ISI) becomes more serious. In a conventional single carrier communication system, time equalization in the form of tap delay line filtering is performed to eliminate ISI. However, in case of wide band channel, the length of the impulse response of the filter used to perform equalization becomes prohibitively large, since it linearly increases with the channel response length.

One way to mitigate the frequency-selective fading, encountered in a wide band channel, is to use a multicarrier technique, which subdivides the entire bandwidth of the channel into smaller subbands, around each subcarrier. Orthogonal frequency division multiplexing (OFDM) is a multicarrier modulation technique which uses orthogonal subcarriers to transmit information. In the frequency domain, since the bandwidth of a subcarrier is designed to be smaller than the coherence bandwidth of the channel, each sub-channel is seen as a flat fading channel which simplifies the equalization process. In the time domain, by splitting a high-rate data stream into a number of lower-rate data streams, that are transmitted in parallel, the OFDM resolves the problem of ISI in wide band communications [26]. But OFDM has its limitations: high Peak-to-Average-Power Ratio (PAPR), high sensitivity to frequency offset, and a need for an adaptive or coded scheme to overcome spectral nulls in the channel [27], [28].

As we noticed in chapter 2, Orthogonal Frequency Multiple Access (OFDMA) technique is used in the downlink of 3GPP LTE, and Single Carrier Frequency Division Multiple Access (SC-FDMA) technique, a newly developed multiple access scheme, is adopted in the uplink of 3GPP LTE. In this chapter, we give an overview of these multiple access schemes and show some research results on their Bit Error Rates (BER) and PAPR characteristics.

3.2. Concepts of OFDMA

OFDMA allows the base station to communicate with several mobile stations at the same time. According to [2], OFDMA is the access multiplexing scheme for OFDM. The OFDMA herits all the properties of the OFDM and exhibits some new features. Multiplexing provides package of many user packets into one frame. As a result, multiplexing becomes very efficient in the sense that overheads caused by inter frame spacing is minimized. Let us overview the principles of OFDM.

In the following subsections are revisited some of the most important principles of OFDM.

3.2.1. Principles of OFDM

3.2.1.1. Evolution to OFDM

OFDM is an appealing technology used for high-speed data communication systems [1]. Its concept is based on spreading the high speed data to be transmitted over a large number of low rate carriers. The carriers are orthogonal to each other and frequency spacing between them are created by using the Fast Fourier Transform (FFT), which is an efficient implementation of Discrete Fourier Transform (DFT). OFDM evolved from two important techniques, frequency division Multiplexing (FDM) and multicarrier communication. The FDM technique divides the available bandwidth into many non overlapping subbands and allows multiples users to access a system simultaneously (Figure 3.1).

Each user transmits its data on different subcarrier. To avoid interference, guard bands are assigned between subbands. Since any information is not transmitted into guard bands, they introduce spectrum inefficiency.

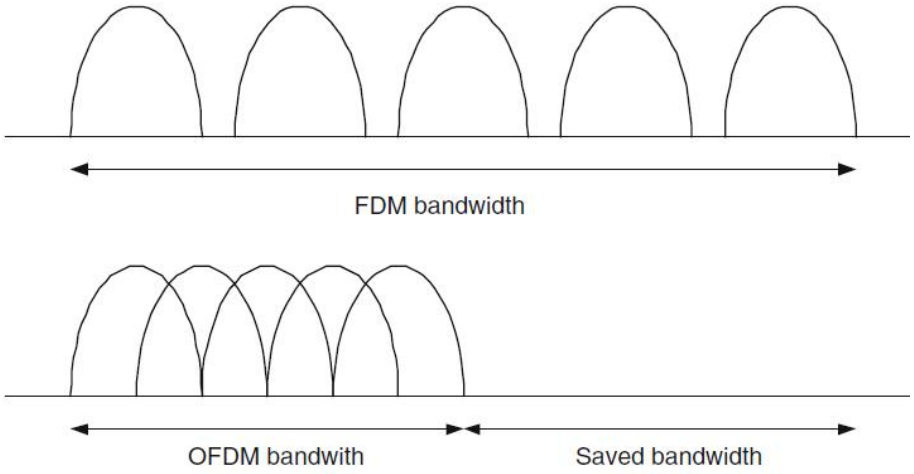

Figure 3.1: Comparison of OFDM and FDM.

With multicarrier communication, an user can split the data into multiple sub-streams and transmit them in parallel. In multicarrier FDM, the user data is converted from serial to parallel. The parallel data sub-streams are sent over multiple subcarriers. At the receivers, the parallel data is combined back into serial data stream. A higher data rate can be achieved by multicarrier communication [1].

OFDM adds the orthogonal feature into multicarrier FDM. The subcarriers are designed to be orthogonal. Orthogonality means no interference. This allows subbands to overlap and saves bandwidth. Therefore, OFDM obtains both higher data rates and good spectrum efficiency. The history of OFDM is presented in Table 3.1.

1957: Kineplex, multicarrier HF modem;
1966: Chang, Bell Labs: OFDM paper and US patent 3488445;
1971: Weinstein and Ebert proposed the use of FFT and guard interval

1985: Cimini described the use of OFDM for mobile communications;
1985: Telebit Trailblazer Modem incorporates a 512-carrier Packet Ensemble Protocol;
1987: Alard and Lasalle: Coded OFDM for digital broadcasting;
88: TH-CSF LER, first experimental Digital TV link in OFDM, Paris area;
1989: OFDM international patent application PCT/FR 89/00546, filed in the name of THOMSON-CSF, Fouche, de Couasnon, Travert, Monnier and others;
1990: TH-CSF LER, first OFDM equipment field test, 34 Mbps in a 8-MHz channel, experiments in Paris area;
1990: TH-CSF LER, first OFDM test bed comparison with VSB in Princeton, USA;
1992: TH-CSF LER, second generation equipment field test, 70 Mbit/s in a 8-MHz channel,twin polarizations. Wuppertal, Germany;
1992: TH-CSF LER, second generation field test and test bed with BBC, near London, UK;
1993: TH-CSF show in Montreux SW, 4 TV channel and one HDTV channel in a single 8-MHz Channel;
1993: Morris: Experimental 150 Mbit/s OFDM wireless LAN;
1994: US patent 5282222, method and apparatus for multiple access between transceivers in wireless communications using OFDM spread spectrum;
1995: ETSI Digital Audio Broadcasting standard EUreka: First OFDM-based standard;
1997: ETSI DVB-T standard;
1998: Magic WAND project demonstrates OFDM modems for wireless LAN;
1999: IEEE 802.11a wireless LAN standard (Wi-Fi);
2000: Proprietary fixed wireless access (V-OFDM, Flash-OFDM, etc.);
2002: IEEE 802.11g standard for wireless LAN;
2004: IEEE 802.16-2004 standard for wireless MAN (WiMAX);
2004: ETSI DVB-H standard;
2004: Candidate for IEEE 802.15.3a standard for wireless PAN (MB-OFDM);
2004: Candidate for IEEE 802.11n standard for next-generation wireless LAN;
2005: OFDMA is candidate for the 3GPP Long Term Evolution (LTE) air interface E-UTRA Downlink;
2007: The first complete LTE air interface implementation was demonstrated, including OFDM-MIMO, SC-FDMA and multi-user MIMO uplink.

Table 3.1: OFDM history [2]

3.2.1.2. A simple OFDM System

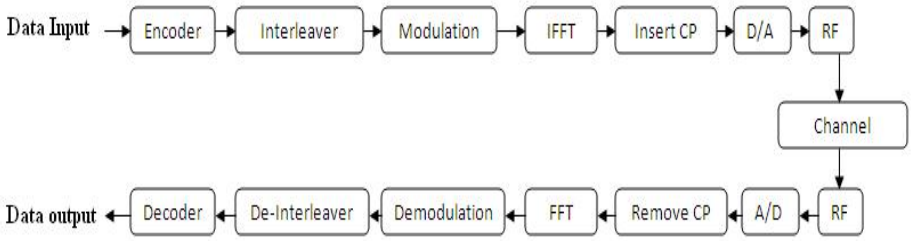

Figure 3.2: A simple OFDM system.

Coding can help a receiver to detect errors and correct some of them. An encoder is used to minimize the error probability of the receiver. It adds redundant nformation into the data stream and transforms the data stream into a new sequence.

Typically, when errors occur in a radio channel, they are not limited to single bit loss. Sudden drops in the received signal, known as fading, result in a series of consecutive bits being lost. This is called burst error, which is more difficult to detect and correct than a single error. Interleaving is usually used to provide protection against burst errors. It is the process of reordering a bit stream. After de-interleaving, the errors are no longer consecutive and became easier to correct. The effect of bit separation provided by interleaving improves the performance of error correcting at the receiver. The coded data comes out of the encoder and is interleaved. The interleaver rearranges the order of bit streams and the de-interleaver at the receiver separates burst errors that occurred in the radio channel. Since the bit errors are no longer consecutive at the input of the decoder at the receiver, the decoder will be more successful in recovering the bit errors.

Modulation is the process of representing data bits with symbols. A constellation diagram is widely used to represent different digital modulation schemes. The points in the constellation diagram represent different symbols. Modulation is divided into two steps. First, data stream is divided into blocks. Data bits in each block are mapped into a constellation diagram (digital modulation). Second, the symbols from the constellation diagram are modulated onto allocated data subcarriers for transmission (OFDM). The most frequently used digital modulation schemes in OFDM systems are Quadrature Phase Shift Keying (QPSK) modulation and Quadrature Amplitude Modulation (QAM) and the subcarrier can be expressed as:

$$\phi_k(t) = e^{j2\pi f_k t} \tag{3.1}$$

where f_k is the frequency of the kth subcarrier. One baseband OFDM symbol is a sum of multiple orthogonal carriers, modulated by the complex data symbols Xk, to be transmitted through the channel:

$$s(t) = \frac{1}{\sqrt{N}}\left(\sum_{k=0}^{N-1} X_k e^{j2\pi f_k t}\right), \qquad 0 \le t \le T \tag{3.2}$$

where T is the length of the OFDM symbol, $j = \sqrt{-1}$. If the digital symbols to be transmitted, X_k, came from different users, then OFDM transforms into OFDMA. This requires perfect synchronization of the system, but brings an additional dimension of multiple accesses too. Thus, apart from the time division multiple access (all the carriers that compose different OFDM symbols may be dedicated to different users, on a symbol-by-symbol basis), a frequency division multiple access may be achieved. This means that, for the duration of a single OFDM symbol, the carriers may be shared by different users, according to the scheduling made by the Media Access Control (MAC) layer. Most of the OFDM/OFDMA practical implementations are based on the computation of the Inverse Fast Fourier Transform (IFFT) in the modulator and of the direct transform in the demodulator. This allows simple, signal-processing based implementation of the multi-carrier modulation, eliminating the need for expensive oscillators required to generate the orthogonal carriers. The IFFT converts the information on subcarriers into time domain signal.

Inter Carrier Interference (ICI) occurs due to a Doppler frequency shift, produced by users' mobility, that results in the loss of subcarriers orthogonality. Inter Symbols Interference (ISI) occurs as a consequence of multipath propagation of the electromagnetic wave which carries the OFDM signal. To overcome these problems, OFDM systems use Cyclic Prefix (CP). With the aid of CP, the convolution of the OFDM signal with the channel's impulse response, which express the noiseless component at the input of the receiver transforms into a circular convolution (which is specific for periodical signals). Extending OFDM symbols into periodical symbols can help the spectral analysis at the receiver maintain the orthogonality of subcarriers. This means that redundant information is sent out to make sure that analysis can be conducted on the undistorted information. This is also called cyclic extension [29]. It is implemented by copying a portion of the original symbol from the end and attaching it in the front or copying the front and attaching it to the end as it can be seen in Figure 3.3.

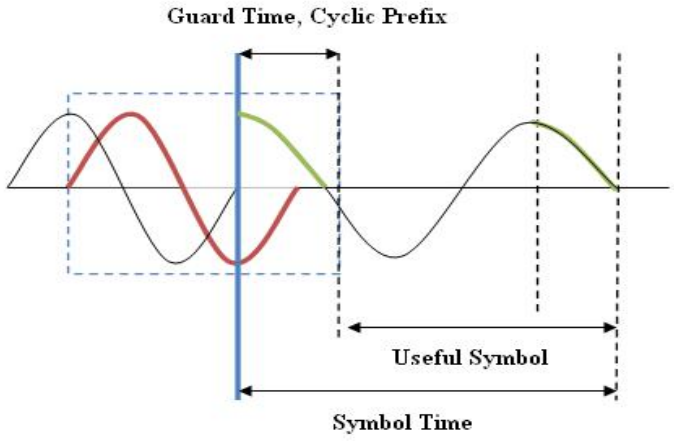

Figure 3.3: Cyclic Prefix [30].

With cyclic prefix, the delayed version of a previous symbol cannot shift onto the current symbol, so ISI is eliminated. Also, CP provides redundant information and allows spectral analysis in the receiver to maintain the orthogonality of subcarriers. Therefore ICI is overcome.

If a CP is used in the guard period between successive blocks of duration τ, the constructed OFDM symbol over a period can be written as:

$$s(t) = \frac{1}{\sqrt{N}}\left(\sum_{k=0}^{N-1} X_k e^{jk2\pi f_k t}\right), \qquad -\tau \le t \le T \tag{3.3}$$

To avoid the ISI, the length of the time interval denoted by τ must be bigger than channel impulse response length τ_h. The CP requires more transmit energy and reduces the bit rate to $(Nb/(T+\tau))$, where b is the number of bits that can be transmitted by a subcarrier [2].

After CP addition, the signal passes the Digital to Analog (D/A) conversion block, where the digital signal is converted into analog signal. Then the spectrum of the analog signal is translated into a high frequency band and sent over the air by the Radio Frequency (RF) block. D/A conversion is performed by electronic

circuits.At the far end of the communication channel, the noiseless component of the received signal becomes:

$$y(t) = s(t) * h(t) = \frac{1}{\sqrt{N}} \sum_{k=0}^{N-1} H_k X_k \phi_k(t), \qquad 0 < t < T \tag{3.4}$$

where:

$$H_k = \int_0^{\tau_h} h(t) e^{j2\pi f_k t} dt \tag{3.5}$$

Hence, the kth subcarrier, has now a channel component Hk, which is the Fourier transform of h(t) at the frequency fk..
The OFDM symbol is next sampled (tk=kT/N) in the receiver and demodulated with FFT. Consequently, the received data has the following form:

$$y_k = H_k X_k \ , \qquad k=0,\ldots, N-1. \tag{3.6}$$

The received actual data can be rearranged back into a serial data stream. Next, the serial data stream passes the De-interleaver and finally the decoding function is performed.

Also note that the spectrum of OFDM subcarriers decays slowly. This causes spectrum leakage to neighboring bands. Pulse shaping is used to change the spectral shape by either commonly used raised cosine time window or passing through a filter. An OFDM system design considers setting the guard interval (τ) as well as the symbol time (T) and FFT size with respect to desired bit rate B and given tolerable delay spread of paths composing the communication channel [1].

3.2.2 OFDMA Implementation in 3GPP LTE Downlink

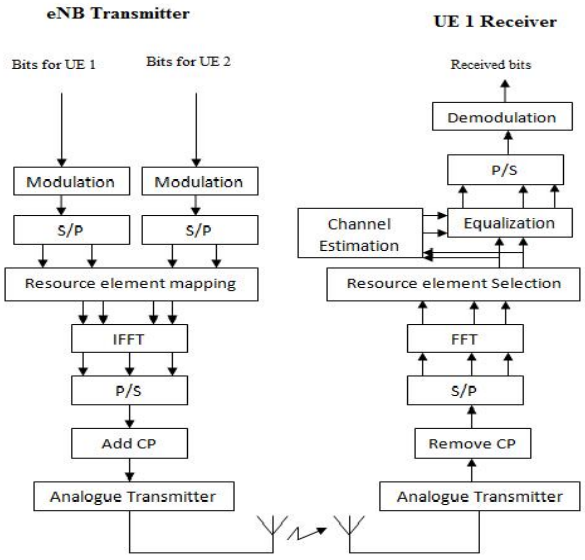

Figure 3.4: OFDMA system.

OFDMA is used in LTE downlink when the transmitter is the eNB and the receiver is the UE (Figure 3.4). According to the standard [31], the supported modulation schemes are QPSK, 16QAM, and 64QAM. Scrambling and interleaving are also supported. For channel coding, both Tail biting Convolutional coding and Turbo coding are used.

Downlink physical channels are implemented by OFDMA which is controlled from higher protocol layers. Resource blocks from physical protocol layer are allocated to users by the scheduler, which is located on a higher protocol layer. In Figure 3.5 is presented a downlink resource block, which represents the smallest element of resource allocation. LTE frames are 10 ms in duration and they are divided into 10 sub-frames where each sub-frame is further divided into two slots, each one of 0.5-ms duration. Slots consist of either 6 or 7 OFDM symbols, as can be seen in Figure 3.6, depending on whether the normal or extended cyclic prefix is used. Longer cyclic prefix is desired to address longer fading that can be encountered in multi-cell broadcast service or very large cell deployments.

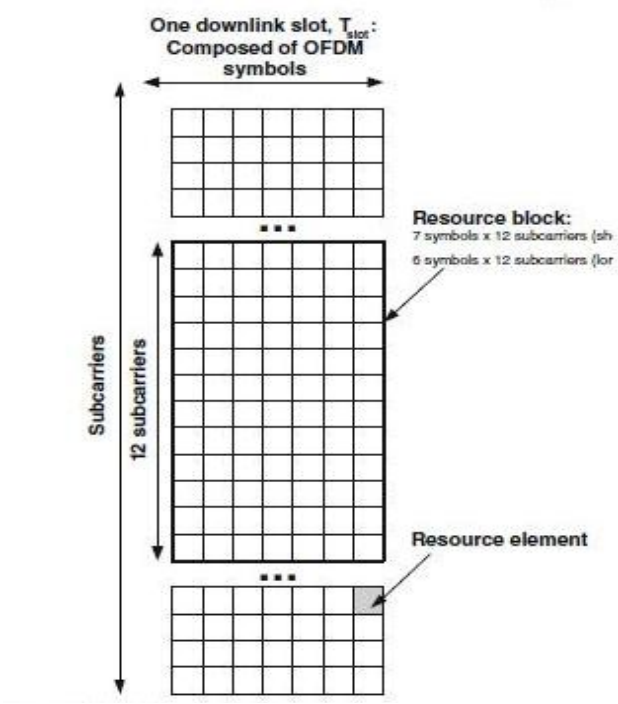

Figure 3.5: Downlink resource block [2].

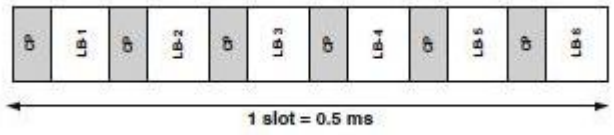

Figure 3.6: Slot structure for 3GPP LTE FDD Downlink.

Parameters for OFDMA downlink are shown in Table 2 for system bandwidth ranging from 1.25 MHz to 20MHz. The number of available subcarriers changes depending on the transmission bandwidth; however, OFDM downlink transmission scheme uses fixed subcarrier spacing regardless of transmission bandwidth. Pilot symbols are used to estimate the channel impulse response Hk and for time and frequency synchronization. The orthogonal pilots sequence or a pseudo-random numerical sequence is used in order to avoid interference; a specific set out of 510 unique orthogonal sequences is assigned to each cell in order to distinguish it from others.

Bandwidth (MHz)	1.25	2.5	5	10	15	20
Sub-frame Duration (ms)	0.5	0.5	0.5	0.5	0.5	0.5
Subcarrier spacing (KHz)	15	15	15	15	15	15
Sampling Frequency (MHz)	1.92	3.84	7.68	15.36	23.04	30.72
Occupied subcarriers/FFT size	76/128	151/256	301/512	601/1024	901/1536	1200/2048
Long CP (s/samples)	16.67/32	16.67/64	16.67/128	16.67/256	16.67/384	16.67/512
Short CP	4.69/9	4.69/18	4.69/36	4.69/72	4.69/108	4.69/144
Resource block Bandwidth (KHz)	180	180	180	180	180	180
No of available RBs	6	12	25	50	75	100

Table 3.2: Parameters for the downlink transmission scheme for OFDMA [8].

3.2.3. Multiple Input Multiple Output OFDMA

LTE PHY can employ multiple transceivers at the base station in order to enhance robustness and data rate. The Multiple Input Multiple Output (MIMO) is supported either with single or multiple-users. The maximum number of code words is 2 regardless of the number of transmit antennas since there are at most two receive antennas. In addition, codebook based precoding with a single precoding feedback and rank adaptation with single rank feedback is supported as well. Typical gains with MIMO are listed in Table 3.3.

In Figure 3.7, it is presented an Alamouti-based 2×1 MIMO system. Downlink is considered as a double codeword system in which two parallel transmitters are used and combined at the later stage with a precoding matrix. OFDM mapper finally performs the modulation. Pilot signal are transmitted at spaced subcarriers and channel impulse estimates for subcarriers that do not bear a pilot are computed with interpolation. When a pilot is transmitted in one antenna, the other antennas are set to idle to maintain the orthogonality [2].

MIMO	1×1	1×2	2×2	2×4	4×2	4×4
Bps/Hz/sector	1.2	1.8	2.8	4.4	3.7	5.1

Table 3.3: OFDMA performance at 2.5 GHz with 10 MHz, TDD [4].

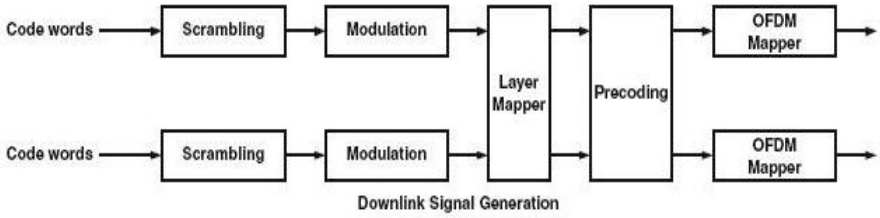

Figure 3.7: Downlink signal generation for MIMO 2×1 LTE [2].

3.3. Concepts of SC-FDMA

As already noticed, the uplink transmission in LTE is realized with SC-FDM.

3.3.1. Overview

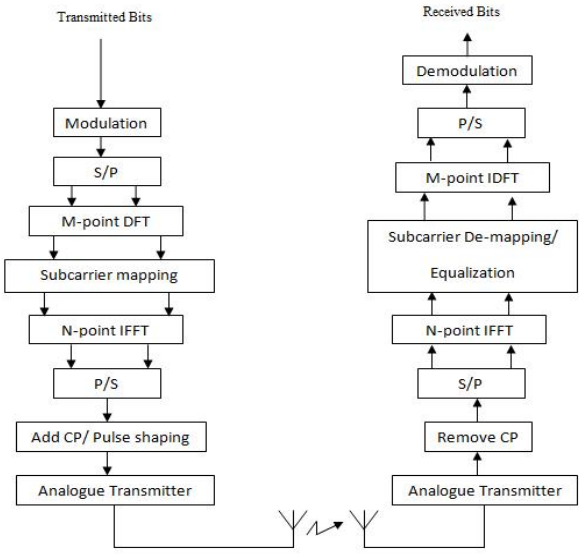

Figure 3.8: Transceiver structure of SC-FDMA [32].

Single carrier Frequency Division Multiple Access (SC-FDMA) systems utilize single carrier modulation and frequency domain equalization. SC-FDMA is a multiple access technique used in LTE Uplink. SC-FDMA is an extension of Single Carrier modulation with Frequency domain Equalization (SC-FDE) to accommodate multiple-users access [32]. The Peak-to-Average-Power Ratio (PAPR) in SC-FDMA, which is a typical problem in multiple access techniques, is lower than in OFDMA [33]. In the

following we give an overview of SC-FDMA signal processing chain. In Figure 3.8 is presented an SC-FDMA transceiver.

The input of the transmitter and the output of the receiver are complex modulation symbols. Practical systems dynamically adapt the modulation technique to the channel quality, using QPSK in weak channels and up to 64-level QAM in strong channels. The data block consists of *M* complex modulation symbols. The *M*-point Discrete Fourier transform (DFT) produces *M* frequency domain symbols that modulate *M* out of *N* orthogonal subcarriers spreaded over a bandwidth. Then, the SC-FDMA system can handle up to *Q* (*N/M*) orthogonal source signals with each source occupying a different set of *M* orthogonal subcarriers. Figure 3.9 shows the generation of SC-FDMA transmitted symbols.

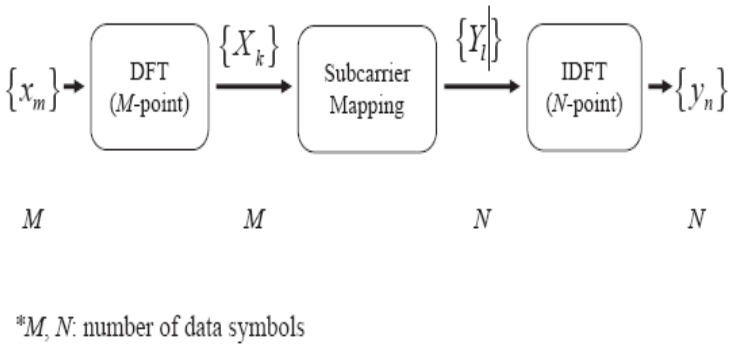

Figure 3.9: Generation of SC-FDMA transmitted symbols.

There are *N* subcarriers among which *M* subcarriers are occupied by the input data *(M < N)* where x_m *(m=0, 1, …, M-1)* represents modulated source symbols and X_k *(k=0, 1, …, M-1)* represent *M* samples of the DFT of x_m.. Y_l (*l*=0, 1, …, *N*-1) represent the frequency domain samples after subcarrier mapping and y_n (*n*=0, 1, …, *N*-1) represent the transmitted time domain channel symbols obtained from the inverse DFT (*IDFT*) of Y_l. The subcarrier mapping block assigns frequency domain modulation symbols to subcarriers. The parallel-to-serial converter places y_0, y_1, …, y_{n-1} in a time sequence suitable for modulating a radio frequency carrier and transmission to the receiver.

Let us prove, in the following, that the system in Figure 3.9 implements a SC transmission.

The signal obtained after DFT can be written as:

$$X_k = \sum_{m=0}^{M-1} x_m e^{-jk\frac{2\pi}{M}m}, \tag{3.7}$$

where $j = \sqrt{-1}$. Without restraining the generality, we can ignore for the moment the subcarrier mapping block. As in OFDMA, *N* point IDFT transforms the subcarriers amplitudes to a complex time domain signal:

$$y_n = \sum_{k=0}^{N-1} X_k e^{j\frac{2\pi}{N}nk}. \tag{3.8}$$

If we replace X_k by its value from equation (7), then we obtain the following equation:

$$y_n = \sum_{k=0}^{N-1}\left(\sum_{m=0}^{M-1} x_m e^{-j\frac{2\pi}{M}mk}\right)e^{j\frac{2\pi}{N}kn} = \sum_{m=0}^{M-1} x_m \sum_{k=0}^{N-1} e^{-j2\pi\left(\frac{m}{M}-\frac{n}{N}\right)k} \tag{3.9}$$

or:

$$y_m = \sum_{n=0}^{M-1} x_n \sum_{k=0}^{N-1} e^{-j2\pi k\left(\frac{n}{M}-\frac{m}{N}\right)} \tag{3.10}$$

But:

$$\sum_{k=0}^{N-1}\left(e^{-j2\pi\left(\frac{n}{M}-\frac{m}{N}\right)}\right)^k = \frac{1-\left(e^{-j2\pi\left(\frac{n}{M}-\frac{m}{N}\right)}\right)^N}{1-e^{-j2\pi\left(\frac{n}{M}-\frac{m}{N}\right)}} = \frac{\left(e^{-j2\pi\left(\frac{n}{M}-\frac{m}{N}\right)}\right)^{\frac{N}{2}}}{\left(e^{-j2\pi\left(\frac{n}{M}-\frac{m}{N}\right)}\right)^{\frac{1}{2}}}\cdot\frac{2j\sin\left(\pi N\left(\frac{n}{M}-\frac{m}{N}\right)\right)}{2j\sin\left(\pi\left(\frac{n}{M}-\frac{m}{N}\right)\right)} =$$

$$= e^{-j2\pi\left(\frac{n}{M}-\frac{m}{N}\right)\left(\frac{N-1}{2}\right)}\frac{\sin\left(\pi N\left(\frac{n}{M}-\frac{m}{N}\right)\right)}{\sin\left(\pi\left(\frac{n}{M}-\frac{m}{N}\right)\right)} = e^{-j\pi\left(\frac{n}{M}-\frac{m}{N}\right)(N-1)}p[n,m] \tag{3.11}$$

where:

$$p[n,m] = \frac{\sin\left[\pi\frac{N}{M}n-m\pi\right]}{\sin\left[\frac{\pi}{M}n-\frac{\pi}{N}m\right]}$$

So, it can be written:

$$y_m = \left(\sum_{n=0}^{M-1} x_n p[n,m]e^{-j\pi\frac{N-1}{M}n}\right)\cdot e^{j\pi m\frac{N-1}{N}} \tag{3.12}$$

This is a single carrier amplitude modulated signal with the carrier frequency of $\frac{N-1}{N}\pi$.

The transmitter in Figure 3.8 inserts the CP in order to provide a guard time to prevent ISI due to multipath propagation and also performs a linear filtering operation referred to as Pulse Shaping in order to reduce Out-Of-Band signal energy. One commonly used Pulse shaping filter is the raised-cosine filter [32].

The receiver removes the inserted cyclic prefix (CP) and transforms the received signal to the frequency domain via DFT in order to recover the subcarriers. The de-mapping operation isolates the *M* frequency domain samples of each source signal. The equalization is necessary to combat ISI because SC-FDMA uses single carrier modulation. The equalized symbols are transformed back into the time domain by IDFT and detection and decoding take place in the time domain.

From multiple user access perspective in the uplink (UL), the base station separates the users in the frequency domain during subcarrier de-mapping process, before performing the basic SC-FDMA (Figure 3.10).

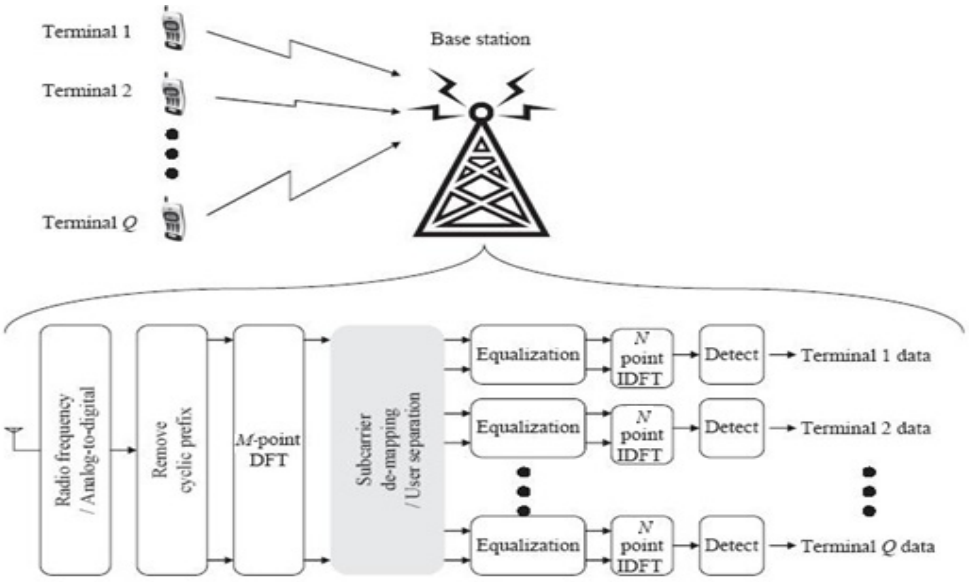

Figure 3.10: SC-FDMA receiver structure from a multiple user access perspective in the uplink [32].

SC-FDMA incorporates the signal processing elements of OFDMA and adds a DFT at the input of the transmitter and a corresponding IDFT at the output of the receiver.

3.3.2. Subcarrier Mapping

The subcarrier mapping in SC-FDMA can be performed by two methods: localized subcarrier mapping (referred to as LFDMA) and distributed subcarrier mapping (referred to as DFDMA). In the LFDMA mode, DFT outputs of the input data are allocated over consecutive subcarriers, whereas in the DFDMA mode, the DFT outputs of the input data are allocated over the entire bandwidth, zeros occupying the unused subcarriers (Figure 3.11). In both modes, the IDFT in the transmitter assigns zero amplitude to the N-M unoccupied subcarriers. The case of N= Q×M for the distributed mode with equidistance between occupied subcarriers is referred to as Interleaved FDMA (IFDMA) [34], [35]. In this case:

$$p[n,m]=\frac{sin\left(\pi N\left(\frac{n}{M}-\frac{m}{N}\right)\right)}{sin\left(\pi\left(\frac{n}{M}-\frac{m}{N}\right)\right)}=\frac{sin\left(\pi QM\left(\frac{n}{M}-\frac{m}{QM}\right)\right)}{sin\left(\pi\left(\frac{n}{M}-\frac{m}{QM}\right)\right)}=\frac{sin(\pi(Qn-m))}{sin\left(\pi\frac{Qn-m}{QM}\right)}=\delta[Qn-m] \quad (3.13)$$

and:

$$y_m = \left(\sum_{n=0}^{M-1} x_n \delta[Qn-m] e^{-j\pi \frac{N-1}{M} n} \right) \cdot e^{j\pi m \frac{N-1}{N}} = x_{\frac{m}{Q}} e^{-j\pi \frac{QM-1}{M} \frac{m}{Q} + j\pi m \frac{QM-1}{QM}} = x_{\frac{m}{Q}} e^{j\pi m \frac{QM-1-QM+1}{QM}} = x_{\frac{m}{Q}}. \quad (3.14)$$

So:

$$y_m = \begin{cases} x_{\frac{m}{Q}}, & \text{if} \quad m \vdots Q \\ 0, & \text{otherwise} \end{cases}, \quad (3.15)$$

operation which can be performed directly in time domain. Hence, IFDMA is a special case of SC-FDMA and it is very efficient in that the transmitter can modulate the signal strictly in the time domain without the use of DFT and IDFT.

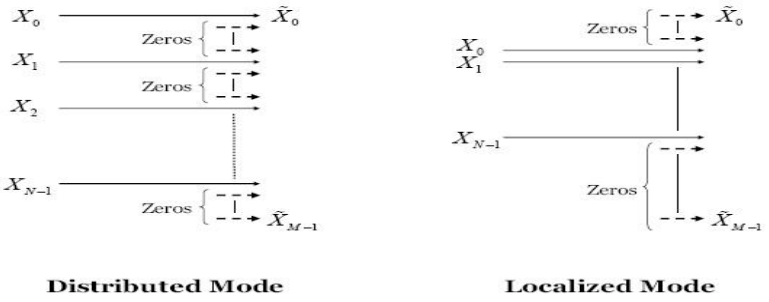

Figure 3.11: Subcarrier mapping modes; distributed and localized.

Figure 3.12 shows three examples of SC-FDMA transmit symbols in the frequency domain for *M*=4 symbols per block, *N*=12 subcarriers, and *Q*= *N/M*=3 terminals. In the LFDMA mode, the four modulation symbols occupy subcarriers 0, 1, 2, and 3*: $Y_0 = X_0$, $Y_1 = X_1$, $Y_2 = X_2$, $Y_3 = X_3$,* and $Y_i = 0$ *for* $i \neq 0, 1, 2, 3$. In the distributed mode with modulation symbols equally spaced over all the subcarriers, $Y_0 = X_0$, $Y_2 = X_1$, $Y_4 = X_2$, $Y_6 = X_3$, and in the interleaved mode, Y0 = X_0, $Y_3 = X_1$, $Y_6 = X_2$, $Y_9 = X_3$.

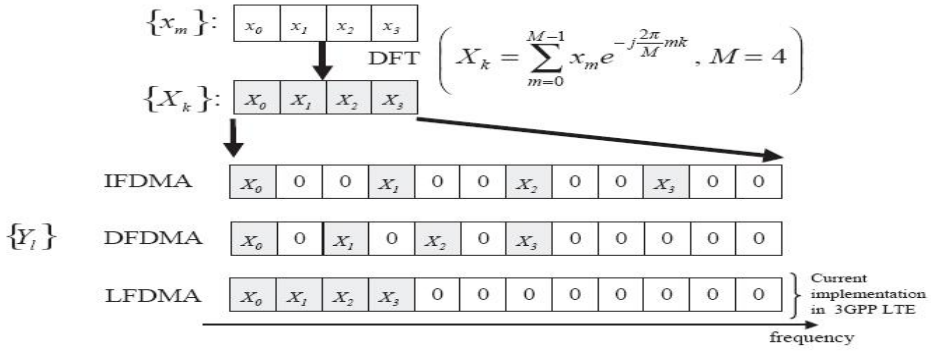

Figure 3.12: An example of different subcarrier mapping schemes for M = 4, Q = 3, and N = 12.

3.3.3. SC-FDMA Implementation in 3GPP Long Term Evolution

SC-FDMA is used in LTE downlink when the transmitter is the UE and the receiver is the eNB. We describe the physical layer implementation of SC-FDMA in 3GPP LTE according to [36]. Both TDD and FDD modes are available, but FDD is currently more popular.

3.3.3.1. Modulation and Channel Coding

In the uplink, the data are mapped onto signal constellation that can be QPSK, 16QAM, or 64QAM. Turbo code based on 3GPP UTRA Release 6 is used for Forward Error Correcting (FEC).

3.3.3.2. Sub-frame structure

The basic sub-frame structure in the time domain is shown in Figure 3.13.

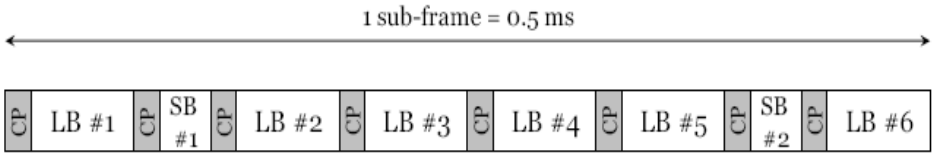

Figure 13: Basic sub-frame structure in time domain.

Band-width (MHz)	Sub-frame Duration(ms)	LB size (μ/# of occupied subcarriers/FFT size)	SB size (μ/# of occupied subcarriers/FFT size)	CP duration (μ/# of subcarriers)
20	0.5	66.67/1200/2048	33.33/600/1024	(4,13/127) or (4.39/135)
15	0.5	66.67/900/1536	33.33/450/768	(4.12/95) or (4.47/103)
10	0.5	66.67/600	33.33/300	(4.1/63) or (4.62/71)
5	0.5	66.67/300	33.33/150	(4.04/31) or (5.08/39)
2.5	0.5	66.67/150	33.33/75	(3.91/15) or (5.99/23)
1.25	0.5	66.67/128	33.33/38	(3.65/7) or (7.81/15)

Table 3.4: Parameters for Uplink SC-FDMA Transmission scheme in 3GPP LTE.

It has duration of 0.5 ms and consists of six blocks (LB) and two short blocks (SB). Cyclic Prefix (CP) is added in front of each block. Long blocks are used for control and/or data transmission and short blocks are used for reference (pilot) signals for coherent demodulation and/or control/data transmission. Both localized and distributed subcarrier mapping data use the same sub-frame structure. Table 3.4 shows the Uplink parameters for SC-FDMA transmission scheme in 3GPP LTE.

3.3.3.3. Reference (Pilot) Signal structure

Reference signals are received and used by the base stations for uplink channel estimation in coherent demodulation/detection and for possible channel quality estimation for channel dependent scheduling. The reference signals can be constructed using Constant Amplitude Zero Auto-Correlation (CAZAC) sequences such as Zadoff-Chu poly-phase sequences. Zadoff-Chu CAZAC sequences are defined as:

$$a_k = \begin{cases} e^{-j2\pi\frac{r}{L}\left(\frac{k^2}{2}+qk\right)}, & k = 0,1,\dots,L-1 \quad for\ L\ even \\ e^{-j2\pi\frac{r}{L}\left(\frac{k(k+1)}{2}+qk\right)}, & k = 0,1,\dots,L-1 \quad for\ L\ odd \end{cases} \tag{3.16}$$

where r is any integer relatively prime to L and q is any integer [37].
The Zadoff-Chu CAZAC sequence has the following properties:

- Constant amplitude;
- Zero circular autocorrelation;
- Flat frequency domain response;
- Circular cross-correlation between two sequences is low and it has constant magnitude provided that L is a prime number.

3.3.4. MIMO for SC-FDMA Uplink

Transmitter for MIMO SC-FDMA system architecture is shown in figure 3.14 and receiver structure is shown in Figure 3.15. One can see from the figure that transmitter can be configured for single or double codeword operation.

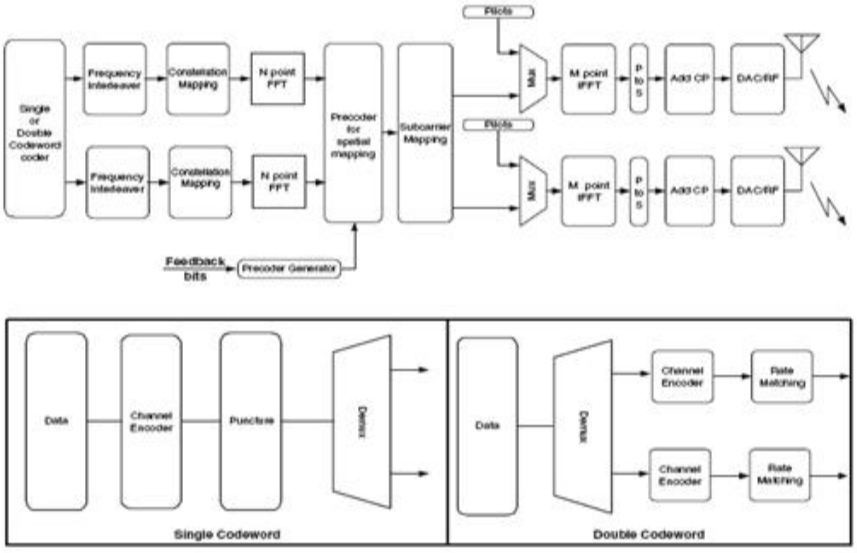

Figure 14: MIMO SC_FDMA transmitter for single and mobile code-words.

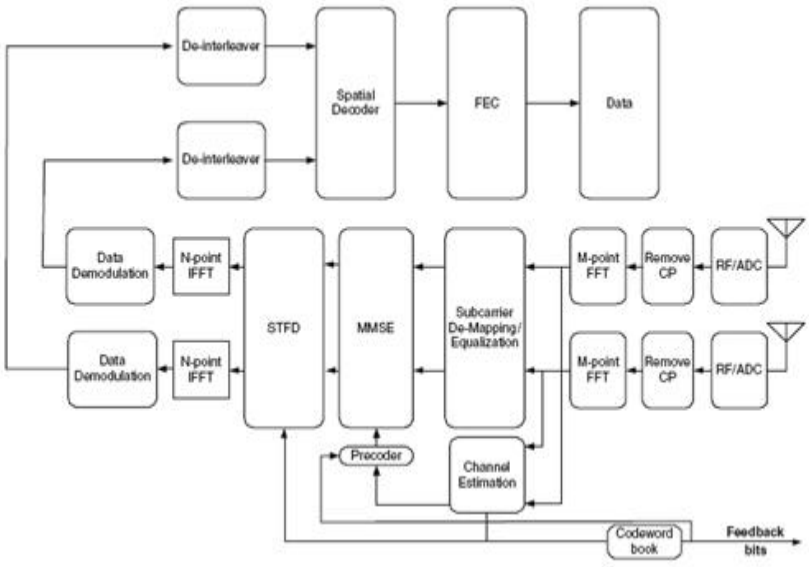

Figure 3.15: MIMO SC-FDMA receiver for single code-word.

According to [2], performance comparison between single code-word and double code-word indicates that they show different performances in different SNR levels with transmit beamforming for 2×2 MIMO.13 Performance of double code-word system shows higher throughput at lower SNR, and opposite is true at higher SNR. Double code-word system in the lower SNR region has one eigenmode that has higher SNR than the total system SNR. Consequently, that stream contributes some successful transmission while the lower SNR stream generally does not. However, at high SNR, lower stream reduces the total throughput because it still has a relatively dominant error rate. On the other hand, in single code-word system, the upper SNR stream protects the lower SNR stream due to the coding. As a result, lower error rate is achieved at higher SNR.

3.4. Simulation of OFDMA and SC-FDMA in Matlab

In this section we present some simulation results of OFDMA and SC-FDMA in different scenarios. The following results were obtained by considering a simple Rayleigh flat fading channel with the standard deviation equal to $1/\sqrt{2}$ and an Additive White Gaussian Noise (AWGN) channel. We simulate the baseband system presented in figure 3.8 by considering 512 subcarriers and a CP length equal to 20.

In Figure 3.16, we can see that the Symbol Error Rate (SER) performance of SC-FDMA (IFDMA) in flat Rayleigh fading channel is poorer than SER performance on AWGN channel, it can be observed that fading channel and the absence of direct view path produce a deterioration of performance of about 2 dB when SER= 10^{-5}.

In Figure 3.17 is shown the SER performance of SC-FDMA for two different subcarrier mapping schemes, IFDMA and LFDMA, in flat fading Rayleigh channel. We can observe the similarity between their SER performances.

A salient advantage of SC-FDMA over OFDMA is the lower PAPR because of its inherent single carrier structure. The lower PAPR is greatly beneficial in the uplink communications where the mobile terminal is the transmitter. Time domain samples of SC-FDMA modulated signals are different depending on the subcarrier mapping scheme and we can expect different PAPR characteristics for different subcarrier mapping schemes [32]. If X is data vector of length N, time domain vector in the transmitter $\mathbf{x}=[\mathbf{x_0},\ldots,\mathbf{x_{n-1}}]$=IDFT(X) and the PAPR is defined as:

$$PAPR\ (\mathrm{x}) = \frac{\|\mathrm{x}\|_{\infty}^{2}}{E\left(\|\mathrm{x}\|_{2}^{2}\right)/N}, \tag{3.17}$$

where E(·) denotes expectation and $\|.\|_{\infty}$.and $\|.\|_2$ represent the ∞-norm and the 2-norm respectively. Therefore the denominator in the right hand side member of equation (3.17) represents the average power. When N is large, the distribution of the output time vector converges to a Gaussian due to central limit theorem. Hence, the probability that the PAPR is above a threshold λ is written as:

$$\Pr\{PAPR>\lambda\}=1-\left(1-e^{-\lambda}\right)^{N}. \tag{3.18}$$

Unlike OFDM, statistical properties of PAPR for single carrier modulations are not easily obtained analytically [38]. We thus resort to numerical analysis by simulations to investigate the PAPR properties.

To compare the PAPR of OFDMA and SC-FDMA, a MATLAB simulation was done [32] with the same input parameters for both multiple access techniques. The SC-FDMA signal is passed through a raised-cosine pulse shaping filter and rectangular pulse shaping filter respectively. The OFDMA signal is not pulse shaped. We computed the Complementary Cumulative Distribution Function (CCDF) of PAPR, which is the probability that PAPR is higher than a certain PAPR value $PAPR_0$, ($Pr\{PAPR>PAPR_0\}$). In Figure 3.18, the CCDF of PAPR of IFDMA, LFDMA and OFDMA are presented.

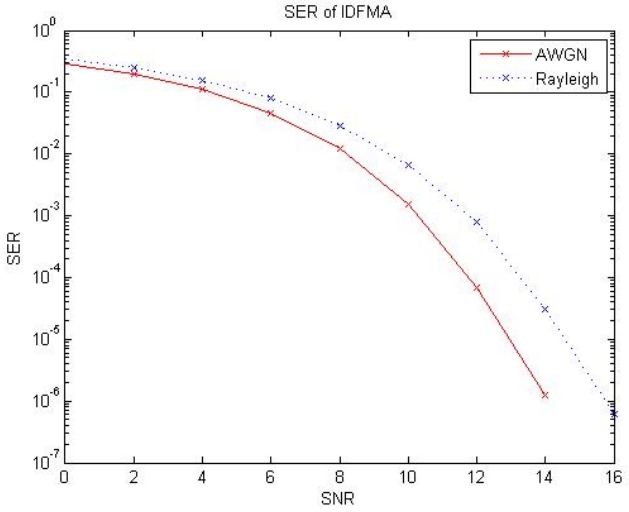

Figure 3.16. SER for SC-FDMA in AWGN and Rayleigh channel.

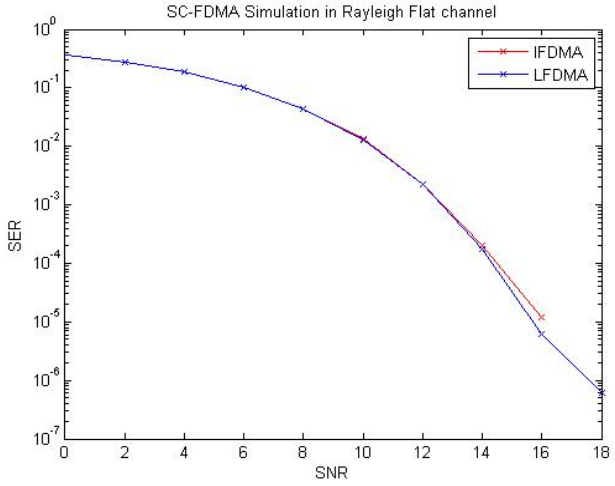

Figure 3.17. Comparison of SER IFDMA and LFDMA in flat fading Rayleigh channel.

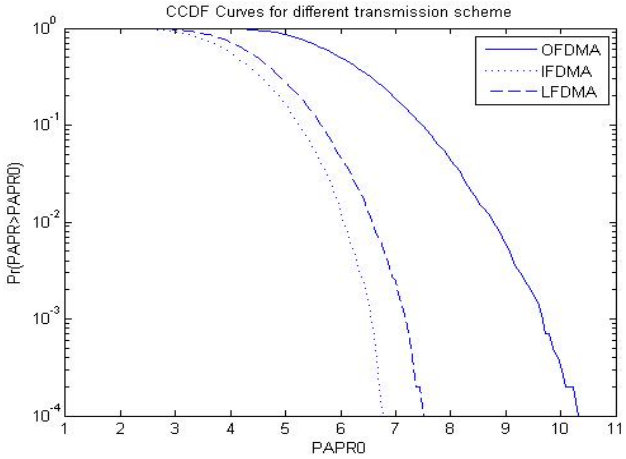

Figure 3.18: Comparison of CCDF of PAPR for IFDMA, LFDMA, and OFDMA with total number of subcarriers N = 512, and QPSK modulation.

We can see that both cases of SCFDMA have indeed lower PAPR than that of OFDMA. Also, it can be observed analyzing last figure that IFDMA has the lowest PAPR.

As a conclusion, we have proved first that the SC-FDMA has good performance on AWGN and flat fading Rayleigh channels (see Figure 3.16). Next, we have compared the two types of subcarriers mappings used in SC-FDMA, the IFDMA and the LFDMA, in a flat fading Rayleigh scenario and we have proved the superiority of IFDMA (see Figure 3.17). Finally we have proven the superiority of the SC-FDMA versus the OFDMA from the PAPR point of view. Both SC-FDMA types of mapping schemes produce small PAPR values for the same value of PAPR0 than the OFDMA (see Figure 3.18).

From the informatics point of view, we have added at the simulator in [32] a new function associated with the flat fading Rayleigh channel, and we have used the new simulator to appreciate the CCDF of PAPR of an OFDMA transmission system [39].

3.5. Summary

In this chapter, we presented the multiple access schemes for 3GPP LTE in Uplink and Downlink. We illustrated in details SC-FDMA and OFDMA and their implementation in LTE. We compared subcarrier mapping in SC-FDMA and the PAPR of SC-FDMA and OFDMA by simulation using Matlab. Next, we will present PAPR and its reduction techniques in more details.

CHAPTER 4

PEAK-TO-AVERAGE POWER RATIO

4.1. Introduction

The great value of the Peak-to-Average Power Ratio (PAPR) is a typical problem in multicarrier modulation. This high value of PAPR in OFDM is due to the summation of large number of independent amplitude modulated signals using different subcarriers for transmission. The PAPR value is a performance measurement that is indicative of the power efficiency of the transmitter.

One of the most difficult problems in the design of a base station (BS) is the high dynamic required for its power amplifier. The length of the interval of levels of the input signal for which the device has a linear comportment defines the dynamic of a power amplifier. Any non-linearity of the power amplifier produces distortions of the transmitted signal, which affect the performance of the corresponding receiver. Generally, these non-linearities appear at the margins of the interval of levels of the input signal. The amplification of a signal with a high PAPR value requires a power amplifier with an extended dynamic. In consequence, the utilization of signals with reduced PAPR values simplifies the design of power amplifiers for wireless communications.

The transmitter in most radio systems uses High Power Amplifier (HPA). The HPA introduce inter-modulation between subcarriers and additional interference into the system due to its saturation as a consequence of high PAPR of the OFDM systems and leads to an increased Bit Error Rate (BER).

In the case of an ideal linear HPA, where we achieve linear amplification up to the saturation point, we reach the maximum power efficiency when the HPA is operating near the saturation point. A positive PAPR in dB means that we need a power bakeoff to operate in the linear region of HPA. We can express the theoretical relationship between PAPR [dB] and transmit power efficiency as follows [40]:

$$\eta = \eta_{max} 10^{-\frac{PAPR}{20}}, \tag{4.1}$$

where ŋ is the power efficiency and $\eta_{\max}$ is the maximum power efficiency.
In this chapter, we analyze the PAPR characteristics for both OFDMA and SC-FDMA, we investigate the most used PAPR reduction techniques, and we propose new techniques in order to further reduce the PAPR.

4.2. PAPR in OFDMA Systems

Despite of its advantages, one of the major drawbacks of OFDMA is the high PAPR value of the transmitted signals. In OFDMA systems, the time domain signal transmitted over the air is the weighted sum of multiple subcarriers. As the number of subcarriers becomes large, a small percentage of the time domain samples have high magnitudes (i.e. peak values). These peak values can be much larger than the average value that leads to high PAPR.

Since the HPA is linear in a certain range, non-linear distortion occurs at the peak values. Extending the linear range of the HPA significantly increases the cost of the entire communication system and reduces power efficiency. Hence, solving the PAPR issue is a critical requirement for mobile stations in OFDMA systems. It can be observed, analyzing Figure 4.1, that the tails of the spectrum of the signal obtained at the output of the HPA decrease slower than the tails of the spectrum of the signal at its input, which proves that the non linearity of the HPA reduces the spectral efficiency of the OFDM based transmitter [41].

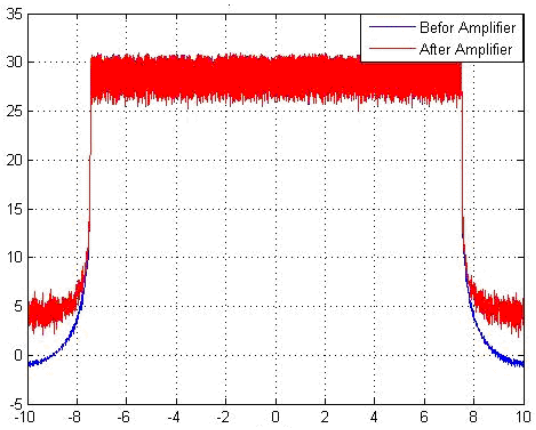

Figure 4.1: Effects of the non linearity of the HPA (Rapp model) on the spectrum of OFDM signals. The spectrum of the signal at the output of the HPA is normalized.

4.2.1. Characteristics of PAPR

Starting from a group of *N* bits $\boldsymbol{X}_k$ and a set of *N* subcarriers $\boldsymbol{f}_k$, an OFDM symbol will be generated by the amplitude modulation of each subcarrier with a corresponding bit. The subcarriers are chosen to be orthogonal, that is $f_k = K.\Delta f$, where $\Delta f = \frac{1}{NT_0}$ and T_0 is the original bit period. Therefore, the complex envelope of the transmitted OFDM signal can be written as:

$$x(t) = \frac{1}{\sqrt{N}} \sum_{k=0}^{N-1} X_k e^{j2\pi f_k t}, \quad 0 \le t \le NT_0 \tag{4.2}$$

In general, the PAPR of OFDM signals is defined as the ratio between the maximum instantaneous power and its average power [42]:

$$PAPR[x(t)] = \frac{\max_{0 \le t \le NT}[|x(t)|^2]}{Pav} \tag{4.3}$$

where P_{av} is the average power of $x(t)$ and it can be computed in the frequency domain because the Inverse Fast Fourier Transform (IFFT) is a (scaled) unitary transformation.

The PAPR of the discrete time sequences typically determines the complexity of the digital circuitry in term of number of bits necessary to achieve a desired signal to quantization noise for both the digital operations and the Digital to Analog Conversion. However, we are often more concerned with reducing the PAPR of the continuous-time signals in practice, since the cost and power dissipation of the analog components often dominate [42].

To better approximate the PAPR of the continuous-time OFDM signals, the oversampling is recommended [42]. It can be implemented by computing an *LN*-point IFFT of the data block with (*L*-1)*N* zero-padding. Therefore, the oversampled IFFT output can be expressed as:

$$x[n] \triangleq \frac{1}{\sqrt{N}} \sum_{k=0}^{N-1} X_k e^{\frac{j2\pi nk}{LN}}, \quad 0 \leq n \leq LN-1 \tag{4.4}$$

The PAPR computed from the *L*-times oversampled OFDM signal can be defined as:

$$PAPR\{x[n]\} = \frac{\max_{0 \leq n \leq LN-1} \left[|x[n]|^2\right]}{E\left[|x[n]|^2\right]}, \tag{4.5}$$

where $E\{.\}$ denotes the expectation operator.

The distribution of PAPR can be expressed in terms of CCDF. When *N* is large, the distribution of the output time vector converges to Gaussian due to Central Limit Theorem [43]. Hence, as already said the probability that the PAPR is above a threshold λ can be written as [43]:

$$\Pr(PAPR > \lambda) = 1 - (1 - e^{-\lambda})^N \tag{4.6}$$

4.2.2. PAPR Reduction techniques in OFDM Systems

Several researchers have proposed schemes for reducing the peak amplitude of the transmitted signal, such as clipping [44], precoding [45], Active Constellation Extension (ACE) [46], Partial Transmit Sequence (PTS) [47], Turbo Coded OFDM [48], and Companding technique [49]. Let us review some typical techniques for PAPR reduction.

4.2.2.1. Clipping

Clipping is a non-linear process and limits the amplitude at some desired maximum level. It is the simplest and most used technique of PAPR reduction. For a multicarrier signal input x(t), the clipping system can be described as follow:

$$y = \begin{cases} x, & |x| \leq A \\ A, & |x| > A \end{cases} \tag{4.7}$$

where A represents the preset clipping level and is a positive real number.

In general, clipping is performed at the transmitter. Despite of PAPR reduction, clipping has two main drawbacks. First, clipping generates self interference by distorting the signal amplitude which increases the BER. It also reduces the spectral efficiency. To overcome these problems in the clipping method,

iterative clipping and filtering is used to obtain the desired PAPR [50], [51]. Figure 4.2 shows the simulation results after four iterative clipping and filtering of a simple OFDM system.

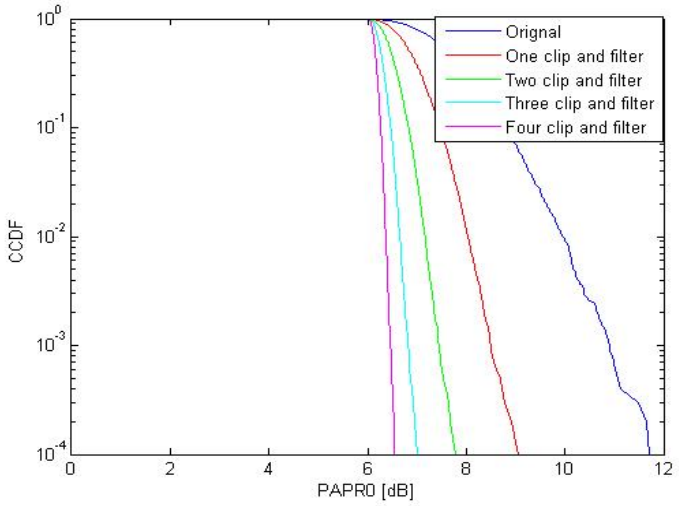

Figure 4.2: PAPR simulation results of Repeated Clipping and Filtering.

4.2.2.2. Companding

The compander consists of a compressor and an expander. The compressor can be a simple logarithm computation block. The inverse system of a compressor is called expander. The compression is applied at the transmitter end after the IFFT process and the expander is applied at the receiver end prior to the FFT block. There are two types of companders that are used in the following of this section, which are described in details in [49]. These two types are the μ-law and the A-law companders [52].

A. μ-law Compander

The μ-law algorithm was primarily used in the digital communication systems of North America and Japan. The μ-law compander employs the logarithmic function at the transmitting side. In general a μ-law compression characteristic is expressed as:

$$y = \frac{V\log\left(1+\mu\frac{|x|}{V}\right)}{\log(1+\mu)}\mathrm{sgn}(x) \tag{4.8}$$

where μ is the parameter which controls the amount of compression, x is the input signal and V is the maximum value of x.

For normalized input signals: $|x| \leq 1$, the input-output equation becomes:

$$y = \frac{\log(1+\mu|x|)}{\log(1+\mu)}\mathrm{sgn}(x) \tag{4.9}$$

The μ -law expander is the inverse of the compressor and has an input-output relation of the form:

$$x = \frac{y}{\mu}\left(e^{\frac{|y|\log(1+\mu)}{v}-1}\right)\mathrm{sgn}(y) \tag{4.10}$$

B. A-law Compander

The characteristic of the A-law compander is given by:

$$y = \begin{cases} \dfrac{1 + \ln A \cdot \|x\|}{1 + \ln A}\mathrm{sgn}(x), & \dfrac{1}{A} \le x \le 1 \\ \dfrac{A\|x\|}{1 + \ln A}\mathrm{sgn}(x), & 0 \le \|x\| \le \dfrac{1}{A} \end{cases} \tag{4.11}$$

where A is the parameter that controls the amount of compression.

In Figure 4.3, we present a simulation result of simple OFDM system with subcarriers compressed using A-law which uses QPSK modulation in an AWGN channel. It can be observed that PAPR is reduced using companding technique.

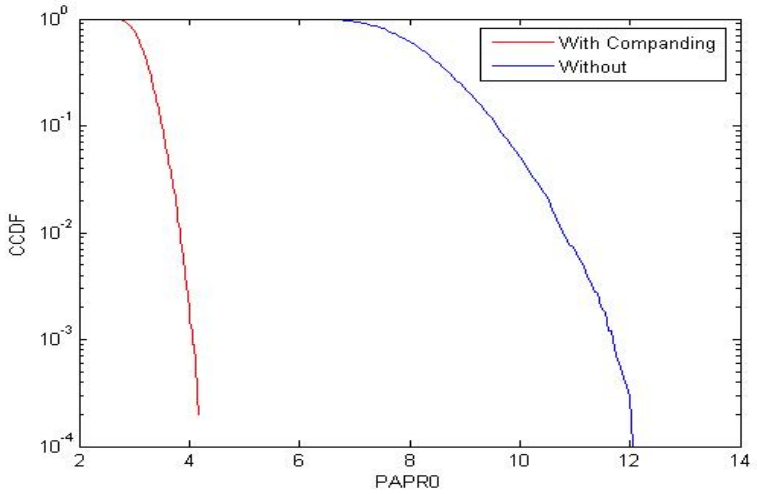

Figure 4.3: CCDF performance of companding technique with A-Law, A=87.

Companding can be seen as a special case of clipping technique [42]. The difference between clipping and companding is that the companding transform compress original OFDM signal using the strict monotone increasing function, so the compressed signal at the transmitter can be recovered through the expander function at the receiver. However, the clipping scheme clips large signal when the amplitude of the original OFDM signal is larger than a given threshold, and thus the clipped signal cannot be recovered at the receiver.

4.2.2.3. Partial Transmit Sequences: PTS

PTS is an important method for PAPR reduction; it is already known that the OFDMA signals generated by PTS are interdependent. PTS divides the frequency

vector into some sub-blocks before applying a phase transformation. In a typical OFDM system with PTS, the input data block *X* is segmented into *M* disjoints sub-blocks, which are represented by the vectors $\{X^{(m)}, m = 0,1, \dots, M-1\}$, [52]. Therefore we can get:

$$X = \sum_{m=0}^{M-1} X^{(m)} \tag{4.12}$$

where $X^{(m)} = [X_0^m\ X_1^m \dots X_{N-1}^m]$, with $X_k^m = X_k$ or 0. The segmentation methods can be classified into three categories [47]: adjacent partition, interleaved partition and pseudorandom partition. Then, the sub-blocks $X^{(m)}$ are transformed into *M* time-domain PTSs:

$$x^{(m)} = [x_0^m\ x_1^m \dots x_{LN-1}^m] = IFFT_{LN\times N}[X^{(m)}] \tag{4.13}$$

Then, these sequences are combined using complex phase weights: $b = [b_1\ b_2 \dots b_M]$ selected to minimize the PAPR.
That is, the PAPR is reduced by the weighted combination of *M* sub-blocks. The resulting time domain signal is given by:

$$x'(b) = \sum_{m=0}^{M-1} b_m\, x^{(m)}. \tag{4.14}$$

Therefore, there are two important issues that should be solved in PTS: high computational complexity for searching the optimal phase weights and the overhead of the optimal phase factors as side information needed to be transmitted to receiver for the correct decoding of the transmitted bit sequence. The allowable phase weights are $b_m = e^{j\phi_m}$ where ϕ_m can be chosen freely within [0, 2π], for convenience we can write:

$$X'(\phi) = \sum_{m=0}^{M-1} e^{j\phi_m} X^{(m)} \tag{4.15}$$

where $\phi = [\phi_0\ \phi_1 \dots \phi_M]$. Hence, the objective of the PTS scheme is to design an optimal phase weight for each sub-block that minimizes the PAPR. The problem can be formulated mathematically in the following form: minimize $|X'(\phi)|$; subject to $0 \le \phi_m \le 2\pi$, *m*=1, 2,..., *M*.

The PTS technique can be implemented in OFDM systems as it is shown in Figure 4.4.

Furthermore, we present in Figure 4.5, the performance of this technique in OFDM using QPSK modulation and 128 subcarriers. It can be observed that the use of PTS results in lower PAPR values.

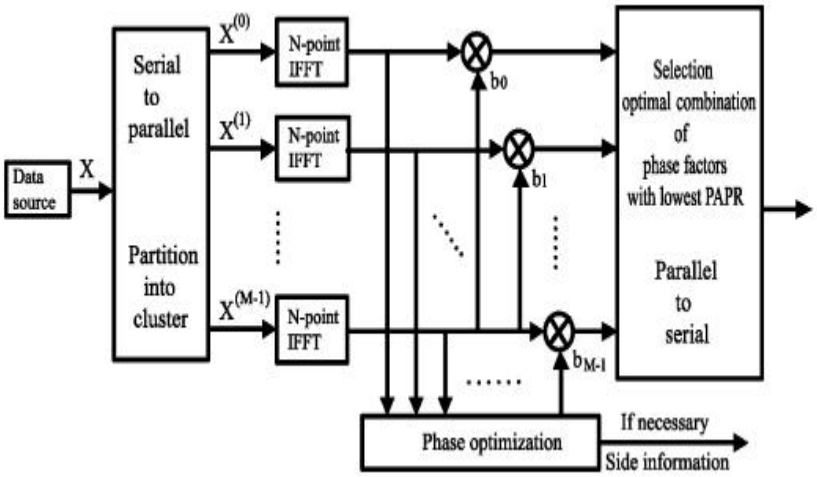

Figure 4.4: PTS technique implementation.

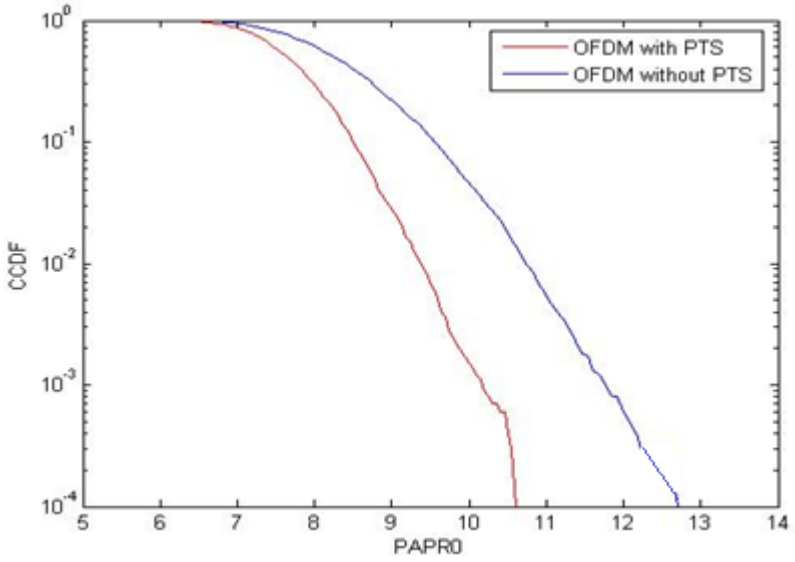

Figure 4.5: CCDF performance for PTS technique.

4.2.2.4. Selected Mapping technique: SLM

SLM outperforms PTS in terms of PAPR reduction versus redundancy, but PTS is considerably better with respect to PAPR reduction versus additional system complexity [53].

Figure 4.6 describes the block diagram of OFDM transmission with SLM PAPR reduction in which the input data sequences are first multiplied by V different phase factors, each of length N, $B_v=[b_{v,0}, b_{v,1}, \ldots, b_{v,N-1}]$ (v=0, 1, …, V-1), in order to

generate alternative input sequences. Then the IFFT is performed for each alternative vector to generate alternative OFDM signal:

$$x^v(t) = \frac{1}{\sqrt{N}} \sum_{n=0}^{N-1} X_n b_{v,n} e^{j2\pi f_n t}, \quad 0 \le t \le NT \tag{4.16}$$

Only OFDM variant with the minimum PAPR is selected for transmission. The implementation of SLM requires *V* IFFT operations and the number of required bits as side information is $[log_2 V]$ for each data block. Therefore the ability of PAPR reduction in SLM depends on the number of phase factors *V*. In Figure 4.7, CCDF performance for SLM method is presented for different values of *V*.

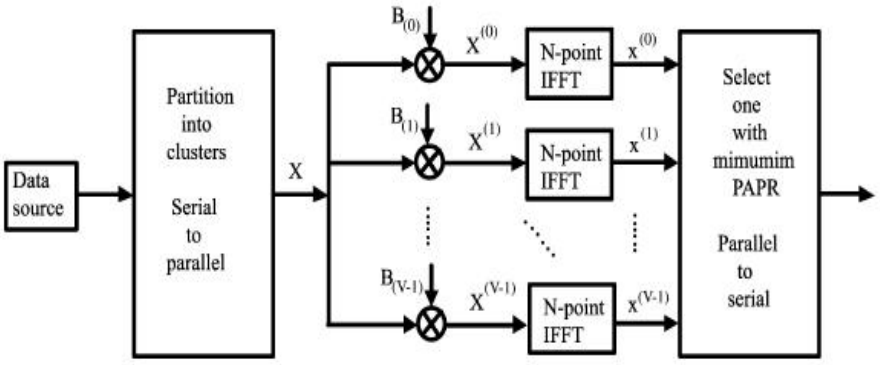

Figure 4.6: the block diagram of OFDM transceiver using SLM PAPR reduction method.

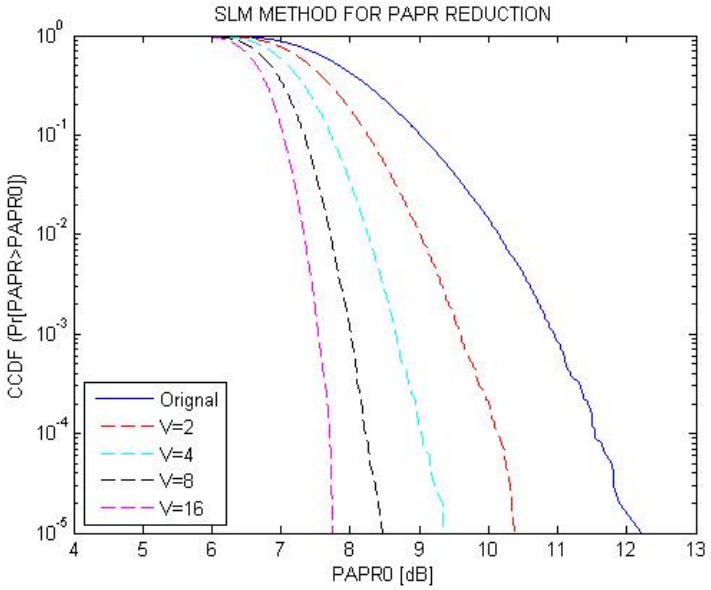

Figure 4.7: CCDF performance of SLM method for different values of V.

4.2.2.5. Tone Reservation

The idea of Tone Reservation (TR) comes from the fact that a certain set of sub-channels (known for the transmitter and receiver) in an OFDM system can be reserved to design a signal that will be used to offset any large peaks from data-bearing sub-channels [54]. The TR technique reserves some tones for generating a PAPR reduction signal instead of data transmission. Figure 4.7 describes the block diagram of TR [54]. The objective is to find the time domain signal c to be added to the original time domain signal x in order to reduce the PAPR.

Let $\{c=c_n;\ n=0,\ 1,\ \ldots,\ N\text{-}1\}$ denote the complex symbols for tone reservation. After TR, the data vector will be $x+c$. Since the inverse Fourier Transform is a linear operation, the resulted OFDM signal can be expressed as:

$$X_{TR} = IDFT(x + c) = X + C \tag{4.17}$$

where $C=IDFT(c)$ and $X=IDFT\ (x)$.

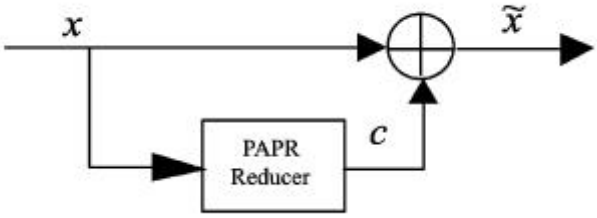

Figure 4.8: Block diagram of TR technique for PAPR reduction.

The main idea of TR is to find out the proper c to make the vector X_{TR} with lowest PAPR. Therefore, we must solve a convex optimization problem that can easily be seen as a linear programming problem [42]. Figure 4.9 shows CCDF performance when a TR is applied to a simple OFDM system.

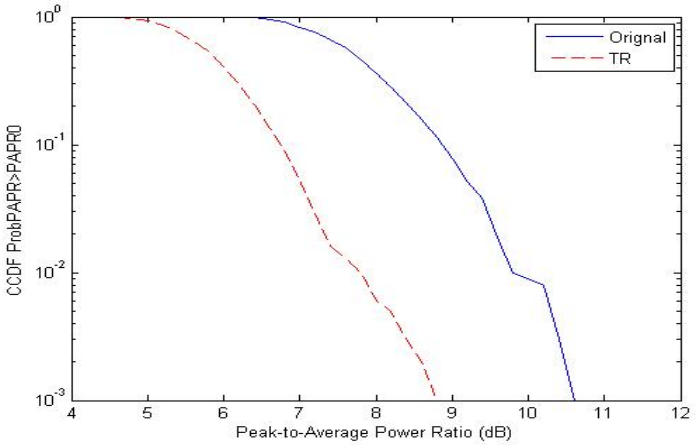

Figure 4.9: CCDF performance of Tone Reservation technique.

4.2.3. Selection Criteria of PAPR Reduction Technique

In [42], authors noticed that several techniques for PAPR reduction were proposed when the first time OFDM was proposed. But some of these solutions affect the system performance. Therefore, it is very important to consider the following factors when choosing PAPR reduction methods:

- High Capability of PAPR reduction technique: It is primary factor to be considered in selecting the PAPR reduction technique with as few harmful side effects such as in-band distortion and out-of-band radiation.
- Low average power: The PAPR can be reduced through the increase of average power of the original signals; this method requires a larger linear operation region in HPA and thus results in the degradation of BER performance.
- Low implementation complexity: Generally, techniques more complex exhibit better ability of PAPR reduction. However, in practice, both time and hardware requirements for the PAPR reduction should be minimal.
- No bandwidth expansion: The bandwidth is a valuable resource in communication systems. The bandwidth expansion directly results in the data code rate loss due to side information (such as the phase factors in PTS). Moreover, the side information could be received in error unless some ways of protection such as channel coding are employed. Therefore, when channel coding is used, the loss in data rate is increased further due to side information. Therefore, the loss in bandwidth due to side information should be avoided or at least be kept minimal.
- No BER performance degradation: The aim of PAPR reduction is to obtain better system performance including BER than that of the original OFDM system. Therefore, all the methods, which have an increase in BER at the receiver, should be regarded with more attention in practice. Moreover, if the side information is received in error at the receiver than the BER performance is reduced.
- Without additional power needed: The design of a wireless system should always take into consideration the efficiency of power consumption. If an operation of the technique which reduces the PAPR needs more additional power, it degrades the BER performance when the transmitted signals are normalized back to the original power signal.
- No spectral spillage: The PAPR reduction technique selected does preserve OFDM attractive technical features such as immunity to the multipath fading. Therefore, the spectral spillage should be avoided in the PAPR reduction.
- Other factors: It also should be paid more attention on the effect of the non-linear devices used in signal processing loop in the transmitter such as DACs, mixers and HPAs, since the PAPR reduction mainly avoid non-linear distortion due to these memory-less devices. At the same time, the cost of these non-linear devices is also an important factor to design the PAPR reduction scheme.

4.3. PAPR in SC-FDMA Systems

In this section, we describe the PAPR of SC-FDMA signal for both mapping schemes. Therefore, we analyze the PAPR of IFDMA and LFDMA.

Let $\{x_m: m=0, 1, \ldots, M-1\}$ be data symbols to be modulated. Then, $\{X_k: k=0, 1, \ldots, M-1\}$ are frequency domain samples after DFT of x_m, $\{X_l: l=0, 1, \ldots, N-1\}$ are frequency domain samples after subcarrier mapping and $\{x_n: n=0, 1, \ldots, N-1\}$ are time symbols after *IDFT* of X_l. The complex pass-band transmit signal of SC-FDMA can be presented as:

$$x(t) = e^{jwt} \sum_{n=0}^{N-1} x_n P(t - n\check{\mathrm{T}}) \tag{4.18}$$

where w is the carrier frequency of the system, $P(t)$ is the baseband pulse, and $\check{\mathrm{T}}$ is the duration of the transmitted symbol x_n. According to [55], in the following, a Raised-Cosine (RC) pulse and a square raise-cosine (RRC) pulse are considered, which the widely used pulse shapes in wireless communications are. The following are time and frequency expressions of these pulse shapes:

$$P_{RC}(f) = \begin{cases} \check{\mathrm{T}}, & 0 \le |f| \le \frac{1-\alpha}{2\check{\mathrm{T}}} \\ \frac{\check{\mathrm{T}}}{2}\left\{1 + \cos\left[\frac{\pi\check{\mathrm{T}}}{\alpha}\left(|f| - \frac{1-\alpha}{2\check{\mathrm{T}}}\right)\right]\right\}, & \frac{1-\alpha}{2\check{\mathrm{T}}} \le |f| \le \frac{1+\alpha}{2\check{\mathrm{T}}} \\ 0, & |f| \ge \frac{1-\alpha}{2\check{\mathrm{T}}} \end{cases} \tag{4.19}$$

$$p_{RC}(t) = \frac{\sin\left(\frac{\pi t}{\check{\mathrm{T}}}\right).\cos\left(\frac{\pi\alpha t}{\check{\mathrm{T}}}\right)}{\frac{\pi t}{\check{\mathrm{T}}.\left(1-\frac{4\alpha^2 t^2}{\check{\mathrm{T}}^2}\right)}} \tag{4.20}$$

$$P_{RRC}(f) = \sqrt{P_{RC}(f)} \tag{4.21}$$

$$p_{RRC}(t) = \frac{\sin\left(\frac{\pi t}{\check{T}}(1-\alpha)\right)+4\alpha\frac{t}{\check{T}}cos\left(\frac{\pi t}{\check{T}}(1+\alpha)\right)}{\frac{\pi t}{\check{T}}.\left(1-\frac{16\alpha^2 t^2}{\check{T}^2}\right)} \ , \tag{4.22}$$

The PAPR for transmit signal $x(t)$ can be computed as follows:

$$PAPR = \frac{peak\ power\ of\ x(t)}{average\ power\ of\ x(t)} = \frac{\max_{0\le t\le N\check{\mathrm{T}}}|x(t)|^2}{\frac{1}{N\check{\mathrm{T}}}\int_0^{M\check{\mathrm{T}}}|x(t)|^2 dt} . \tag{4.23}$$

Without pulse shaping, or equivalently using rectangular pulse shaping, symbol rate sampling will give the same PAPR as in the continuous time case since SC-FDMA signal is modulated over single carrier. Thus, the PAPR without pulse shaping with symbol rate sampling can be expressed as follows:

$$PAPR = \frac{\max_{m=0,1,\ldots,M-1}|x_m|^2}{\frac{1}{M}\sum_{m=0}^{M-1}|x_m|^2} \tag{4.24}$$

According to [55], the amplitude of a single carrier modulated signal does not have a Gaussian distribution unlike OFDM signals and it is difficult to derive analytically the exact form of the distribution. Thus, we resort to numerical analysis to investigate the PAPR properties.

The CCDF of PAPR is presented in Figure 4.10 for IFDMA and LFDMA using 512 subcarriers; QPSK symbol constellation and Raised Cosine pulse were considered. It can be observed, analyzing Figure 4.10, that IFDMA has lower PAPR than LFDMA. As a conclusion, to fully exploit the low PAPR advantage of SC-FDMA, IFDMA is more suitable than LFDMA, when choosing subcarrier mapping method.

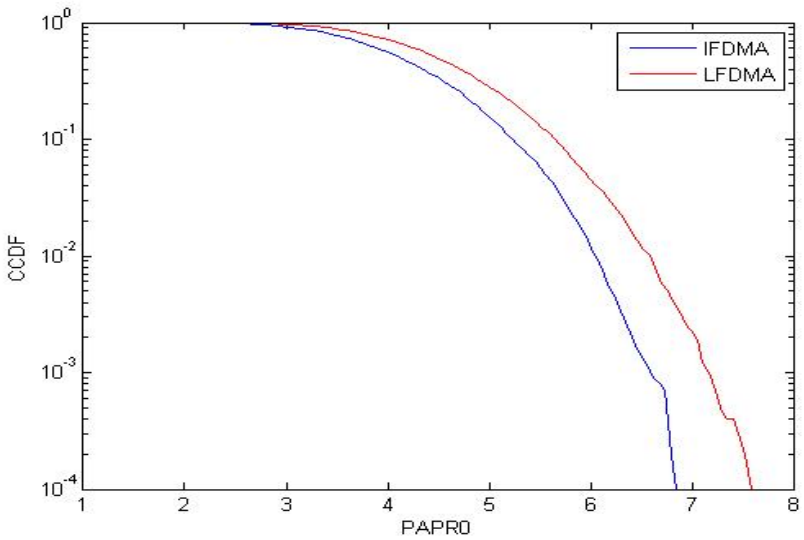

Figure 4.10: CCDF performance of IFDMA and LFDMA using 512 subcarriers and QPSK modulation.

4.4. Proposed PAPR reduction techniques

The goal of this section is to present other PAPR reduction techniques and to propose new ones.

4.4.1. Pre-coding Techniques in OFDM systems for PAPR reduction

In this section, we review and analyze some pre-coding techniques in OFDM and highlight their superiority versus other PARR reduction techniques mentioned in literature**.**

4.4.1.1. Pre-coding techniques

The goal of pre-coding techniques is to obtain a signal with lower PAPR than in the case of OFDM without pre-coding techniques and to reduce the interference produced by multiple users. The PAPR reduction must compensate the non-linearities of the HPA producing the reduction of the BER. Some pre-coding techniques are presented in the following [56].

a. **The Discrete Cosine Transform**

Mathematically, the unitary Discrete Cosine Transform (DCT) of an input sequence *x* is:

$$y(k) = w(k)\sum_{n=1}^{N} x(n)cos\frac{\pi(2n-1)(k-1)}{2N}, \quad k = 1, \dots, N \tag{4.25}$$

where the analysis window *w* can be expressed as:

$$w(k) = \begin{cases} {}^{1}/_{\sqrt{N}} & , \quad k = 1 \\ \sqrt{{}^{2}/_{N}} & , \quad 2 \le k \le N \end{cases} \tag{4.26}$$

a. Zadoff-Chu sequences

Zadoff-Chu codes are the special case of the generalized Chip-Like polyphase sequences having optimum correlation properties [57]. Indeed, Zadoff-Chu sequences of length *L* offer an ideal periodic autocorrelation and a constant magnitude ($\sqrt{L}$)periodic cross-correlation. They are defined by:

$$Z(k) = \begin{cases} e^{\frac{j2\pi r}{L}(\frac{k^2}{2}+qk)} & \text{for } L \text{ even} \\ e^{\frac{j2\pi r}{L}(\frac{k(k+1)}{2}+qk)} & \text{for } L \text{ odd} \end{cases} \tag{4.27}$$

where *k*=0, 1… *L*-1, *q* is any integer, *r* is the code index, prime with *L* and $j = \sqrt{-1}$. Consequently, if *L* is a prime number, the set of Zadoff-Chu codes is composed of *L*-1 sequences.

b. Walsh-Hadamard Transform

The Walsh-Hadamard Transform (WHT) is a non sinusoidal, orthogonal technique that decomposes a signal into set of basic functions. These functions are Walsh functions, which are square waves with values of +1 or -1.

The WHT is used in a number of applications, such as image processing, speech processing, filtering, and power spectrum analysis. Like the FFT, the Walsh–Hadamard transform has a fast version, the Fast Walsh–Hadamard Transform (FWHT). The FWHT is able to represent signals with sharp discontinuities more accurately using fewer coefficients than the FFT. Both the FWHT and the inverse FWHT (IFWHT) are symmetric and thus, use identical calculation processes. The FWHT and IFWHT for a signal $x(t)$ of length *N* are defined as:

$$y_n = \frac{1}{N}\sum_{i=0}^{N-1} x_i \mathrm{WAL}(n,i) \tag{4.28}$$

$$x_i = \frac{1}{N}\sum_{n=0}^{N-1} y_n WAL(n,i) \tag{4.29}$$

where i = 0,1,..., *N*-1 and WAL(n,i) are Walsh functions.

Finally, it must be mentioned the fact that the single carrier Frequency Division Multiplexing used in LTE in uplink is implemented by DFT pre-coding.

4.4.1.2. Simulation results

In this section, the PAPR of OFDM with different pre-coding techniques has been evaluated by simulation. The block implementation is shown in Figure 4.11, where the pre-coding matrix corresponds to different pre-coding techniques used in our simulations.

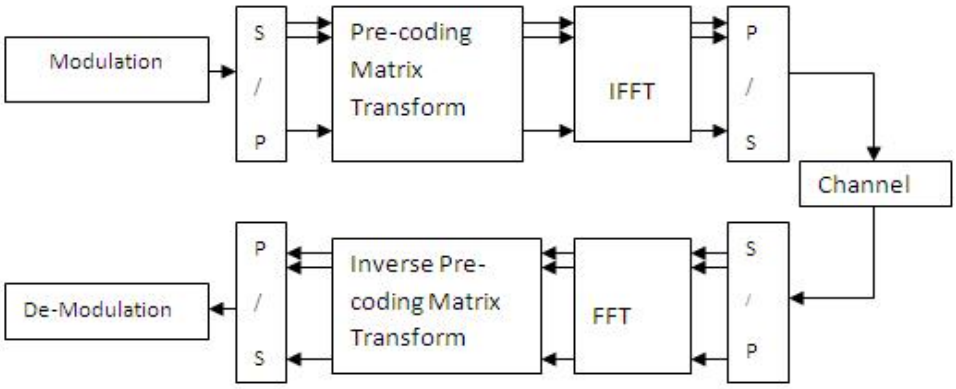

Figure 4.11: Block scheme of pre-coding technique in OFDM system.

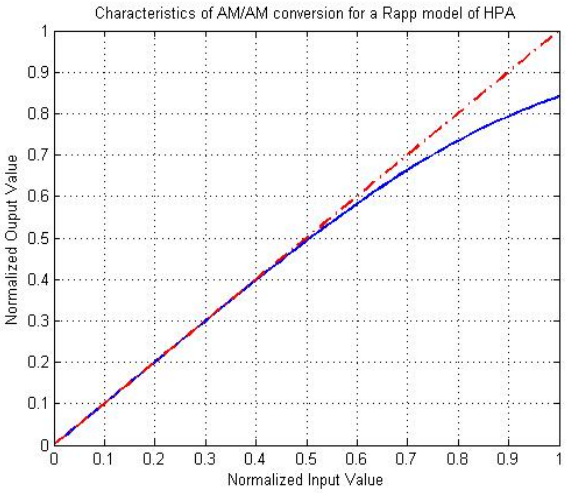

Figure 4.12: Characteristics of AM/AM conversion of a Rapp model.

The simulation results were obtained by considering an Additive White Gaussian Noise (AWGN) channel, the signal is modulated by M-QAM (where M=16,

64 and 256) , *N*=64 and for the HPA we have considered the Rapp model illustrated in Figure 4.12.

The encoding was realized in the transmitter before the computation of IFFT and the corresponding decoding was realized in the receiver after the computation of FFT. Figures 4.13, 4.14, and 4.15 represent the PAPR distributions obtained for different pre-coding techniques: DCT, Discrete Sine Transform (DST), Zadoff-Chu sequences (ZCT), FWHT and the Discrete Fourier Transform (DFT), with 16, 64, and 256 QAM. We can observe in Figure 4.14 that at CCDF=10^{-2}, the PAPR is reduced by approximately 5.2 dB for DFT and Zadoff-Chu, by 1.8 dB for DCT and 1 dB for FWHT pre-coding based OFDM systems.

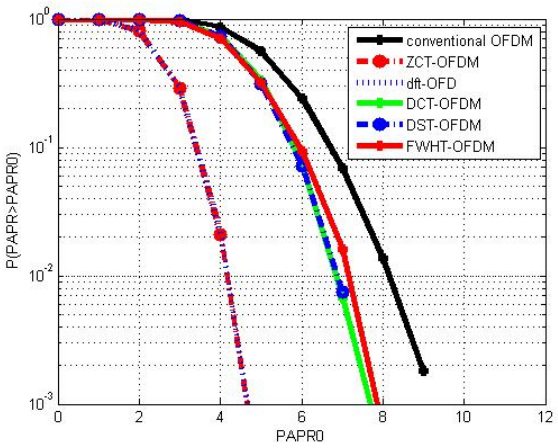

Figure 4.13: CCDF for different pre-coding techniques with 16 QAM.

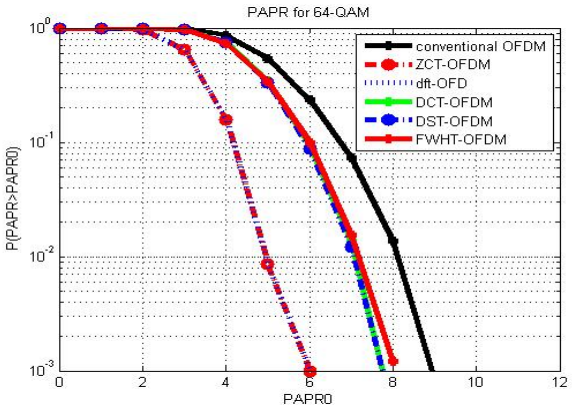

Figure 4.14: CCDF for different pre-coding techniques with 64 QAM.

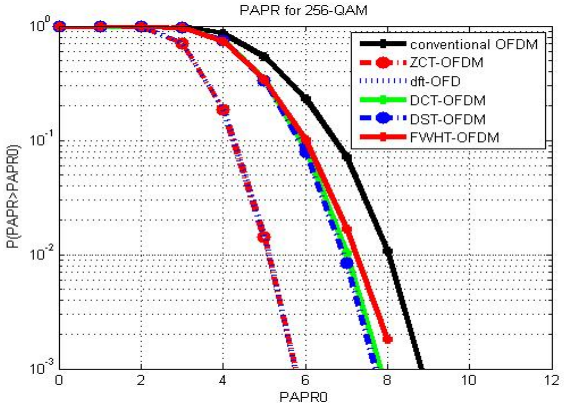

Figure 4.15: CCDF for different pre-coding technique with 256QAM.

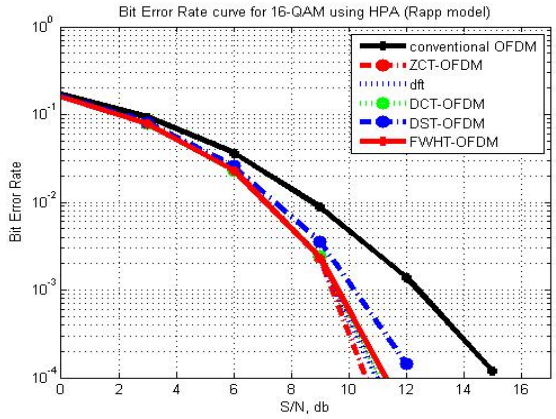

Figure 4.16: BER performances for OFDM with and without pre-coding techniques.

In Figure 4.16 are represented the BER performances of different pre-coding based OFDM systems using the HPA (Rapp model). We can observe that the pre-coding based OFDM systems compensate the non-linearities introduced by HPA and have better performance than simple OFDM system.

These pre-coding techniques based OFDM systems produce low PAPR than simple OFDM system. Furthermore, the DFT and ZCT are better than other pre-coding techniques because they produce the lowest PAPR. Additionally, these techniques introduced no signal degradation representing better PAPR reduction methods than others [42] because they do not require any power increment, complex optimization and side information to be sent to the receiver. This also explains the selection of the DFT pre-coding technique in LTE uplink implemented as PAPR reduction mechanism. Additionally, as it is highlighted in [57], ZCTOFDM systems also take advantage of the time-varying behavior of the wireless communication channel, due to the good correlation properties of the Zadoff-Chu sequences, offering substantial performance gain in fading channels.

4.4.2. Combined Partial Transmit Sequence and Companding for PAPR Reduction in OFDM Systems

In this section, we propose a new PAPR reduction technique, which combines Partial Transmit Sequence (PTS) and companding techniques. Some simulation results are presented, commented, and compared with the results obtained applying PAPR reduction methods already proposed in literature.
The proposed technique is shown in Figure 4.17.

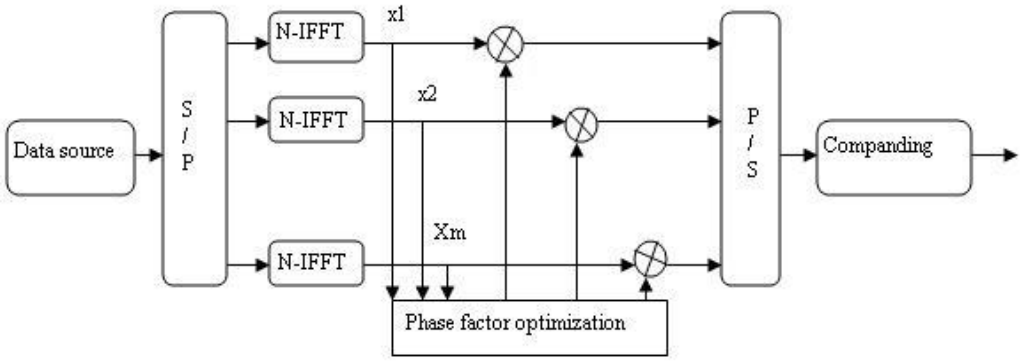

Figure 4.17: Block diagram of the proposed PAPR reduction method based on combining PTS and Companding techniques.

The main idea of the proposed scheme is to use a combination of two PAPR reduction methods. First, the PTS approach is used and second the signal with the lowest PAPR is submitted to the companding technique. The intention of this combination is to obtain a signal with lower PAPR than in the case of the PTS method. In this section we will present some simulation results obtained using different scenarios for PAPR reduction for OFDM signals. The results presented in the following were obtained by considering an Additive White Gaussian Noise (AWGN channel, 512 subcarriers and a QPSK modulation. Figure 4.18 shows the CCDF performance of the proposed technique (PTS + companding) for different values of μ. The peak power at CCDF=10^{-4} is reduced by approximately 3dB, 8.5dB, 9.2 dB for μ= 2, μ=75, μ=255 respectively in comparison with the corresponding value obtained without any PAPR reduction technique. In Figure 4.19 is presented the CCDF performance of the proposed scheme compared with those of the system without any PAPR reduction, of the system equipped only with the PTS technique and of the system equipped only with the companding technique. It can be observed that the PAPR value improves by 2dB for CCDF = 10^{-4} for PTS technique, by 8.5 dB for the companding technique, and by 9.2dB for the proposed technique in comparison with the value obtained for the system without any reduction technique. In Figure 4.20 are presented the BER performances of the proposed scheme compared with the original system over a flat fading Rayleigh channel without mobility and the same value of μ (μ=255).

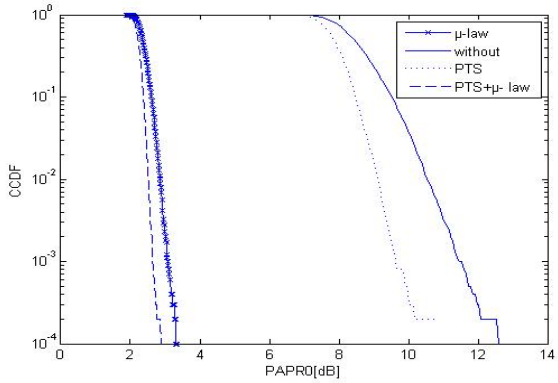

Figure 4.18: CCDF performance for different PAPR reduction techniques.
For the proposed method a value of μ =255 was used.

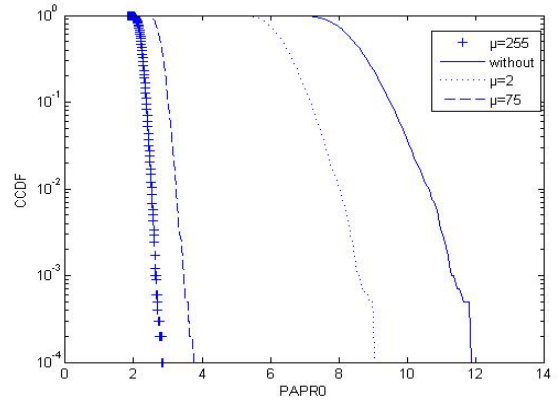

Figure 4.19 CCDF performance of the proposed method for different values of μ

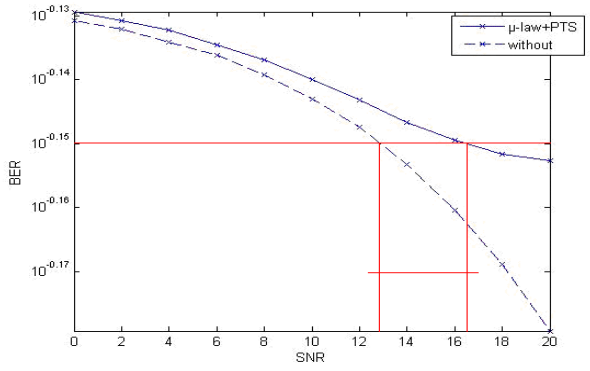

Figure 4.20: BER performance comparison for OFDM system
with and without PAP reduction.

We can observe that BER increases for the system with PAPR reduction scheme because the signal is distorted. The mean BER degradation is of 4 dB. The BER results can be improved by channel coding, for example using turbo-codes. The simulations results obtained prove the good performance of the approach proposed, better than the performance that can be obtained using only one of the two composing methods applied separately.

4.4.3. PAPR reduction Using Soft Reduction Companding for SC-FDMA

We propose a new PAPR reduction scheme based on combining the Soft Reduction transform and Companding system. It can be implemented in SC-FDMA system at the Cyclic Prefix output. Figure 4.21 presents the principle of the A-law/μ-Law soft reduction technique (ASR/μSR).

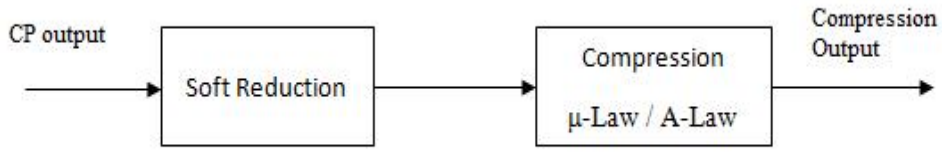

Figure 4.21: Soft reduction compressor.

First the soft reduction transform is applied to the CP output *x*, the resulting signal can be written as:

$$x_{SR} = \frac{x}{(1+x^2)^{1/2}} \tag{4.29}$$

Then we apply the A-Law compressor on the soft reduction output x_{SR} in order to obtain the following signal:

$$Y_{ASR} = \begin{cases} \frac{1+\log(A.|x_{SR}|)}{1+logA} sgn(x_{SR}); & \frac{1}{A} \leq |x_{SR}| \leq 1 \\ \frac{A.|x_{SR}|}{1+logA} sgn(x_{SR}); & 0 \leq |x_{SR}| \leq \frac{1}{A} \end{cases} \tag{4.30}$$

where *A* is the compression parameter. The custom value of *A* used in Europe is of 87.6 [58].
We can also use the μ-Law compressor which has the same basic features and implementation advantages as the A-Law compressor. After the μ-Law compression, the signal can be expressed as follow:

$$Y_{\mu SR} = V.\frac{\log\left(1+\mu\frac{|x_{SR}|}{V}\right)}{\log(1+\mu)} sgn(x_{SR}) \quad (4.31)$$

where μ is the compression parameter. In the United States and Japan the custom value of μ is 255 [58].
For normalized input signal: $|x_{SR}| \leq 1$, we can write $Y_{\mu SR}$ as:

$$Y_{\mu SR} = \frac{\log(1+\mu|x_{SR}|)}{\log(1+\mu)} sgn(x_{SR}) \quad (4.32)$$

By using soft reduction at the output of the Cyclic Prefix insertion block, signal peaks are attenuated. Then, the application of the compression (A-law, μ-Law) leads to the amplification of the reduced signal x_{SR} while giving gain superiority to lower amplitudes and decreasing even more PAPR [55]. We can choose the compressor parameter in function of the BER deterioration while we are interested in reducing PAPR without deteriorating BER.
In order to verify the performance of the proposed companding scheme, we simulated the SC-FDMA system with parameters presented in the following table.

Table 4.1: Simulation parameters.

Total number of subcarriers	512
Subcarrier mapping scheme	LFDMA
Channel	AWGN
Channel estimation	MMSE
Modulation	QPSK and 16QAM

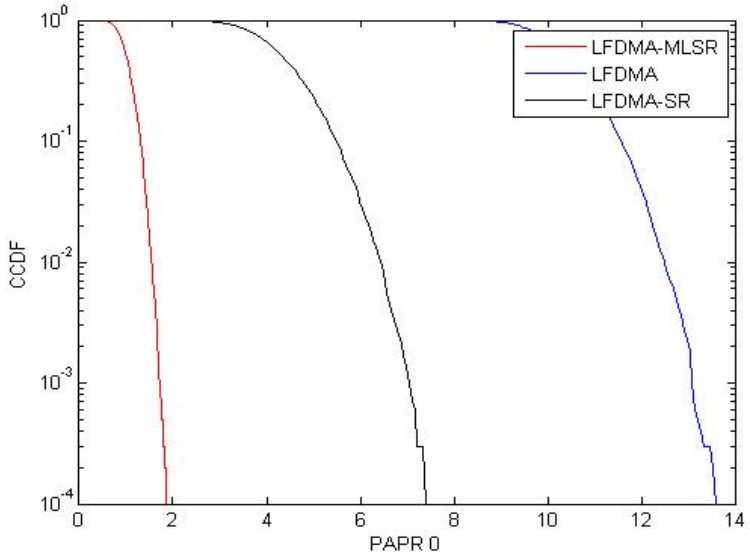

Figure 22: CCDF performance of LFDMA with μ-Law compressor and Soft reduction.

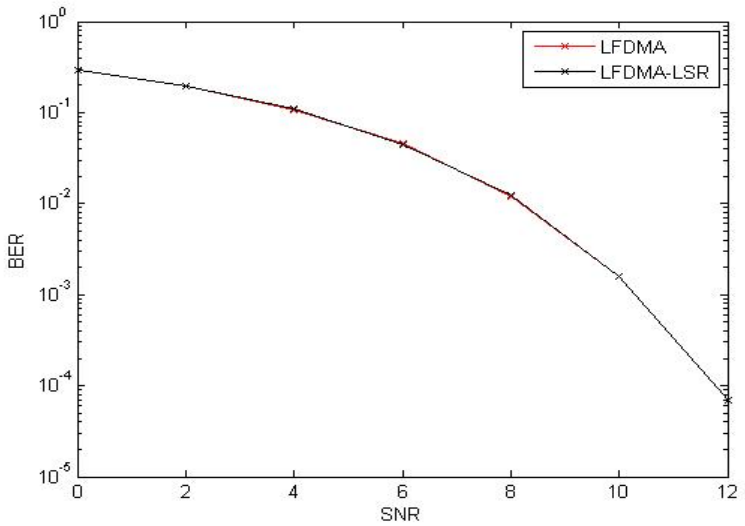

Figure 4.23: BER performance of the LFDMA with the proposed scheme in comparison with the original LFDMA system.

Figure 4.22 shows the Complementary Cumulative Distribution Function of the PAPR with the proposed reduction scheme. With this scheme, the PAPR was reduced by 12 dB at CCDF=10^{-4}.

We analyzed also the BER of LFDMA with our companding function and we presented the BER performance in Figure 4.23 where BER performance is compared to simple LFDMA. We can easily observe that this companding function produce no BER degradation.

As a conclusion, by a simple PAPR reduction technique, we obtained good PAPR result without deteriorating the BER curves and this is the principle goal.

4.5. Summary

In this chapter, we gave an overview of PAPR parameter in OFDMA and SC-FDMA. We investigated the existing reduction techniques and we proposed new techniques. Next, we will focus on the channel estimation.

CHPATER 5

CHANNEL ESTIMATION

5.1. Introduction

The transmitted signal over the wireless channel is perturbed by the Additive White Gaussian Noise (AWGN) whose samples are statically independent. This channel model represents the start point to understand the performance of communication systems. It is the ideal radio channel; the received signal would consist of only a single direct path signal, which would be a perfect reconstruction of the transmitted signal.

In the following, we analyze the wireless channel and channel estimation techniques, and then we introduce our approach.

5.2. Wireless channel

In wireless communication system, signal may be transmitted over multipath; this phenomenon is called multipath propagation. It results in receiving different versions of the transmitted signal at the receiver where all the received signals are accumulated together creating a non-AWGN model for the wireless channels. Since an AWGN model does not describe the wireless channels, it is important to find other models that represent the channels. The multipath propagation produces fluctuations of the phases and amplitudes of the received signal.

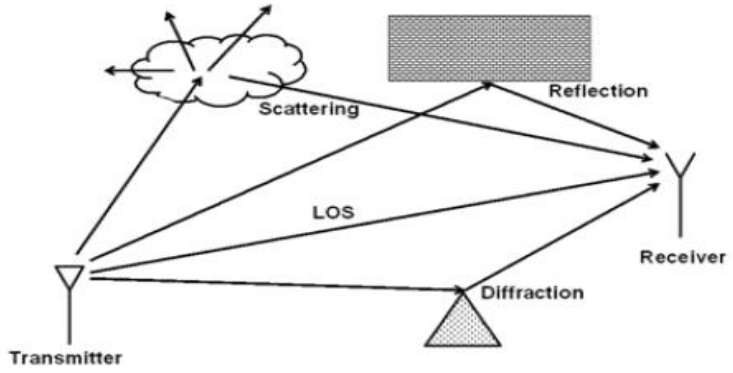

Figure 5.1: Different phenomena which perturb propagation in wireless communications [59].

Figure 5.1 presents an example of multipath propagation. LOS means Line of Sight and indicates the presence of a direct path between the transmitter and the receiver. The received signal through the LOS is usually the strongest signal. The electromagnetic wave may be reflected diffracted or scattered as well.

The effects of these propagation mechanisms and their combinations may reduce the power of the transmitted signal. There are two general aspects of such a power reduction: the first one consists in large-scale effects, which characterize the signal power over large distances. This aspect is called attenuation or path loss and sometimes large-scale fading. The second one is small-scale fading, also called just fading, which characterizes the signal transmission over short distances or short time intervals.

5.2.1. Attenuation

Attenuation is the drop of signal power during transmission over the wireless channel. Also called large-scale fading, attenuation can be caused by any objects that obstruct the LOS signal from the transmitter to the receiver. The average received power P_r is proportional to d^{-v} where d is the distance between the transmitter and the receiver, and v is the path loss exponent. Thus we have,

$$P_r = \beta d^v P_t \tag{5.1}$$

where P_t is the transmitted power and β is a parameter that depends on the frequency and other factors [59]. For propagation in urban area, v>2 is chosen.
Hence, the path loss L_{path} at the distance d with respect to the reference distance d_0 is,

$$L_{path} = \beta_0 + 10\log_{10}\frac{d}{d_0} \tag{5.2}$$

where β_0 ist the measured path loss at distance d_0.
In many practical situations, the environment (such as building height) can randomly affect the path loss by shadowing. Hence, the path loss will be expressed as,

$$L_{path} = \beta_0 + 10\log_{10}\frac{d}{d_0} + X \tag{5.3}$$

where $\boldsymbol{X}$ is a zero-mean Gaussian random variable in dB with typical standard deviation between 5 and 12 dB.

5.2.2. Fading

The transmitted signal is received in two or more versions by the receiver at slightly different time. The interference between these signals produces the fading or small-scale fading. These multipath signals (waves) combined produces the received signal which can vary widely in amplitude and phase; it is random in nature and its strength changes rapidly over a small period of time. The multipath propagation increases the time required for the signal to reach the receiver over the baseband period and results Inter-Symbol Interference (ISI). Figure 5.2 depicts a deterministic model for multipath time-varying channel.

Let us define the delay spread. For that, let us consider p_i and τ_i the power and delay of the i-th path, according to [59], the weighted average delay is:

$$\bar{\tau} = \frac{\sum_{i=1}^{I} p_i \tau_i}{\sum_{i=1}^{I} p_i} \tag{5.4}$$

The delay spread is defined as,

$$\sigma_\tau = \sqrt{\overline{\tau^2} - \bar{\tau}^2}, \tag{5.5}$$

where
$$\overline{\tau^2} = \frac{\sum_{i=1}^{I} p_i \tau_i^2}{\sum_{i=1}^{I} p_i}. \tag{5.6}$$

Finally, the channel coherence bandwidth B_c is approximated by:

$$B_c = \frac{1}{5\sigma_\tau}. \tag{5.7}$$

When the channel has a constant gain and linear phase response over a bandwidth then τ=0; in other words $h(t,\tau)=\alpha(t)\delta(\tau)$. Also, the channel coherence bandwidth B_c is much larger than signal bandwidth. In this case the transmitted signal is affected by flat fading (Figure 5.3).

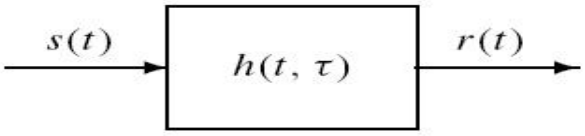

Figure 5.2: A deterministic channel model.

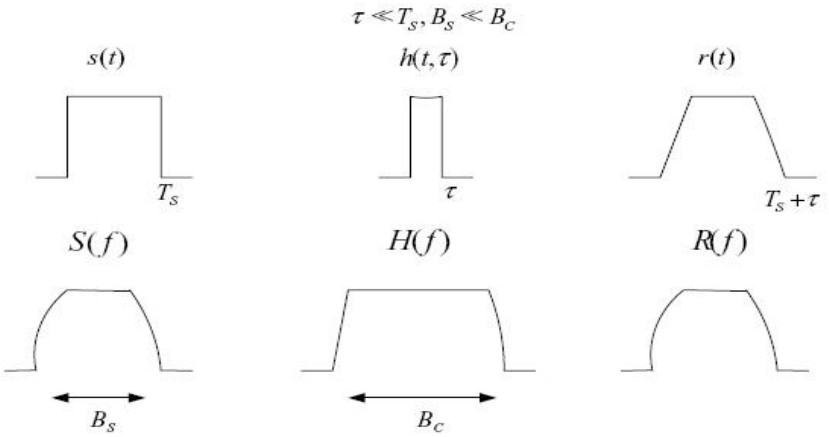

Figure 5.3: Example of propagation on a flat fading channel: *s* – signal transmitted, *h* – channel's impulse response, *r* – received signal.

When the channel has a constant gain and linear phase over a bandwidth that is smaller than the signal bandwidth, ISI appears and signal is distorted. In this case the transmitted signal is affected by frequency selective fading (Figure 5.4).

Doppler shift in frequency is another independent phenomenon caused by mobility which can affect the quality of transmission. If we consider a signal

associated to an electromagnetic wave with a wavelength of λ and a mobile receiver with a velocity of v, the Doppler shift is given by:

$$f_d = \frac{v}{\lambda}\cos\theta \tag{5.8}$$

where θ is the angle between the direction of the motion of the mobile and the direction of the arrival of the wave.

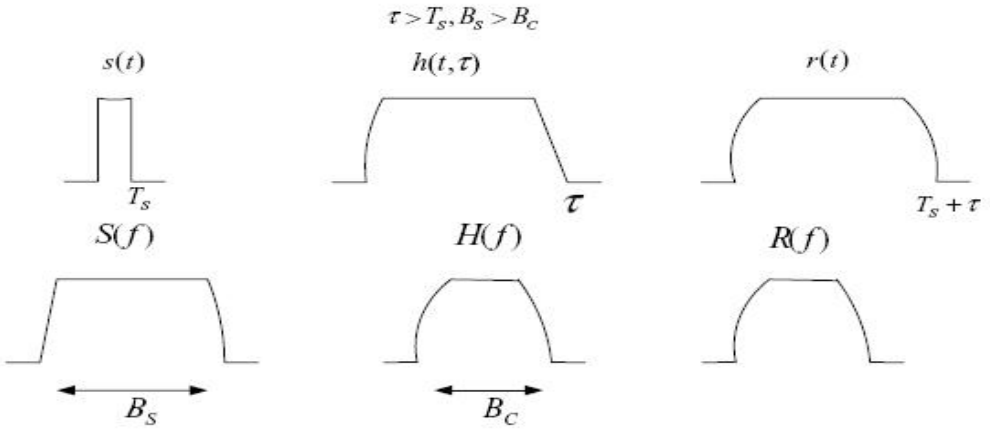

Figure 5.4: Example of propagation on a frequency selective fading channel.

The amount of frequency changes due to the Dopller effect depends on the relative motion between the source and receiver and on the speed of propagation of the wave.

A Doppler shift causes significant problems if the transmission technique is sensitive to frequency carrier offsets or the relative speed is higher, which is the case for OFDM [59], [60].

5.2.3. Fading channel statistical models

There are two statistical models for the flat fading communication channels. In the presence of LOS the Ricean model is used. When the LOS path is absent, it is preferable to use a Rayleigh model.

5.2.3.1. Rayleigh fading channel model

The received signal can be expressed as follows:

$$r(t) = \sum_{i=1}^{I} a_i \cos(2\pi f_c t + \phi_i) + \eta(t) \tag{5.9}$$

where a_i and ϕ_i are the amplitude and phase of the *i*-th component, respectively, and $\eta(t)$ is the Gaussian noise and I is the number of paths.
Equation (5.9) can be expanded as

$$r(t) = \cos(2\pi f_c t)\sum_{i=1}^{I} a_i \cos(\phi_i) - \sin(2\pi f_c t)\sum_{i=1}^{I} a_i \sin(\phi_i) + \eta(t) \tag{5.10}$$

In practical cases, the value of I is large, so the central limit theorem can be used. The envelope of the received signal is:

$$R = \sqrt{A^2 + B^2} \tag{5.11}$$

where

$$B = \sum_{i=1}^{I} a_i \sin(\phi_i) \quad \text{and} \quad A = \sum_{i=1}^{I} a_i \cos(\phi_i) \tag{5.12}$$

A and *B* are zero-mean Gaussian random variables, the envelope *R* follows a Rayleigh distribution whit the probability density function (pdf):

$$f_R(r) = \frac{r}{\sigma^2} \exp\left(\frac{-r^2}{2\sigma^2}\right), \quad r \geq 0 \tag{5.13}$$

where σ^2 is the variance of the random variables *A* and *B*.
For the baseband digital signal, after the matched filter and the sample and hold blocks, the output r_t (of the matched filter after demodulation) is:

$$r_t = \alpha s_t + \eta_t \tag{5.14}$$

where s_t and η_t are the discrete-time forms of *s*(*t*) and η(*t*); the transmitted signal and noise, respectively. α is a complex Gaussian random variable. The real and imaginary part of α are zero-mean Gaussian random variables and the amplitude $|\alpha|$ is called Rayleigh random variable.
Hence, equation (5.14) is a fading channel model, α is the path gain and η_t is usually AWGN.

5.2.3.2. Ricean fading channel model

In Ricean fading channel model, the Gaussian random variables A and B are not zero-mean, because a LOS path exists between the transmitter and the receiver, and a dominant stationary component exists in addition to random multiple paths. As a result, the distribution of the envelope random variable, *R*, is a Ricean distribution as expressed in equation (5.15) [59].

$$f_R(r) = \frac{r}{\sigma^2} \exp\left(\frac{-(r^2+D^2)}{2\sigma^2}\right) I_0\left(\frac{Dr}{\sigma^2}\right), \quad r \geq 0,\ D \geq 0 \tag{5.15}$$

where *D* is the peak amplitude of the dominant signal and $I_0(.)$ is the modified Bessel function of the first kind and of zero-order.

When the dominant signal disappears, the Ricean distribution converges to a Rayleigh distribution. The discrete-time input-output relationship in the case of Ricean fading channel model is also expressed as in equation (5.14) except that the real and imaginary parts of the path gain α are Gaussian random variables with non-zero means. Hence, the distribution of the amplitude $|\alpha|$ is Ricean instead of Rayleigh.

5.2.3.3. Frequency selective fading models

Frequency selective fading produces ISI. As a result, the channel can be modeled by the sum of a few weighted delta functions with different delays each

one describing a different path. In this case, the corresponding discrete time input-output relationship is:

(5.16)

The path gains α^j are independent complex Gaussian distributions and η_t represents the receiver's noise which usually is AWGN. In the case of Rayleigh fading, they are i.i.d complex Gaussian random variables. A special case that has been extensively utilized in the literature is the case of a two-ray Rayleigh fading model. For a two-ray Rayleigh fading model [60], we have

(5.17)

where the real and imaginary parts of a^0 and a^1 are i.i.d zero-mean Gaussian random variables.

5.3. Channel estimation techniques

Channel estimation techniques in multiple access communication systems can be divided in two major categories: non-blind and blind estimation. Non-blind estimation is based on the knowledge of previous channel estimations or some portion of the transmitted data like pilot symbols or training sequences. This a priori knowledge of the transmitted data sequences makes the estimation task easier and faster than in the case of the blind estimation techniques. Its main drawback is the consequent reduction of the spectral efficiency. The blind estimation is based on the received data and statistically estimates the channel behavior without any further knowledge; the blind estimation techniques perform the estimation by considering the second order statistics of the received data without any a priori knowledge of pilot symbols or previous channel estimation. Its advantage is the high spectral efficiency, because there is no need to transmit extra data symbols for training purpose. But to achieve reliable estimations, second order statistics of the received data require long estimation time [61], [62].

We can also find in literature examples for the use of the so called semi-blind estimation technique, where (they) are combined blind and non blind estimation algorithms. In [63], the authors used a periodic sequence of pilot symbols and first order statistic of the time domain received signals (symbols) in order to estimate the frequency-selective channel in OFDM systems. Also in [64], the authors proposed a semi-blind estimation algorithm which can learn channel coefficients accurately when only short training is available; they used blind channel estimation algorithms to improve the quality of the channel knowledge obtained from the short training. In the following, we will consider the SISO OFDM system presented in Figure 5.5, in order to introduce some basic channel estimation techniques.

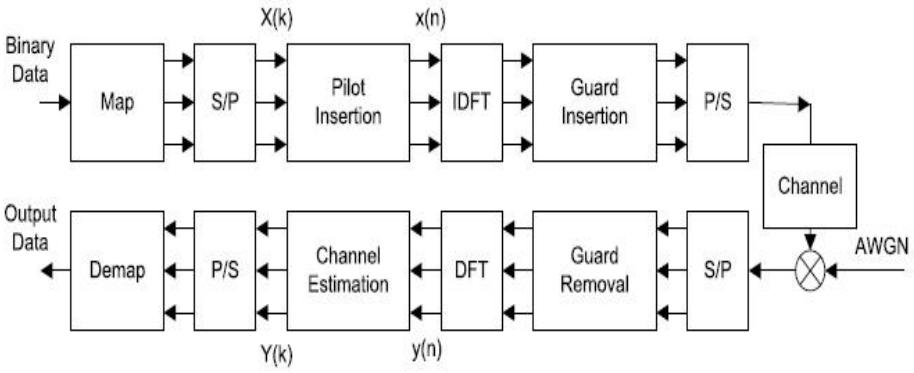

Figure 5.5: Baseband SISO OFDM system (using pilots for channel estimation) [65].

5.3.1. Non-Blind Channel Estimation

Some of the subcarriers composing the OFDM symbol transmitted represent pilots (with known amplitude at the channel's input), distributed in frequency in the entire baseband. Measuring their amplitudes at the output of the channel, we can identify the magnitudes of the channel's frequency response at the corresponding frequencies. Interpolating these magnitudes, the magnitude of the frequency response of the channel can be estimated.

5.3.1.1. Pilot Arrangement

There are three basics types of channel estimation based on pilot structures depending on arrangement of pilots: Block type, Comb-Type, and Lattice type [66].

5.3.1.1.1. Block-Type Pilot Arrangement

In block-type pilot based channel estimation, known OFDM symbols, in which all subcarriers are used as pilots, are transmitted periodically. If the channel is constant during the block transmission, there will be no channel estimation error since the pilots are sent at all subcarriers [65]. In Figure 5.6, a block type of pilot arrangement is depicted. In this type of estimation, a frequency-domain interpolation is performed in order to estimate the channel along the frequency axis. To keep track of the time-varying channel characteristics, the pilot symbols must be placed as frequently as the coherence time indicates. As the coherence time is the inverse of the Doppler frequency, $f_{Dopller}$ the pilot symbol period, S_t, must satisfy the following inequality:

$$S_t \leq \frac{1}{f_{Dopller}} \tag{5.18}$$

Since pilot tones are inserted into all subcarriers of OFDM symbols periodically in time, the block-type pilot arrangement is suitable for frequency-selective channels. However, for the fast fading channels, it might incur too much overhead to track the channel variation by reducing the pilot symbol period.

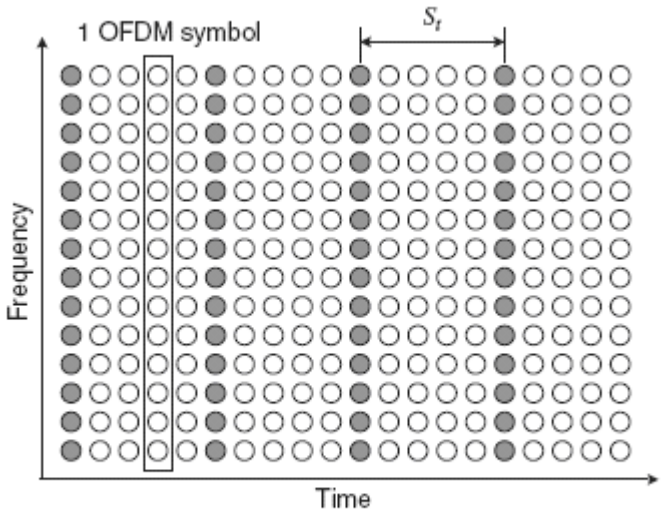

Figure 5.6: All subcarriers of an OFDM symbol represent pilots.

The block-type pilot based channel estimation can be performed by using Least Square (LS) or Minimum Mean Square Error (MMSE) techniques. In the following we present both LS and MMSE estimation techniques.

- **Least Square channel estimation: LS**

LS is a basic non-blind estimation technique, its goal is to minimize the square distance between the received signal *y* and the transmitted signal *x*. We consider only a single transmit and single receive antenna (i.e. SISO model). Hence, we can express the relationship between ***X*** and ***Y*** as,

$$\boldsymbol{Y} = \boldsymbol{X}.\boldsymbol{H} + \boldsymbol{W} \tag{5.19}$$

where *H* and *W* are the matrices representing the channel and the AWGN noise, respectively;
X= diag {*X* (0), *X* (1), …, *X*(*N*-1)};
Y=[*Y* (0), *Y* (1), …, *Y*(*N*-1)]^T;
W=[*W* (0), *W* (1), …, *W*(*N*-1)]^T;
H=[*H* (0), *H* (1), …, *H*(*N*-1)]^T=*DFT*$_N${*h*}=*F*.*h*;

$\boldsymbol{F} = \begin{bmatrix} W_N^{00} & \dots & W_N^{0(N-1)} \\ W_N^{(N-1)0} & \dots & W_N^{(N-1)(N-1)} \end{bmatrix}$; $W_N^{nk} = \frac{1}{N} e^{-j2\pi(\frac{n}{N})k}$; *h* the channel impulse response.

By considering negligible the noise contribution, the LS estimation of *h* in the frequency domain is:

(5.20)

Hence, the LS estimation in frequency domain (***H***) of *h* is,

(5.21)

(5.22)

It should be noted that *X* includes only non-zero data symbols and as such, matrix inversion is possible. Note that this simple LS estimate (for) does not exploit the correlation of channel across frequency carriers and across OFDM symbols.
The time domain LS estimation is given by the IDFT of ,

(5.23)

The Mean Square Error (MSE) is usually considered as the performance criterion (of) for channel estimates, and it is defined by,

(5.24)

An LS technique is utilized to get initial channel estimates at the pilot subcarriers [67] which are then further improved via different methods (as for example interpolation). In general, LS estimation technique has low complexity but it suffers (from) of high mean square error.

- **Minimum Mean Square Error: MMSE**

The MMSE is another (basic) channel estimation technique based on the knowledge of the second order statistical description of the channel conditions in order to minimize the Mean Square Error (MSE). If the time domain channel vector *h* is Gaussian and uncorrelated with the channel noise *w*, the frequency domain MMSE estimate of *h* is given as [68]:

(5.25)

where

(5.26)

(5.27)

are the cross covariance matrix between *h* and *Y* and the auto-covariance matrix of *Y*. R_{hh} is the auto-covariance matrix of *h* and σ^2 represents the noise variance .
The time domain MMSE estimate of the channel impulse response *h* can be expressed as,

(5.28)

The MMSE estimator yields much better performance than LS estimator, especially under the low SNR scenarios. But the major drawback of MMSE estimate is its high computational complexity.

- **Estimation with Feedback**

Channel estimation with decision feedback equalizer can be used in OFDM systems by utilizing the pilots to estimates the channel response using LS or MMSE algorithms. When the channel is slow fading, the channel estimation inside the block can be updated using the decision feedback equalizer at each subcarrier.
Let $H_i = \{H_{k,i}\}$ denotes the channel frequency response for the k^{th} subcarrier and the i^{th} symbol. For each coming symbol and for each coming subcarrier, the transmitted symbol is estimated from the previous $H_{k,i}$ using the formula,

$$X_{k,i+1} = \frac{Y_{k,i+1}}{H_{k,i}} \tag{5.29}$$

The estimated received symbols $X_{k,i+1}$ are used to make decision about the real transmitted symbols values (considered known in the training phase). The estimated channel frequency response is updated by:

$$H_{k,i+1} = \frac{Y_{k,i+1}}{X_{k,i+1}} \tag{5.30}$$

Consequently, $H_{k,i+1}$ is used as a reference for the next symbol, indexed by i+2, for the channel equalization.

The fast fading channel will cause the complete loss of estimated channel parameters. Therefore, as the channel fading becomes faster, there happens to compromise between the estimation error due to the interpolation and the error due to loss of channel tracking [65].

5.3.1.1.2. Comb-Type Pilot Arrangement

In Comb-Type pilot arrangement, as depicted in Figure 5.7, every OFDM symbol contains pilot tones located at subcarriers with uniform repartition on the frequencies' axis, which are used for a frequency-domain interpolation to estimate the channel frequency response (along the frequency axis). In order to keep track of the frequency-selective channel characteristics, the pilot symbols must be placed as frequently as coherent bandwidth is. As the coherence bandwidth is determined by an inverse of the maximum delay spread σ_{max}, the pilot symbol period, S_f, must satisfy the following inequality [66]:

$$S_f \leq \frac{1}{\sigma_{max}} . \tag{5.31}$$

The Comb –Type arrangement is suitable for fast-fading channels, but not for frequency- selective channels.

The N_P pilot signals are uniformly inserted into the OFDM symbol $X(k)$ according to the equation:

$$X(k) = X(mL + l) = \begin{cases} x_p(m) & l = 0 \\ inf.data & l = 1, \dots N_P \end{cases} \quad (5.32)$$

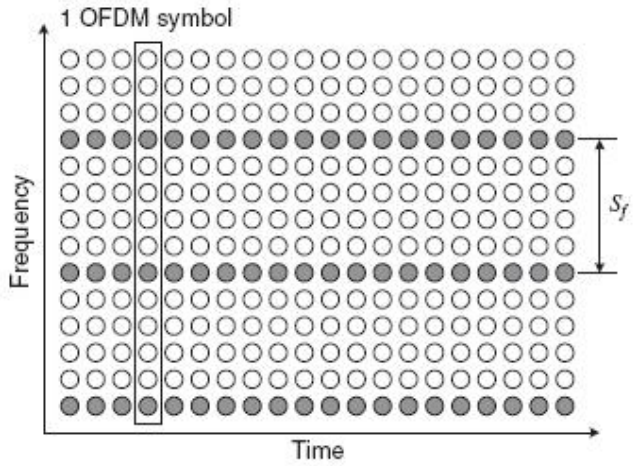

Figure 5.7: The pilots are allocated to some subcarriers of OFDM symbol only, equally spaced on the frequencies axis.

where $L = \frac{number\ of\ carriers}{N_P}$ and $x_p(m)$ is the m^{th} pilot carrier value. Let $\{H_P(k), k = 0, 1, \dots N_P\}$ be the frequency response of the channel at the frequencies of pilot subcarriers. By using the LS estimation, the estimate of the channel at pilot subcarriers frequencies is given by:

$$H_e(k) = \frac{Y_P(k)}{X_P(k)} \quad k = 0, \dots L - 1 \quad (5.33)$$

where $Y_P(k)$ and $X_P(k)$ are the spectra of output and input signals at the k^{th} pilot sub-carrier frequency respectively.

Since LS estimate is susceptible to noise and Inter Carrier Interference (ICI), the MMSE estimator is proposed while compromising computational complexity. Since MMSE includes the matrix inversion at each iteration, the simplified linear MMSE estimator is suggested in [69], where the inverse is needed to be calculated only once. The complexity is further reduced with a low-rank approximation by using Singular Value Decomposition (SVD). Let us describe the Linear Minimum Mean Square Estimator in the following paragraph.

- **Linear Minimum Mean Square Error: LMMSE**

The goal of the use of LMMSE channel estimator is to minimize the estimation's MSE. According to [70], the LMMSE of the channel frequency response is given by:

$$H_P^{LMMSE} = R_{HH_P}(R_{H_PH_P} + \sigma_\mu^2(XX^H)^{-1}))\widetilde{H}_p^{LS} \quad (5.34)$$

where R_{HH_P} represents the cross-correlation matrix between all subcarriers and the subcarriers with reference signals. $R_{H_PH_P}$ represents the autocorrelation matrix of the subcarriers. The high complexity of LMMSE estimator (5.34) is due to the inversion matrix lemma. Every time data changes, inversion is needed. The complexity of this estimator can be reduced by averaging the transmitted data. Therefore, we replace the term $(XX^H)^{-1}$ in the equation (5.34) with its expectation $E[(XX^H)^{-1}]$.

- **Interpolation Techniques in Comb-Type Pilot Arrangement**

To estimate the channel for data, the responses to pilot subcarriers must be interpolated. Popular interpolation methods include linear interpolation, second-order polynomial interpolation and cubic spline interpolation.

An efficient interpolation technique is necessary in Comb-Type pilot arrangement based channel estimation, in order to estimate the channel at data subcarriers frequencies by using the channel information at pilot subcarriers frequencies. According to [65], the linear interpolation method performs better than piecewise-constant interpolation. By using the linear interpolation, we obtain the channel estimation at the data subcarriers frequencies indexed by *k* where $mL \le k \le (m+1)L$, denoted as H_e:

$$H_e(k) = H_e(mL + l) \quad 0 \le l \le L \tag{5.35}$$

$$H_e(k) = (H_P(m+1) - H_P(m))\frac{l}{L} + H_P(m) \tag{5.36}$$

However, the second-order interpolation is better than linear interpolation [65]. Hence, the channel estimation using the second-order interpolation can be expressed as follow [71]:

$$H_e(k) = H_e(mL + l) \quad 0 \le l \le L \tag{5.37}$$

$$H_e(k) = c_1 H_P(m-1) + c_0 H_P(m) + c_{-1} H_P(m+1) \tag{5.38}$$

where
$$\begin{cases} c_1 = \frac{\alpha(\alpha-1)}{2} \\ c_2 = -(\alpha-1)(\alpha+1) \qquad \alpha = \frac{1}{N} \\ c_{-1} = \frac{(\alpha+1)}{2} \end{cases} \tag{5.39}$$

The low-pass interpolation (*interp function in MATLAB*) is performed by inserting zeros into the original sequence and then applying a low-pass FIR filter, that allows the original data to pass through unchanged and interpolates between such that the MSE between the interpolated points and their ideal value is minimized.

5.3.1.1.3. Lattice type Pilot Arrangement

In Lattice-Type pilot arrangement, pilot tones are inserted along both the time and frequency axes with given periods. As depicted in Figure 5.8, the pilot tones scattered in both time and frequency axes facilitate time/frequency-domain interpolations for channel estimation. Let S_t and S_f denote the periods of pilot

symbols in time and frequency, respectively. In order to keep track of the time-varying and frequency-selective channel characteristics, the pilot symbol arrangement must satisfy both equations (5.18) and (5.31), such that:

$$S_f \leq \frac{1}{\sigma_{max}} \quad \text{and} \quad S_t \leq \frac{1}{f_{Doplller}}, \tag{5.40}$$

where $f_{Doplller}$ and σ_{max} denote the Doppler spreading and maximum delay spread, respectively.

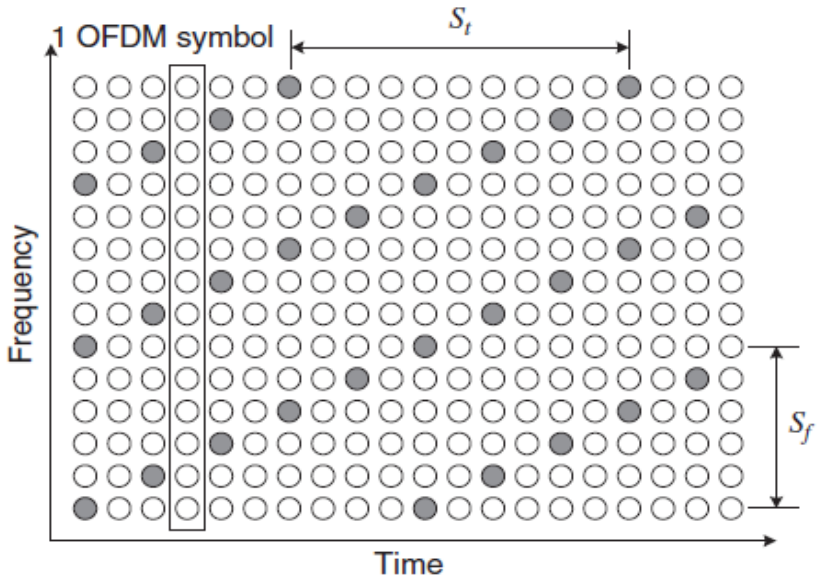

Figure 5.8: Lattice-Type pilot arrangement.

5.3.1.2. Training symbol based channel estimation

Training symbols can be used for channel estimation, usually providing a good performance. However, their transmission efficiencies are reduced due to the required overhead of training symbols such as preamble or pilot tones that are transmitted in addition to data symbols. The LS and MMSE techniques are widely used for channel estimation when training symbols are available [66].

5.3.2. Blind Channel Estimation

Using Blind Estimation Techniques, the channel can be estimated without resorting to the preamble or pilot signals. Many blind channel estimation algorithms have been proposed in the last years, most of these algorithms share the hypothesis that the input signal is unknown. Such blind technique has advantage of avoiding the overhead produced by training signals. However, it often needs a large number of received symbols to extract statistical properties, as for example the blind estimation techniques based on Constant Modulus Algorithm (CMA) [74]. Also, the

subspace based channel estimation technique is another blind (technique) method developed for OFDM systems and based on the use of the second order statistical and orthogonal properties of a received signal. The channel can be also estimated by using the properties of the noise subspace, which is orthogonal to the signal subspace, this method is called subspace-based channel estimation and needs a high computational complexity to separate the signal subspace and the noise subspace.

In the following, we present some blind channel estimation techniques and next we introduce our proposed technique based on denoising by Haar wavelet.

5.3.2.1. Subspace Methods

Subspace methods are applications of Second Order Statistics (SOS) based algorithms, consisting of estimating the unknown parameters by exploiting the orthogonality of subspaces of certain matrices obtained by arranging in a prescribed order the second order statistics of the observation [75]. Either signal subspace or noise subspace may be used independently in the subspace –based blind channel estimation method [76].

Let s_k denote the symbol emitted by the digital source at time kT, where T is the symbol duration. This discrete time signal is modulated, filtered, sent through the wireless communication channel, filtered, and demodulated. The resulting baseband signal is continuous in time, and given by:

$$x_c(t) = \sum_{k=-\infty}^{\infty} s_k h_c(t - kT) + v_c(t) \ , \tag{5.41}$$

where $h_c(t)$ is the continuous-time channel impulse response, which is assumed to have finite support; and $v_c(t)$ is the additive noise that is assumed to be stationary and uncorrelated with s_k.

The corresponding fractionally spaced discrete time model can be obtained either by sampling the signal received on several sensors at the emission duration, by oversampling the signal received on a single sensor, or by combining both techniques [76]. Consider oversampling the signal by a factor L. If $x_c(t)$ is sampled at $t=nT/L$, then the equation (5.44) can be written as [77]:

$$x_c(t) = \sum_{k=-\infty}^{\infty} s_k h_c\left(n\frac{T}{L} - kT\right) + v_c\left(n\frac{T}{L}\right). \tag{5.42}$$

We can also write:

$$x(n) = \sum_{k=-\infty}^{\infty} s_k h(n - kL) + v_c(n). \tag{5.43}$$

The noiseless outputs have a periodically time-varying correlation with period L. In general, periodically correlated signals are conveniently represented by a vector stationary process. The Single-Input Single Output (SISO) system of (5.43) has an equivalent MIMO description as:

$$x_i(n) = \sum_{k=-\infty}^{\infty} s_k h_i(n - kL) + v_i(n). \tag{5.44}$$

We can express $x(n)$ in a vector form as:

$$X(n) = \sum_{k=-\infty}^{\infty} s_k h(n - k) + V(n), \tag{5.45}$$

by letting,

$$X(n)=\begin{bmatrix} x_0(n) \\ . \\ . \\ . \\ x_{L-1}(n) \end{bmatrix} \quad , h(n)=\begin{bmatrix} h_0(n) \\ . \\ . \\ . \\ h_{L-1}(n) \end{bmatrix} \text{ and } V(n)=\begin{bmatrix} V_0(n) \\ . \\ . \\ . \\ V_{L-1}(n) \end{bmatrix}$$

We suppose that $h(0) \neq 0$. The system (5.48) can be expressed in matrix form as:

$$\boldsymbol{X}(n)=\boldsymbol{H_N s}(n)+\boldsymbol{V}(n) \tag{5.46}$$

where $\boldsymbol{H_N}$ is a $NL \times (N+L_h-1)$ block Toeplitz matrix, $s(n)$ is $(N+L_h-1)\times 1$ vector, $\boldsymbol{V}(n)$ and $\boldsymbol{X}(n)$ are $NL \times 1$ vectors.

$$\boldsymbol{H_N}=\begin{bmatrix} h(0) & h(1) & \cdots & h(L_h-1) & \cdots & 0 \\ 0 & h(0) & h(1) & \cdots & \cdots & 0 \\ \vdots & \ddots & \ddots & \ddots & \vdots & \\ 0 & \cdots & h(0) & \cdots & h(L_h-1) & \end{bmatrix}$$

$$\boldsymbol{X}(n)=\begin{bmatrix} x(n) \\ x(n-1) \\ \vdots \\ x(n-N+1) \end{bmatrix}, \boldsymbol{s}(n)=\begin{bmatrix} s(n) \\ s(n-1) \\ \vdots \\ s(n-N-L_h+2) \end{bmatrix}, \boldsymbol{V}(n)=\begin{bmatrix} \mathrm{v(n)} \\ \mathrm{v(n-1)} \\ \vdots \\ \mathrm{v(n-N+1)} \end{bmatrix}. \tag{5.47}$$

Assume that $\boldsymbol{X}(n)$ given in Equation (5.46), is wide-sense stationary process, and the signal $\boldsymbol{s}(n)$ and the noise $\boldsymbol{V}(n)$, are mutually independent. The covariance matrix of $\boldsymbol{X}(n)$ is:

$$R_x = E(\boldsymbol{X}(n)\boldsymbol{X}^H(n)) \tag{5.48}$$

where $E(.)$ denotes mathematical expectation. Since the additive measurement noise is assumed to be independent of the transmitted sequence, R_x is expressed using equation (5.46) as:

$$R_x = \boldsymbol{H_N} R_s \boldsymbol{H_N^H} + R_{\boldsymbol{V}} \tag{5.49}$$

where $R_s = E(\boldsymbol{s}(n)\boldsymbol{s}^H(n))$ is the transmitted signal covariance matrix, and $R_{\boldsymbol{V}} = \boldsymbol{E}(\boldsymbol{V}(n)\boldsymbol{V}^{\boldsymbol{H}}(n)) = \boldsymbol{\sigma^2} I$ is the noise covariance matrix.

Using Eigen Value Decomposition (EVD), eigenvectors corresponding to the L_h+N-1 largest values span the signal subspace defined by the columns of $\boldsymbol{H_N}$. The remaining $r = NL-L_h-N+1$ eigenvectors span the noise subspace. The corresponding eigen values are all equal to noise variance, σ^2. But the noise subspace eigenvectors g_i are orthogonal to channel matrix [78]

$$\boldsymbol{H_N}^{\boldsymbol{H}} g_i = 0\,,\ i=1,\ldots,r \tag{5.50}$$

This orthogonality of the signal and noise subspaces allows the estimation of the channel impulse response vector,

$$\boldsymbol{h} = \begin{bmatrix} h(0) \\ . \\ . \\ . \\ h(L_h - 1) \end{bmatrix}. \tag{5.51}$$

One of the important advantages of subspace based methods is its deterministic property. That is, the channel parameters can be recovered perfectly in the absence of noise using only finite set of data samples without any statistical assumption over the input data.
However, subspace based methods are computationally very intensive and difficult to implement. The main reason is that they require non-parallelizable EVD, to extract the noise or the signal [75].

5.3.2.2. Constant Modulus Algorithm

The Constant Modulus Algorithm (CMA) is one the most studied and implemented techniques in blind estimation; it was developed by Godard in [74] and Treichler in [79]. CMA employs the Constant Modulus (CM) criterion in its cost function, which penalizes deviations of the modulus of the estimated signal away from a constant [80].

As mentioned before and according to [78], the CM cost function assigns penalty to deviation in the modulus of the output signal; this function can be expressed as [80]:

$$J_{pq}^{CM} = E[(\|y(n)\|^p - \gamma)^q], \tag{5.52}$$

where p and q are positive integers and γ is a positive constant related to the CM of the signal constellation. It is called also the dispersion constant [78], and $y(n)$ is the blind estimator output.

Many algorithms can be conceived from the equation (5.55) by choosing special values of the couple (p,q).

The CMA is obtained by choosing (p,q) equal to (2,2) [80] and the channel estimation is performed by minimizing the J_{22}^{CM} cost function which can be expressed as:

$$J_{22}^{CM} = E[(\|y(n)\|^2 - \gamma)^2], \tag{5.53}$$

and the dispersion constant will be [21]:

$$\gamma = \frac{E[|s(k)|^4]}{E[|s(k)|^2]} \tag{5.54}$$

CMA method is used mainly to estimate and equalize source constellations that have a constant envelope, such as GMSK and M-PSK, however, it has been demonstrated that the constant modulus criterion can be used also for the source estimation that do not have a constant envelope, such as 16-QAM. The dispersion constant γ is selected depending on the modulation scheme. For example, in [81], the authors selected $\gamma = 1.0$ for M-PSK and $\gamma = 1.32$ for 16-QAM.

5.4. Blind Estimation Technique Based on Denoising for LTE DL and UL

The goal of this technique is to perform blind estimation based on denoising for LTE in UL and DL. The idea of this technique comes from a paper published by Professor David Donoho from Stanford University in 1992, which introduced the term denoising in connection with the adaptive non-linear filtering applied in the wavelets domain, [82]. This paper produced a high interest in the world of science and represents a source of inspiration for a huge number of papers which were already published and continue to appear. Despite its advantages, this method was not systematically exploited in communications yet.

Let us suppose that the signal $s[k]$ is additively perturbed by the white Gaussian noise $n[k]$. This is the well known scenario of the AWGN channel. The received signal has the expression: $x[k]=s[k]+n[k]$. To estimate the signal, Donoho, [82], proposed the following three steps method:

1) Computation of the Discrete Wavelet Transform (DWT) of the signal $x[k]$ obtaining the wavelet coefficients sequence, $y[k] = s[k] + n[k]$, where the noise $n[k]$ is white and Gaussian (WGN) [83]. The approximation y_{ia} and details y_{id} sequences are separated.
2) A non linear filtering is applied to the sequence of detail coefficients obtained:

$$y_{0d}[k] = \begin{cases} sgn\{y_{id}[k]\}(|y_M[k]| - t), & |y_M[k]| > t \\ 0, & if\ not \end{cases} \tag{5.55}$$

where t is a threshold.
3) The approximation coefficients sequence y_{ia} is concatenated with the new detail coefficients sequence y_{0d} obtaining the new sequence of wavelet coefficients $y_0$and is computed its inverse DWT (IDWT). The estimation of the signal $s[k]$, denoted by $s_0[k]$ is obtained.
The non linear filter applied at the second step is named soft-thresholding. The success of the Donoho's estimation procedure is assured by an appropriate choice of the threshold's value t. If $t = 3\sigma_n$, where σ_n represents the standard deviation of the noise n, then the probability that y_{0d} to be affected by noise is of 0.2% (rule of three sigma). The standard deviation σ_n can be estimated using the same DWT coefficients:

$$\hat{\sigma} = \frac{median\{|y_{id1}[k]|\}}{0.6745} \tag{5.56}$$

where y_{id1}represents the sequence of details from the first decomposition level.

In [83] is proposed a blind threshold selection method which maximizes the output signal to noise ratio, SNR_0. Starting from a small value of t, in [83] is proved also that SNR_0 increases with the increasing of t till an optimal value t_{opt}. Depending on the value of the input signal to noise ratio SNR_i, the value of t_{opt} could become superior to the maximum value of the useful component of the sequence. In this case the soft thresholding filter removes all the detail wavelet coefficients. So, in the case of low SNR_i , the Donoho's denoising method supposes only the separation of the approximation coefficients, all the detail coefficients being met to zero. The step 2, supposing filtering in the wavelet domain, is no longer necessary. We will show in the following that the case of fading channels corresponds to very low SNRi.

We have find only two references dealing with applications of the Donoho's denoising method in communications [83] and [84].

In [83] is proposed to perform a denoising operation before the interpolation, to improve the precision of the estimation of the frequency response of the channel. In [84] is proposed a blind estimation method for the detection of images in mobile wireless networks based on the association of the interleaved convolutional coding with a denoising method.

The idea of the proposed technique is the inclusion of a denoising system in the chain of wireless receiver based on OFDMA and SC-FDMA, to improve their Bit Error Rate (BER) [85], [86].

The architecture of the proposed blind estimator is presented in Figure 5.9. The blind estimation is performed after IDFT computation in OFDMA and DFT computation in SC-FDMA at the receiver of each scheme. The proposed denoising system implements the simplified variant of the Donoho's denoising method, without filtering, which consist in meting all the DWT detail coefficients to zero.

Figure 5.9: The architecture of the proposed blind estimation system.

The blind estimator is implemented with the aid of an interpolator (Upsampling system in Figure. 5.9) with an interpolation factor of 8. So, our blind estimation system is composed by the interpolator, followed by the denoising system and by down sampling system having the down sampling factor of 8. This last system selects each of the fourth samples from a group of 8 consecutive samples of its input signal.

5.4.1. Simulation Results

To simplify our simulations, we have considered the case of one user equipment with single transmitter and single receiver antenna (SISO system). We simulated the OFDMA and SC-FDMA transmission chain already described including or not the blind Estimation (BE), we used QPSK modulation and flat fading Rayleigh channel model. For subcarrier mapping in SC-FDMA, we simulated the IFDMA scheme. The denoising was performed using DWT computed with the Haar mother wavelets for six iterations. We have selected Haar mother wavelets because it has the best time localization, which is more important than the frequency localization in case of flat fading channels.

We performed the simulations in Matlab, in order to evaluate the performance of the proposed blind estimation technique.

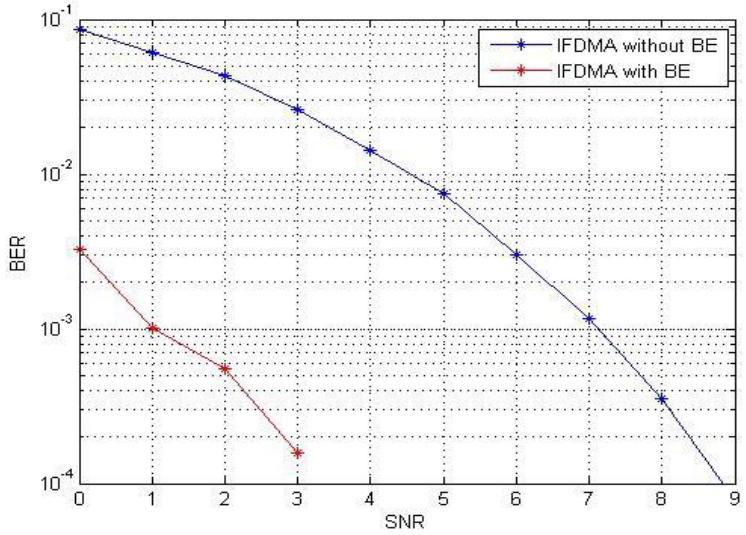

Figure 5.10: A comparison of the performance BER (SNR) obtained with and without blind estimation in SC-FDMA (IFDMA) system.

Figure 5.11 shows a comparison of BER performance of an OFDMA system equipped or not with the proposed blind estimation technique.

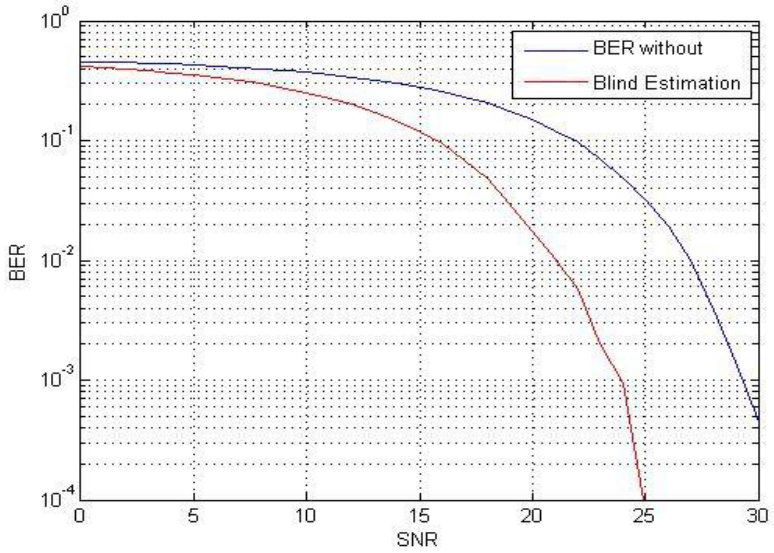

Figure 5.11: A comparison of the performance BER (SNR) obtained with and without blind estimation in OFDMA system.

Fig 5.10 shows a comparison of BER performance of SC-FDMA communication system equipped or not equipped with blind estimation technique. At SNR=3dB, the BER is approximately 0.0002 when the blind estimation technique is used and about 0.005 without the proposed technique. At BER equal to 0.0001 the

gain of SC-FDMA equipped with the blind estimation based on denoising is about 6 dB. These results prove also the good performance of the proposed technique.

At SNR= 20dB, the BER decreases below 0.01 when the blind estimation is implemented. At this value of BER, the gain of OFDMA equipped with the proposed blind estimation technique versus the conventional OFDMA is about 5.2 dB. This value is high enough to recommend the use of the proposed blind estimation technique. Such BER gains can be attained normally only with the aid of powerful channel coding techniques as for example the Turbo-codes.

Comparing the experimental results, it can be observed that the blind estimation improves substantially the performance of both types of communication systems, so the contribution of this technique is very important. The proposed blind estimation method is simpler than the non blind estimation methods, because it does not require the channel estimation. It could be used for channel estimation as well for both OFDMA and SC-FDMA which are used in LTE technology. The DWT computation algorithm implemented with the Haar mother wavelets is faster than the FFT algorithm. The soft thresholding filter is also very fast. So, the blind estimation method proposed in this paper is faster than the non blind estimation methods which are based on iterative algorithms and permits the tracking of faster time varying channels. The simulation results presented highlight the very good quality of the proposed estimation method outperforming the results obtained using other equalization methods as for example the zero forcing method. Such results can be obtained on AWGN channels only with the aid of coding techniques which are redundant and require important computing resources.

5.5. Summary

In this chapter, first we investigated the wireless channels and we gave an overview of some estimation techniques; finally, we developed and introduced a new blind estimation technique based on denoising, and then we implemented this new technique in OFDMA and SC-FDMA for one user case.

CHAPTER 6

CONCLUSIONS

This thesis is dedicated to the implementation of LTE at the air interface level. LTE was introduced in order to support high data rates, mobility and reduce latency. It enhances the air interface by exploiting OFDMA in the Downlink and SC-FDMA in the Uplink along with CP, adaptive modulation and coding schemes, advanced MIMO techniques, supporting both FDD and TDD, and offers all IP-based services.

The prominent advantage of SC-FDMA over OFDMA is that SC-FDMA transmitted signal has lower PAPR; for this reason SC-FDMA is used in LTE uplink communication. The PAPR parameter is a very important benefit for the mobile user equipment in term of power efficiency.

6.1. Contributions

In this work, we investigated the following items.

1. In chapter 3, we analyzed and compared the multiple access schemes in 3GPP LTE in downlink and uplink; we specifically compared subcarriers mapping in SC-FDMA, and the PAPR in both OFDMA and SC-FDMA. We have shown by simulations, using Matlab simulator, that SC-FDMA has good performance on AWGN and flat fading Rayleigh channel. We have highlighted by simulation also, the superiority of IFDMA over LFDMA. Finally we have shown that both of these mapping schemes produce lower PAPR then in OFDMA.

2. In Chapter 4, we first reviewed the most used PAPR reduction techniques. We also investigated some precoding techniques used in OFDM systems for PAPR reduction; we have shown that these precoding techniques reduce PAPR without signal distortion. We analyzed the Discrete Cosine Transform (DCT), Zaddof-Chu Transform (ZCT), and Walsh-Hadamard Transform (WHT) as coding mechanisms. We simulated these techniques implementing them in an OFDM system by considering a High Power Amplifier (HPA). We have demonstrated that precoding techniques based OFDM system produce lower PAPR than simple OFDM system. Furthermore, these techniques introduce no signal degradation. Also, we proposed two PAPR reduction techniques. The first one was applied for OFDMA systems and consists of the combination of Partial Transmit Sequence and Companding techniques. Simulation results show that PAPR has been reduced but with BER degradation. This drawback can be ameliorated by channel coding. The second PAPR reduction technique proposed consist of the use of Soft

Reduction and Companding after the cyclic prefix insertion in SC-FDMA communication systems. We have shown by simulations that this technique produces lower PAPR than the first one, without deteriorating the BER curves.

3. In Chapter 5, we have designed a new blind estimation technique based on denoising for the uplink and downlink in LTE. We have also implemented and simulated this technique in both OFDMA and SC-FDMA scenarios by considering SISO system. We have shown, by simulation, that the blind estimation improves substantially the performance of both types of communication systems, so the contribution of this technique is very important. The DWT computation algorithm implemented with the Haar mother wavelets is faster than the FFT algorithm. The soft thresholding filter is also very fast. So, the proposed blind estimation technique is faster than non blind estimation methods which are based on iterative algorithms and permits the tracking of faster time varying channels.

6.2. Perspectives

For future work, we list the following items:

- Design and implementation of more sophisticated PAPR reduction techniques in LTE UL and DL communications. The signal degradation is still a big problem when reducing the peak power. Other precoding and postcoding techniques could be applied in the future in OFDMA and SC-FDMA systems, in order to mitigate this problem and reduce the PAPR in the same time.
- Analyze the impact of interferences on the proposed estimation technique. We have considered a SISO system in our simulation in order to attend our contributions. MIMO systems along with coding, as for example the Turbo Codes, could be applied in the future, to include the effect of interferences.
- Implementation of the proposed blind estimation technique in LTE simulator [3] and WiMAX simulator [87].

Bibliography

[1] E-learning course, "LTE Overview." Award Solutions. Inc 2012. 2100 Lakeside Blvd., Suite 300, Richardson, TX.

[2] M. Ergen, Mobile Broadband: including WiMAX and LTE, Springer Science+Business Media LLC, 2009.3. C. Mehlführer.

[3] C. Mehlführer, J. Colom Ikuno, M. Simko, S. Schwarz, M. Wrulich, M. Rupp: "The Vienna LTE Simulators - Enabling Reproducibility in Wireless Communications Research"; EURASIP Journal on Advances in Signal Processing, Vol. 2011 (2011), 1 - 13.

[4] 3GPP TS 36.300 V8.8.0 (2009-03)," 3GPP Technical Specification Group Radio Access Network; Evolved Universal Terrestrial Radio Access (E-UTRA) and Evolved Universal Terrestrial Radio Access Network (E-UTRAN); Overall description; Stage 2(Release 8).

[5] M Mouly, MB Pautet, T Haug, The GSM System for Mobile Communications (Telecom Publishing, Palaisea, 1992).

[6] Frederic Michaud."GPRS &EDGE, First steps toward wireless EPFL-course Mobile network", 2004.

[7] TS 100 521 V66.1.0 (1999-05), "Digital cellular telecommunications system (Phase 2+); Network functions (GSM 03.01 version 6.1.0 Release 1997).

[8] 3GPP TS 23.101 (v 3.1.0) (2000-12) Technical specification "3rd Generation Partnership Project; Technical Specification Group Services and System Aspects General UMTS Architecture (3G TS 23.101 version 3.1.0).

[9] JS Lee, LE Miller, CDMA Systems Engineering handbook (Artech House Publishers, Boston, 1982).

[10] 3GPP TS 44.001 V4.0.0 (2001-03) , 3rd Generation Partnership Project; Technical Specification Group Core Network; Mobile Station - Base Station System (MS - BSS) interface; General aspects and Principals. (Release 4).

[11] 3GPP TS 44.001 V5.0.0 (2002-06) Technical specification, "3rd Generation Partnership Project; Technical Specification Group Core Network; Mobile Station - Base Station System (MS - BSS) interface; General aspects and principles (Release 5).

[12] 3GPP TS 44.001 V6.0.0 (2004-12) Technical specification, "3rd Generation Partnership Project; Technical Specification Group Core Network; Mobile Station - Base Station System (MS - BSS) interface; General aspects and principles (Release 6).

[13] AM Rao, A Weber, and S Gllamudi, R. Soni, "LTE and HSPA +: revolutionary and evolutionary solutions for global mobile broadband." Bell Labs Tech. J 13(4), 7-34 (2009).
[14] [14] 3GPP TS 44.001 V7.0.0 (2007-06) Technical specification, "3rd Generation Partnership Project; Technical Specification Group Core Network; Mobile Station - Base Station System (MS - BSS) interface; General aspects and principles (Release 7).
[15] Robert Volesky. "IS-95 StandardPower Control and RAKE Receiver." Iowa State University EE 521 Robert Volesky 29 Nov 00.
[16] Raymond Steele, Chin-Chum Lee and Peter Gould,"GSM, cdmaOne and 3G systems.", 2001 John Wiley & Sons Ltd.
[17] T Ojanpera, R. Prasad, WCDMA: Towards IP Mobility ans Mobile interbet (Artech House publishers, boston, 2001).
[18] "EV-DO Rev.A and B: wireless Broadband for the masses", Qualcomm Incorporated, December 2007.
[19] E.dahlman, S. Parkvall, J. Skoid, and P. Beming, 3G Evolution-HSPA and LTE for Mobile Broaband, 1st ed. Academic Press, 2007.
[20] Ralf Zartenar, Ralf Klüber, Tilo Hamann, Caglar Ekmen, Markus Bieling, Marcus Brunner, and Hakan Ekmen, "LTE/SAE, Drivers, Benitfits and challenges". P3communications GmbH, version 1.0, 2011.
[21] [21] 3GPP 36.321, "E-UTRA Medium Access Control (MAC) Protocol Specification, "Rel 8.
[22] 3GPP 36.322, " E-UTRA Radio Link Control (RLC) Protocol Specification, " Rel8
[23] 3GPP TS 36.323, "E-UTRA Packet Data Convergence Protocol (PDCP) Specification, "Rel 8.
24 3GPP Technical Specification 36.211, version 8.4.0, "Physical Channels and Modulation," September 2008.
[25] 3GPP Technical Specification 36.300, version 8.3.0, "Evolved universal Terrestrial Radio Access (E-UTRA) and Evolved Universal Terrestrial radio Access Network (E-UTRAN), overall description,)stage 2, January 2008.
[26] R. Van Nee and R. Prasad, "OFDM for Wireless Multimedia Communication", Artech House, 2000.
[27] H. Sari, G.Karam, and I. Jeanclaude,"Transmission Techniques for Digital terrestrial TV Broadcasting", IEEE Commun. Mag., vol. 33, no. 2, pp. 100-109, Feb.1995.
[28] D. Falconer, S. L. Ariyarisitakul, A. Benyamin-Seeyar, and B. Edison, "Frequency Domain Equalization for Single Carrier Broadband Wireless Systems", IEEE Commun Mag., vol. 40, no. 4, pp. 58-66, Apr. 2002.
[29] Christopher Cox, "An introduction to LTE: LTE, LTE Advanced, SAE and 4G Mobile Communications." First Edition. 2012John Wiley and Sons Ltd. Page 61.
[30] "OFDM Overview", Technology Training, Award Solutions. Inc 2012. 2100 Lakeside Blvd., Suite 300, Richardson, TX.
[31] 3GPP TS 3.211 v9.1.0(2010-03 Technical specification):3rd Generation Partnership project; Technical Specification Group radio Access Network; Evolved Universal terrestrial radio Access (E-UTRA); Physical channel and Modulation (Release 9).

[32] Hyung G. Myung and David Goodman, "Single Carrier FDMA A new Air Interface for Long Term Evolution." Wiley Series on Wireless Communications and Mobile computing. October 2008.

[33] H. G. Myung, J. Lim, and D. J. Goodman, "Single Carrier FDMA for Uplink Wireless
Transmission," IEEE Vehicular Technology Mag., vol. 1, no. 3, Sep. 2006.

[34] Sorger, U., De Broeck, I., and Schnell, M., "Interleaved FDMA - A New Spread-
Spectrum Multiple-Access Scheme," *Proc. IEEE ICC '98*, Atlanta, GA, Jun. 1998,
pp. 1013–1017.

[35] Frank, T., Klein, A., and Costa, E., "IFDMA: A Scheme Combining the Advantages of
OFDMA and CDMA," *IEEE Wireless Commun.*, vol. 14, no. 3, June 2007, pp. 9–17.

[36] 3GPP TR 25.814 – 3GPP; Technical Specification Group Radio Access Network; Physical
Layer Aspects for Evolved Universal Terrestrial Radio Access (UTRA) (Release 7).

[37] B. M. Popovic, "Generalized Chirp-like Polyphase Sequences with Optimal Correlation
Properties," IEEE Trans. Info. Theory, vol. 38, Jul. 1992, pp. 1406-1409.

[38] D. Wulich and L. Goldfeld, "Bound of the Distribution of Instantaneous Power in Single Carrier Modulation", IEEE Trans. Wireless Commun., vol. 4, no. 4, pp. 1773–1778, Jul. 2005.

[39] Mountassir Jamal, Balta Horia, Kovaci Maria and Isar Alexandru, "Study of Multiple Access Schemes in 3GPP LTE OFDMA vs. SC-FDMA". 2011 International Conference on Applied Electronics, pilsen, Czech Republic 7-9 September 2011, pages 275-278.

[40] Miller, S.L. and O'Dea, R.J., "Peak Power and Bandwidth Efficient Linear Modulation,"
IEEE Trans. Commun., vol. 46, no. 12, Dec. 1998, pp. 1639–1648.

[41] Jamal Mountassir, Alexandru Isar," Combined Partial Transmit Sequence and Companding for PAPR Reduction in OFDM Systems". Signal Processing and Applied Mathematics for Electronics and Communications, Cluj-Napoca, Romania. August 26-28, 2011.

[42] Tao Jiang, and Yiyan Wu, "An overview: Peak-to-Average Power ratio Reduction Techniques for OFDMA signals." IEEE Transactions on Broadcasting, Vol. 54, NO. 2, June 2008.

[43] Dae-Woon Lim, Seok-Joong Heo, and Jong-Seon No, "An Overview of Peak-to-Average Power Ratio reduction Schemes for OFDM Signals". Journal of Communications and Networks, Vol. 11, No. 3, June 2009.

[44] Gross, R. and D. Veeneman, "Clipping distortion, in DMT ADSL systems," *IEEE Electron. Letter*, Vol. 29, 2080–2081, Nov. 1993.

[45] Davis, J. A. and J. Jedwab, "Peak-to-mean power control in OFDM, Golay complementary sequences, and Reed-Muller codes," *IEEE Trans. Inform. Theory*, Vol. 45, 2397–2417, Nov. 1999.

[46] Korngold, B. S. and D. L. Jones, "PAPR reduction in OFDM via active constellation extension," *IEEE Trans. on Broadcasting,* Vol. 49, 258–268, Sept. 2003.
[47] Muller, S. H. and J. B. Huber, "OFDM with reduced peak-to average power ratio by optimum combination of partial transmit sequences," *IEEE Electron. Letter*, Vol. 33, 368–369, Feb. 1997.
[48] Yung, C., K. Shang, C. Kuan, and C. Mao, "Turbo coded OFDM for reducing PAPR and error rates," *IEEE Transactions on Wireless for Communications*, Vol. 7, No. 1, Jan. 2008.
[49] Proakis, J. G. and M. Salehi, Communication Systems Engineering, *Prentice-Hall, Inc*., 1994.
[50] J. Amstrong, "Peak to average power reduction for OFDM by repeated clipping and fequency domain filtering," IEE Electron. Lett., vol. 38, no. 5, pp. 246–247, Feb. 2002.
[51] X. Li and L. J. Cimini Jr., "Effects of clipping and filtering on the performance of OFDM," IEEE Commun. Lett., vol. 2, no. 5. pp. 131–133, May 1998.
[52] H. Sakran, M. Shokair, and A. Abou Elazn, "Combined Interleaving and Companding for PAPR Reduction in OFDM systems," Progress in Electromagnetic Research C, Vol. 6, 67-78, 2009.
[53] Stefan H. MÄuller and Johannes B. Huber, "A COMPARISON OF PEAK POWER REDUCTION SCHEMES FOR OFDM." In Proc. of the IEEE Global Telecommunications Conference GLOBECOM '97, pp. 1{5, November 1997, Phoenix, Arizona, USA
[54] J. Tellado, "Peak to Average Power Ratio Reduction for Multicarrier Modulation," PhD thesis, University of Stanford, Stanford, 1999.
[55] Hyung G. Myung and David Goodman, "Single Carrier FDMA A new Air Interface for Long Term Evolution." Wiley Series on Wireless Communications and Mobile computing. October 2008.
[56] Jamal Mountassir, Alexandru Isar, Tarik Mountassir" Precoding Techniques in OFDM systems For PAPR Reduction" The 16th IEEE Mediterranean Electrotechnical Conference MELECON 2012, Tunisia, 25-28 March 2012.
[57] I. Baig and V. Jeoti, "PAPR Reduction in OFDM Systems: Zadoff-Chu Matrix Transform Based Pre/Post-Coding Techniques," IEEE Second Conference on Computational Intelligence, Communication Systems and Networks, pp505-510, Pahang, June 2010.
[58] Hyung G. Myung , Junsung Lim, and David j. Goodman, "PEAK-TO-AVERAGE POWER RATIO OF SINGLE CARRIER FDMA SIGNALS WITH PULSE SHAPING", the 17th Annual IEEE International Symposium on Personal, Indoor and Mobile Radio Communications (PIMRC'06). 2006.
[59] Hamid Jafarkhani, "Space-Time coding – Theory and Practice", University of California, Irvine. ISBN: 9780521842914. Publication date: September 2005.pages 5-12.
[60] H. Vincent Poor and Gregory W. Wornel, "Wireless communications", Prentice Hall Signal Processing Series. 2002.
[61] L. Wei, C. Ming, S. Cheng, H. Wang, \A complexity reduced blind channel equalization scheme for OFDM systems", IEEE 17th International Symposium on Personal, Indoor and Mobile Radio Communications, 2006.

[62] R. Boloix-Tortosa, F. J. Simois-Tirado, J. J. Murillo-Fuentes, \Blind adaptive channel estimation for OFDM systems", IEEE 10th Workshop on Signal Processing Advances in Wireless Communications, Jun. 2009.

[63] W. Yang, Y. Cai, Y. Xun, \Semi-blind Channel Estimation for OFDM Systems",
IEEE 63rd Vehicular Technology Conference, May 2006.

[64] Tianbin Wo and Peter Adam Hoeher, "Semi-Blind Estimation for Frequency-Selective MIMO systems."Faculty of Engineering. University of Kiel. Kaiserstr. 2, D-24143 Kiel, Germany.

[65] Sinem Coleri, Mustafa Ergen, Anuj Puri, and Ahmad Bahai, "Channel Estimation Techniques Based on Pilot Arrangement in OFDM Systems," IEEE TRANSACTIONS ON BROADCASTING, VOL. 48, NO. 3, SEPTEMBER 2002.

[66] Yong Soo Cho, Jaekwon Kim, Won Young Yang, and Chung Gu Kang, "MIMO-OFDM Wireless Communications with Matlab". John Wiley & Sons (Asia) Pte Ltd. 2 Clementi Loop, # 02-01, Singapore 129809. 2010.

[67] Mehmet Kemal Ozdemir Logus, Broadband wireless Solutions, inc. and Huseyin Arslan," Channel Estimation for Wireless OFDM Systems, "IEEE Communications Surveys & Tutorials. 2nd quarter 2007.

[68] A. Omri, R. Boullegue, R. Hamila and M. Hasna, "Channel Estimation For LTE Uplink System by Perecption Neural Network", International Journal of Wireless and Mobile Network (IJWMN), Vol. 2, No. 3, August 2010.

[69] U. Reimers, "Digital video broadcasting," IEEE Commun. Mag., vol. 36, no. 6, pp. 104–110, June 1998.

[70] Abdelhakim Khlifi and Ridha Bouallegue, "Performance Analysis of LS and LMMSE Channel Estimation Techniques for LTE Downlink Systems, "International Journal of Wireless & Mobile Networks (IJWMN) Vol. 3, No. 5, October 2011.

[71] M. Hsieh and C.Wei, "Channel estimation for OFDM systems based on comb-type pilot arrangement in frequency selective fading channels," IEEE Trans. Consumer Electron., vol. 44, no. 1, Feb. 1998.

[72] Y. Zhao and A. Huang, "A novel channel estimation method for OFDM Mobile Communications Systems based on pilot signals and transform domain processing," in Proc. IEEE 47th Vehicular Technology Conf., Phoenix, USA, May 1997, pp. 2089–2093.

[73] A. V. Oppenheim and R. W. Schafer, Discrete-Time Signal Processing, New Jersey: Prentice-Hall Inc., 1999.

[74] D. Godard "Self-Recovering Equalization and Carrier Tracking in Two-Dimensional Data Communications Systems," IEEE Transactions on Communications, COM-28, 11, pp. 1867-1875.

[75] P. Sivakumar, M. Rajaram, "Subspace Method based Blind Channel Equalization in OFDM System." European Journal of Scientific Research, ISSN 1450-216X, Vol.61, No.2, pp.314-320. Eurojournals Publishing, Inc 2011.

[76] E. Moulines, P. Duhamel, J. Cardoso, and S. Mayrargue, "Subspace methods for the blind identification of multichannel FIR filters," IEEE Trans. Signal Processing, vol. 43, pp. 516–525, Feb. 1995.

[77] Xiaohua Li and H. Howard Fan," Blind Channel Identification: Subspace Tracking Method without Rank Estimation, " IEEE Transactions on Signal Processing", Vol. 49, No. 10, October 2001.
[78] Visa Koivunen, Juha Laurila, and Ernst Bonek." Blind Methods for Wireless Communication Receivers."
[79] J.R. Treichler and B. G. Agee "A New Approach to Multipath Correction of Constant Modulus Signals," IEEE Transactions on Acoustics, Speech and Signal Processing, ASSP-31, 2, pp. 459-471, 1983.
[80] Marilli Rupia, Panagiotis Tsakalidesb, Enrico Del Rea, Chrysostomos L. Nikias, "Constant modulus blind equalization based on fractional lower-order statistics." Signal Processing 84 (2004) 881 – 894.
[81] J. R. Treichler [1998], "Practical Blind Demodulators for High-Order QAM Signals," Signal Processing, 67, pp. 331-344.
[82] D. Donoho, Denoising by Soft Thesholding, IEEE Transactions on Information Theory, vol. 41, no. 3, May 1995, 613-627.
[83] M. Borda, D. Isar, Whithening with Wavelets. Proceedings of ECCTD'97 Conference, Budapest, August, 1997.
[84] Dong Heon Lee, Suk Chan Kim, Jin Woo Park and Seong Lai Park, "Channel Estimation with Wavelet De-noising for OFDM System in Mobile Environment", Proc. of 12th Int. Conf. on Advanced Communication Technology, Phoenix Park, Korea, Feb. 7-10, 2010.
[85] Jamal Mountassir, "Denoising based blind estimation for Single Carrier Frequency Division Multiplexing (SCFDM)." International Symposium on Electronics and Telecommunications (ISETC), 2012 Nobember10th.
[86] Jamal Mountassir, Daniel Bojneagu, Marius Oltean and Alexandru Isar "Denoising based blind estimation technique for orthogonal frequency division multiplex systems," International Conference on Wireless and Mobile Networks ICWMCN 2011, Paris, France. October 24-25, 2011.
[87] Marius Oltean, Maria Kovaci, Jamal Mountassir, Alexandru Isar, Petru Lazar, A physical layer simulator for WiMAX, 9'th IEEE International Symposium of Electronics and Telecommunications, ISETC 2010, Timisoara, Romania, November 2010, pp. 133-136, ISBN : 978-1-4244-8458-4.